ATOMIC HYDROGEN IN A MAGNETIC TRAP

ACADEMISCH PROEFSCHRIFT

ter verkrijging van de graad van doctor
aan de Universiteit van Amsterdam
op gezag van de Rector Magnificus
Prof. Dr. S. K. Thoden van Velzen
in het openbaar te verdedigen in de Aula der Universiteit
(Oude Lutherse Kerk, ingang Singel 411, hoek Spui),
op maandag 29 mei 1989 te 13.30 uur

door

Raymond van Roijen

geboren te Leiden

Amsterdam 1989

Promotor : prof. dr. J.T.M. Walraven

Faculteit der Natuur- en Sterrenkunde

The work described in this thesis was part of the research program
of the 'Stichting voor Fundamenteel Onderzoek der Materie (FOM)'
and was carried out at the

Natuurkundig Laboratorium der
Universiteit van Amsterdam
Valckenierstraat 65
1018 XE Amstterdam
The Netherlands

where a limited number of copies of this thesis are available

aan mijn moeder
aan mijn vader

Contents

Introduction

The hydrogen atom is fascinating in its simplicity. When properly prepared also a collection of atoms behaves in many respects as a nearly ideal system, well suited for theoretical analysis from first principles. The experiments described in this thesis show the accuracy of such an analysis.

A hydrogen atom is a composite boson, consisting of one electron and one proton. A gas of hydrogen atoms will recombine to molecular hydrogen (H_2), but polarizing the atoms in a strong magnetic field at low temperature can increase the stability dramatically. This was first accomplished experimentally by Silvera and Walraven[1] using a l-He coated cell at low temperature (T <1K) in a high ($B \leq$10T) magnetic field.

Because of the small mass of the atoms and the weak interaction between the particles a gas of spin-polarized atomic hydrogen is a nearly ideal system obeying Bose-statistics,[2] in which macroscopic quantum properties should be observable, such as the gaseous nature of atomic hydrogen even at $T = 0$, and Bose-Einstein condensation (BEC). In a number of experiments, described in two review articles by Silvera and Walraven[3] and Greytak and Kleppner,[4] the stability of the gas was improved and the maximum density increased by orders of magnitude. However, the closest approach to BEC ever reported,[5] was, in terms of density n and temperature T, $n^{2/3}/T \approx 6\times10^{12}\mathrm{cm}^{-2}\mathrm{K}^{-1}$, less than 10% of the minimum condition for BEC. At high densities three particle recombination on the surface leads to rapid destruction of the sample. Soon it was realized that in order to get closer to BEC surface processes had to be eliminated, and proposals were made to trap the atoms using static[6] or dynamic[7] magnetic traps. Stabilizing atomic hydrogen (H) in a static magnetic trap implies using electron spin-up polarized hydrogen (H$\uparrow$) instead of the spin-down state (H$\downarrow$) used in earlier experiments. The H$\uparrow$ are low-field-seekers, which can be trapped in a magnetic field minimum. The construction of a magnetic field maximum in free space, necessary to trap H$\downarrow$, is forbidden by the Maxwell equations.[8]

The spin-up states can relax to the lower, spin-down states (H$\downarrow$), whereas at low temperatures and in moderate magnetic field, i.e. for $B/T \gg 1\mathrm{TK}^{-1}$, the transition from H$\downarrow$ to H$\uparrow$ is energetically forbidden. The relaxation will take place via spin exchange and the dipolar interaction. The rates were calculated by Lagendijk *et al.*[9] and Stoof *et al.*[10]

This thesis describes the construction and application of a static magnetic trap for atomic hydrogen. We demonstrate that densities of up to $3 \times 10^{14}\mathrm{cm}^{-3}$ at temperatures of 80 to 200mK can be achieved with a technically simple method of filling the trap. Double polarization is shown to occur spontaneously in the trapped gas, and the dipolar relaxation rate ($G_{dd} = 1.2(2) \times 10^{-15}\mathrm{cm}^3/\mathrm{s}$) and its field dependance are measured,[11] confirming theoretical predictions. These results show that atomic hydrogen is (again)

a promising material for the achievement of BEC, provided that apart from the present method of cooling the gas, which is shown to impose a lower limit on the temperature, another cooling mechanism is supplied to reach lower temperatures. The density reached was two orders of magnitude higher than that of trapping experiments done at MIT,[12,13] where the technique of 'evaporative cooling' (i.e. letting the most energetic particles escape the trapping region) was used to reach a temperature lower than 3mK.

References

[1]I.F. Silvera, and J.T.M. Walraven, Phys. Rev. Lett. **44**, 164 (1980).

[2]A. Einstein, Preuss. Akad. der Wiss. Sitzungsber. **3**, 18 (1925).

[3]I.F. Silvera, and J.T.M. Walraven, Progr. Low Temp. Phys. edited by D.F. Brewer (North-Holland, Amsterdam, 1986) vol. **X**, 139.

[4]T.J. Greytak, and D. Kleppner, New Trends in Atomic Physics, edited by G. Grynberg and R. Stora (Elsevier, Amsterdam, 1984), vol **II**, 1125;

[5]T. Tommila, E. Tjukanov, M. Krusius, and S. Jaakkola, Phys. Rev. B **36**, 6837 (1987).

[6]H.F. Hess, Bul.Am.Phys.Soc. **30** 854 (1985); Phys.Rev.B(RC) **34** (1986) 3476.

[7]R.V.E. Lovelace, C. Mehanian, T.J. Tommila, and D.M. Lee, Nature **318**, 30 (1985).

[8]W.H. Wing, Progr. Quant. Electr. **8**, 181 (1984).

[9]A.Lagendijk, I.F.Silvera en B.J.Verhaar, Phys.Rev.B (RC) **33** 626 (1986).

[10]H.T.C. Stoof, J.M.V.A. Koelman, and B.J. Verhaar, Phys. Rev. B **38**, 4688 (1988).

[11]R. Van Roijen, J.J. Berkhout, S. Jaakkola, and J.T.M. Walraven, Phys. Rev. Lett. **61**, 931 (1988), included in this thesis as Chapter 4.

[12]H.F.Hess, G.P. Kochanski, J.M. Doyle, N.Masuhara, D.Kleppner and T.J.Greytak, Phys.Rev.Lett. **59**, 672 (1987).

[13]N. Masuhara, J.M. Doyle, J.C. Sandberg, D. Kleppner, and T.J. Greytak Phys. Rev. Lett. **61**, 935 (1988).

Chapter 1

Overview

1.1 The hydrogen atom

The magnetic properties of a hydrogen atom in its electronic ground state ($^2S_{1/2}$) in a magnetic field B are well described with a Hamiltonian of the type[1]

$$H = H_Z + H_{hyp} = -(-g_e\mu_B\vec{s} + g_n\mu_n\vec{i}).\vec{B} + a\vec{i}.\vec{s}, \tag{1.1.1}$$

where H_Z and H_{hyp} represent the Zeeman and the Fermi contact hyperfine interaction respectively. The electron and proton have g factors g_e and g_n respectively, μ_B and μ_n are the Bohr magneton and the nuclear magneton, s and i are the electron and proton spin and a is the hyperfine constant. The gyromagnetic ratios are defined as positive numbers. The energies of the eigenstates, labeled a, b, c, and d in order of increasing energy, are

$$\begin{aligned} E_a &= -\frac{1}{4}a - \frac{1}{2}a[1 + (\mu^+B/a)^2]^{1/2} \\ E_b &= \frac{1}{4}a - \frac{1}{2}\mu^-B \\ E_c &= -\frac{1}{4}a + \frac{1}{2}a[1 + (\mu^+B/a)^2]^{1/2} \\ E_d &= \frac{1}{4}a + \frac{1}{2}\mu^-B. \end{aligned} \tag{1.1.2}$$

Here $\mu^\pm \equiv g_e\mu_B \pm g_n\mu_n$. In Fig. 1.1.1 these energies are plotted as a function of the magnetic field along with the expressions for the states. The simple arrows stand for the electron spin-up ($\uparrow$) and down states ($\downarrow$) respectively, and similarly the barred arrows for the nuclear spin ($\bar{\uparrow}$,$\bar{\downarrow}$). As can be seen in this figure the b and d state are pure states, whereas a and c have a field dependent admixture of the opposite spin. The mixing parameter $\epsilon = \sin\theta$ may be expressed as

$$\sin\theta = \{1 + (\mu^+B/a + [1 + (\mu^+B/a)^2]^{1/2}\}^{-1/2}. \tag{1.1.3}$$

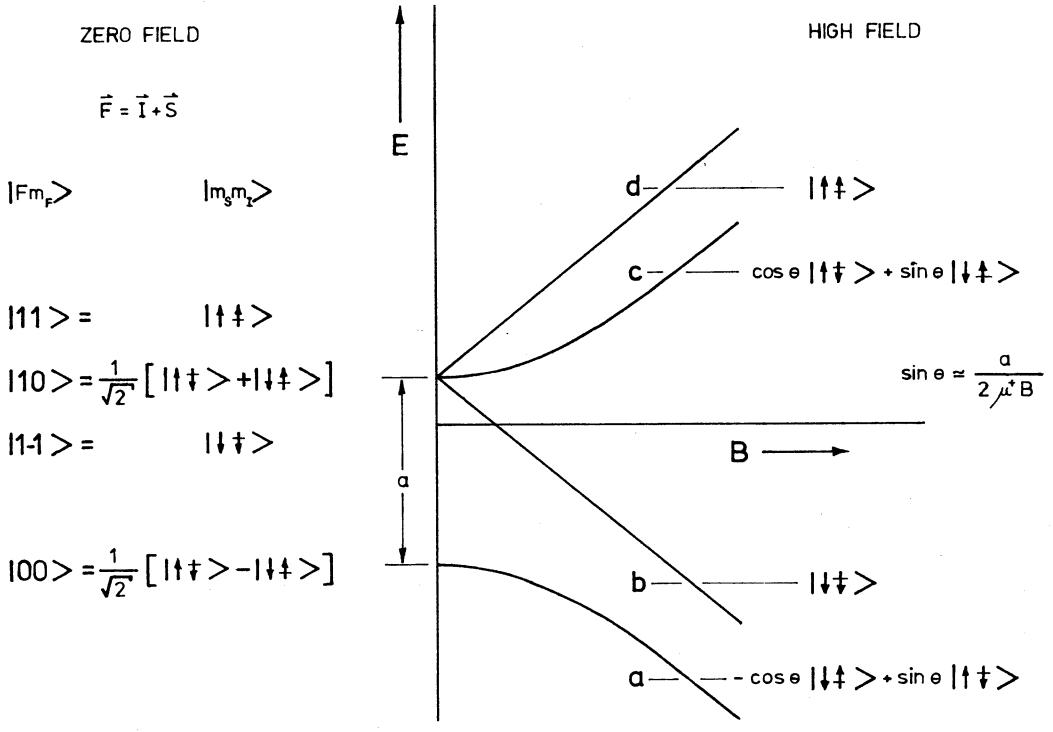

Figure 1.1.1: *Energies of the hyperfine levels of the ground state hydrogen atom in a magnetic field.*

From Fig. 1.1.1 one can also infer the effective magnetic moment μ_H of hyperfine state h, given by $\mu_H(h) = -(\partial E_h/\partial B)$. Fig. 1.1.2 shows the effective magnetic moment as a function of the magnetic field. The effective magnetic moment of the a and c states in a field of 0.1T is $0.9\mu_B$. We will replace the magnetic moment of the hydrogen atom by $\pm\mu_B$ throughout this thesis, because this approximation is valid for the magnetic fields used.

The a and b states have a lower energy in higher field, so atoms in these states will be attracted by a high field (high-field seekers), whereas the c and d states correspond to so-called low-field seekers. This feature of the electron spin-up states enables trapping H-atoms in a minimum B field.

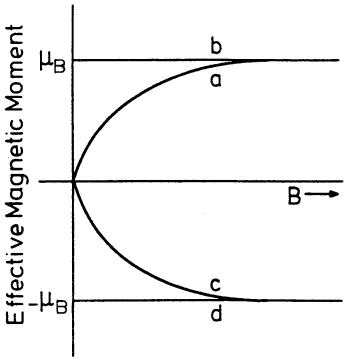

Figure 1.1.2: *The effective magnetic moment μ_H as a function of magnetic field.*

1.2 Interatomic interaction

The interaction between hydrogen atoms can be expressed by the hamiltonian

$$H = H_D + H_{exch} + H_{dd}. \tag{1.2.1}$$

The first two terms are due to the Coulomb interaction, which has a direct and an exchange part. The Coulomb interaction is quite strong and causes the binding of two atoms in the stable hydrogen molecule. The last term is the magnetic dipole-dipole interaction between different atoms.

A pair of hydrogen atoms in zero field will be either in the singlet or in the triplet state. In the presence of a magnetic field the singlet or triplet character is found by calculating $\frac{1}{2}\langle S^2\rangle$, which is 1 for pure triplet, and 0 for a pure singlet state. The interatomic potentials of hydrogen in its electronic ground state, shown in Fig. 1.2.1, were calculated in detail by Kolos and Wolniewicz.[2,3] The singlet potential supports many bound states and is associated with the large dissociation energy of the hydrogen molecule, $\epsilon_{diss}/k_B \approx$ 52000K.[4] In contrast the triplet potential has only a very shallow minimum and no bound states at all. This potential is weaker than other interatomic potentials, as can be seen in Fig. 1.2.2, where it is compared with the He-He interatomic potential. The absence of bound states for the triplet potential leads to the possibility of stabilizing a gas of spin-polarized atomic hydrogen. The degree of polarization determines the amount of singlet interaction in the gas, and thus the stability against recombination through collisions. Note that two hydrogen atoms can only enter a bound state by transferring momentum to a third body, since recombination by radiative transitions are electric-dipole forbidden for the homonuclear diatomic molecule.[5] In experiments the third body may be another hydrogen atom, a helium atom or the surface of the experimental cell. A pair of atoms in the lowest (a) state has $\frac{1}{2}\langle S^2\rangle = \frac{3}{4} + \frac{1}{4}(2\sin^2\theta - 1)^2$, so the interacting pair will display

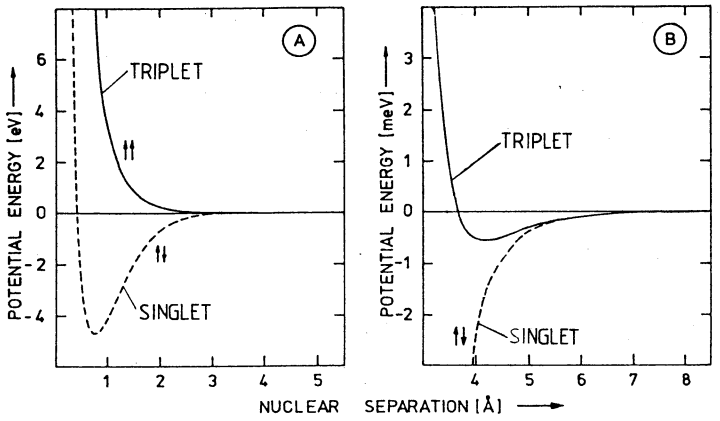

Figure 1.2.1: *The singlet and triplet interatomic potentials of hydrogen atoms. The weak attractive part of the triplet interaction can be seen in the second figure with the expanded vertical axis.*

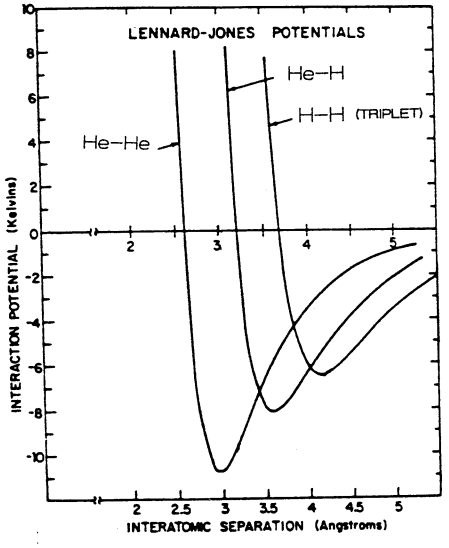

Figure 1.2.2: *The interatomic potentials of He-He, H-H (triplet) and H-He.*

some singlet character, which decreases with increasing field. A pair of b state atoms will have $\frac{1}{2}\langle S^2\rangle = 1$, so it will not form a bound state. Even though only the a and b states are populated in high magnetic field at low temperature in equilibrium, there remains a finite chance of singlet interaction, because of the admixture of electron spin-up in the a state. Similarly in a mixture of c and d states the c state has an admixture of the opposite spin. Only a gas polarized in a pure b or d state will show no singlet interaction at all.

The dipolar interaction can be written as

$$H_{dd} = \frac{\mu_0}{4\pi}\frac{\hbar^2}{2}\frac{1}{r_{ij}^3}\sum_{i,j}\{\gamma_e^2 f(s_i,s_j) - \gamma_e\gamma_n[f(s_i,i_j)+f(i_i,s_j)] + \gamma_n^2 f(i_i,i_j)\}, \qquad (1.2.2)$$

where γ_e and γ_n are the electron and proton gyromagnetic ratio respectively and

$$f(s_i,i_j) = [\vec{s_i}.\vec{i_j} - 3(\vec{s_i}.\hat{r}_{ij})(\vec{i_i}.\hat{r}_{ij})], \qquad (1.2.3)$$

and where r_{ij} is the distance between two spins labeled i and j and $\hat{r}_{ij}$ is a unit vector. In general, the term $f(i_i,i_j)$ is negligible.

1.3 Wall interaction

Apart from the interatomic interaction the atoms will also interact with the walls of the vessel in which they are kept. As can be seen in Fig. 1.2.2 the interaction between hydrogen and helium is quite weak, but stronger than the hydrogen-hydrogen triplet interaction. Mantz and Edwards[6] have calculated the adsorption potential for H on a surface of liquid helium-4 and found a single bound state. For many purposes this state can be separated into a one-dimensional bound state in the z-direction and a free particle motion in the x,y-plane. Recent experimental determinations of the binding energy ϵ_a on ^{4}He were compiled by Hardy *et al*,[7] leading to a best value of ϵ_a/k_B =1.00(5)K. Less accurate data for ^{3}He or ^{3}He-^{4}He mixtures[8,9] yield a binding energy of about 0.4K. The binding energy of any substance other than liquid helium is so high ($\epsilon_a/k_B > 35$K) that no low temperature experiments with atomic hydrogen can be carried out unless a l-helium film covers the walls of the cell. For moderate densities and temperatures of the order of the binding energy there is a simple relation between the bulk (n) and surface density (σ) in equilibrium

$$\sigma = n\Lambda\exp(\epsilon_a/k_BT), \qquad (1.3.1)$$

where $\Lambda = h/\sqrt{2\pi m k_B T}$ is the de Broglie wavelength. This relation holds until $\sigma \approx 10^{13}\text{cm}^{-2}$. The saturated surface coverage[10–12] is about 10^{14}cm^{-2}, as can be seen in Fig. 1.3.1. Recent calculations by Kagan *et al.*[13] show that the saturated coverage may be as high as $2\times10^{14}\text{cm}^{-2}$ due to degeneracy effects on the surface.

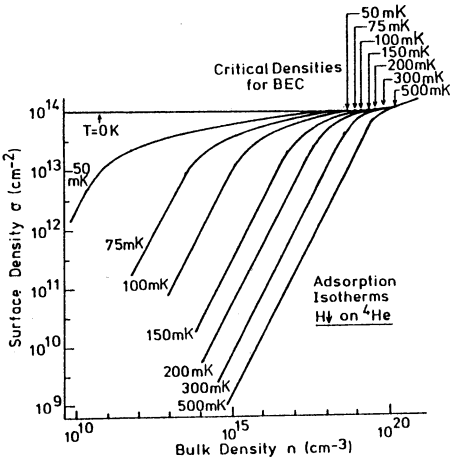

Figure 1.3.1: *Surface vs. bulk density in equilibrium for various temperatures. Note that at any temperature the surface becomes saturated before the critical density for BEC is reached.*

1.4 Statistics

The proton and the electron, both fermions, are tightly bound in the ground state of the atom. Any system with an even number of tightly bound fermions will form a composite boson, because the wave function of two of those composite particles is symmetric. The bosonic nature of the hydrogen atom has also been verified experimentally at low density.[14] Lhuillier and Laloë[15] showed that the indistinguishability of the particles leads to the so-called 'identical-spin rotation effect'. The spin-waves associated with this effect, also containing evidence for the boson-nature of H, were first observed by Johnson *et al.*[16] in a NMR experiment.

The interesting feature of atomic hydrogen compared to other atomic bosons is its extremely large quantum parameter. This causes atomic hydrogen to remain gaseous down to $T = 0$. As such it should be possible to observe quantum degeneracy in a nearly ideal gas.

The distribution function of a Bose gas is

$$N_i = \frac{g}{\exp[(\epsilon_i - \mu)/k_B T] - 1}, \tag{1.4.1}$$

where N_i is the population of state i, g the spin degeneracy, μ the chemical potential and ϵ_i the energy. We express μ in terms of the fugacity $z \equiv \exp(\mu/k_B T)$. If we leave out

the interaction entirely for a moment, the energy will be $\epsilon_i = p_i^2/2m$. The density in a volume V can be found by summation of N_i over all states and $n \equiv N/V$. Converting the summation into an integration over p and separating out the $p = 0$ term, we get after integration

$$n = \frac{N_0}{V} + \frac{g}{\Lambda^3} g_{3/2}(z), \tag{1.4.2}$$

where $g_{3/2}$ is the function

$$g_n(z) = \sum_{l=0}^{\infty} \frac{z^l}{l^n}. \tag{1.4.3}$$

The chemical potential μ is always negative or zero. If μ goes to zero z approaches 1 and the $g_{3/2}$-function goes to a limiting value of $g_{3/2}(1) = 2.612$. This means the population of the ground state N_0 may become a macroscopic number at finite temperature. This population of the zero-momentum state is called Bose-Einstein condensation.[17] From eq. 1.4.2 we can see that N_0 will have to take on some finite value if

$$\frac{n^{2/3}}{T} \geq 11.9 \frac{m k_B}{h^2} g^{2/3}, \tag{1.4.4}$$

where we can take the degeneracy to be one. If we pretend that hydrogen has no interaction we can apply eq. 1.4.4 and find that

$$\left(\frac{n^{2/3}}{T}\right)_c = 6.25 \times 10^{13} \mathrm{cm}^{-2}\mathrm{K}^{-1}. \tag{1.4.5}$$

It is possible to generalize the statistics for various external potential fields.[18] Goldman *et al.*[19] and Bagnato *et al.*[20] have calculated the critical temperature of atomic hydrogen including the interatomic interaction. Assuming an s-wave scattering length[21] $a = 0.72$Å for a gas in a rigid container both authors find a decrease of the critical temperature by 5% for a gas with a density of approximately $2 \times 10^{18}\mathrm{cm}^{-3}$ and $T_c \approx 30$mK. This shows that atomic hydrogen can be treated fairly well as an ideal Bose gas.

1.5 Experiments with H↓

The first experiments with stabilized atomic hydrogen were done in Amsterdam by Silvera and Walraven.[22] They made atomic hydrogen by a discharge in molecular hydrogen gas in a microwave cavity at room temperature. The gas was fed into an experimental cell in a cryostat. The cell was at a temperature of about 0.3K and covered with a l-helium film, to avoid the build-up of high surface density (Section 1.3). The cell was situated in the bore of a magnet, and the experiment was carried out with fields up to 7T. The field attracts the high-field seekers, i.e. the atoms in states a and b (Section 1.1), whereas the c and d state atoms will be repelled. In equilibrium the product of the density of high-$(n_\downarrow)$

and low-field seekers ($n_\uparrow$) in the presence of a magnetic field gradient at a temperature T is given by

$$n_\downarrow(r)n_\uparrow(r) = n_{\downarrow,0}n_{\uparrow,0}\exp\left[\frac{-2\mu_B(B(r)-B_0)}{k_BT}\right], \tag{1.5.1}$$

where n_0 and B_0 are the density and magnetic field respectively at some reference point, and $B(r)$ is the field at point r. For $B(r) = 7$T, $B_0 = 0$, and $T = 0.3$K the exponential factor will be 3.8×10^{13}, so the high and low-field seekers will be almost totally separated. In the first experiments atomic hydrogen was detected by using bolometric detectors. These devices are operated by evaporating the helium film from their surface and measuring the heat subsequently deposited by atoms recombining on the surface.

After this many experiments have been carried out with atomic hydrogen at low temperature,[1] in magnetic fields ranging from 0 to 20T, using bolometric techniques, pressure transducers, NMR, ESR and other detection methods. A result important for the stability of the gas was the achievement of doubly polarized atomic hydrogen (H$\downarrow\downarrow$), since a gas consisting of only b-state atoms is stable against two-body recombination through singlet interaction. As Statt and Berlinsky[23] pointed out, a mixture of a and b state atoms should polarize spontaneously to a pure b state by preferential recombination of a state atoms. Double polarization was first established experimentally by Cline *et al.*,[24] who succeeded in suppressing relaxation induced by magnetic impurities in cell walls,[25] which had frustrated earlier attempts to make doubly polarized hydrogen.[8]

After this result it seemed that the degenerate regime could be reached by increasing the density of the doubly polarized gas. The highest densities were achieved in so-called compression experiments, in which atomic hydrogen gas is compressed in a bubble of liquid helium. The density can be increased by orders of magnitude in this way. Several groups have performed such experiments,[26–29] but were confronted with a three-body recombination process, predicted by Kagan *et al.*[30] Since this process increases with the third power of the density, it forms a major barrier for reaching high densities. Calculations of the three-body recombination rate have been refined and extended to higher fields by the Eindhoven theory group of B.J. Verhaar.[31–34] The highest density reported in a compression experiment was 7×10^{18}cm^{-3} at a temperature of about 0.6K.[28] The critical temperature for this density is 43mK. However, lowering the temperature leads to an increase of the surface density and therefore to increasing surface recombination. Removing the heat of the recombining particles is also a major difficulty because of the Kapitza resistance at the hydrogen-helium interface. Only a strong decrease of the three-body recombination rates in fields higher than used so far seems to offer the possibility of a better result through compression techniques. There are attempts planned to reach BEC in high fields,[35] though the theoretical prediction for recombination in fields higher than 20T are not favorable.[34]

1.6 Alternatives

The strong interaction of hydrogen atoms with helium surfaces appears to be the crucial factor that prohibits the gas to enter the degenerate regime. It can be shown[1] that in equilibrium one does not expect BEC before all surface states have been occupied. This can also be seen in Fig. 1.3.1, where the line of critical density meets the line of saturated surface density. However, the saturated surface density is such that surface recombination is extremely high. Apart from using higher magnetic fields several ways to overcome this difficulty have been suggested.

Kagan *et al.*[36] have proposed to employ a needle with which a local, high magnetic or electric field may be created, where the density could be highly increased, while the 'hot' atoms and molecules produced by recombination would escape without heating the rest of the gas in the high density region. If the recombination loss is compensated by atoms from a large reservoir of low density surrounding the needle, the density could be increased and become sufficient for BEC to occur.

Other approaches are aimed at avoiding the surface altogether. There are several ways to trap neutral atoms, all based on the forces of the electromagnetic field in various manifestations. A light beam tuned near resonance can exert a considerable force on a particle.[37] For some time this technique has been applied for slowing beams of Na-atoms. Raab *et al.*[38] used radiation pressure to trap atoms at a density of 2×10^{11}at cm^{-3} with a lifetime of 2 minutes. A non-resonant technique was proposed by Lovelace *et al.*,[39] namely using an alternating magnetic field with a parabolic field profile to trap atoms who possess a magnetic moment. This method has not been applied experimentally yet. Silvera and Agosta[40] have pointed out a possibility for resonant trapping of atomic hydrogen.

Kügler *et al.*[41] were the first to trap neutral particles, very slow neutrons, in a magnetic storage ring. The first report of trapped neutral atoms was made by Migdall *et al.*,[42] who employed laser light to slow down a beam of sodium atoms, along with trapping in a static 'spheroidal quadrupole' field created by two solenoids in opposition. A 'spheroidal quadrupole' or anti-Helmholtz configuration of magnets creates a field zero at the center of symmetry between the solenoids, while the absolute value of the field increases in all directions around the center. Atoms with a suitable magnetic moment, i.e. such that their energy increases with magnetic field, can be confined in this field. In Migdall's case[42] Na-atoms in the $^3S_{1/2}, m_F = 2$ state, which have a magnetic moment of approximately one Bohr magneton, were trapped.

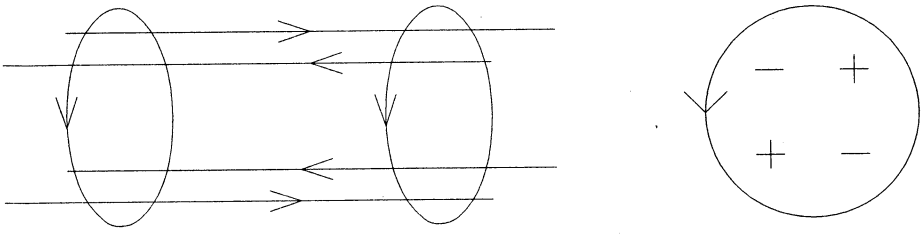

Figure 1.7.1: *Schematic drawing of the currents for a non-zero minimum B-field trap, side-view and top-view. The arrangement of the four parallel conductors is also known as the Joffe-bar geometry.*

1.7 Trapping of H↑

As discussed in Section 1.1 atomic hydrogen atoms can be divided in two species: the atoms in the c or d state (H↑), who will tend to move to low field in a magnetic field gradient (low-field seekers), and those in the a or b state (H↓), which will experience a force in the opposite direction (high-field seekers). Unfortunately the Maxwell equations do not allow the creation of a static magnetic field maximum in free space.[43] Therefore a static trap can only be made for H↑, which is susceptible to relaxation to the a or b state. The simplest way to build such a trap is the anti-Helmholtz geometry mentioned in the previous paragraph. However, in the neighborhood of zero-field so-called Majorana transitions may occur. These transitions happen if the frequency experienced by an atom moving in a region where the direction of the field varies rapidly, is equal to or higher than the frequency of the Zeeman splitting. At low temperature the atoms will be near the minimum, so the frequency of the splitting will be very low and even small fluctuations in the field will be sufficient to induce transitions. For this reason a H↑ trap will preferably be constructed in such a way that the magnetic field minimum has some finite value. An arrangement for a trap with these properties was proposed by Pritchard[44] for confining sodium atoms. A quadrupole field, made by four parallel conductors, would confine the atoms in the plane perpendicular to the conductors. For confinement in the third direction (the z-axis) an ordinary parabolic field, created by two solenoids, may be used. The set-up is drawn schematically in Fig. 1.7.1. Hess[45] suggested that this set-up should be used to confine hydrogen.

In the case of hydrogen we envisioned that filling of the magnetic trap may be done in a very straightforward way. In contrast to sodium traps, we aimed at filling the trap by letting atoms thermalize with the physical cell walls. Crucial for this is the value of the well depth. In a magnetic trap the well depth (ϵ_{tr}) is the difference in potential energy

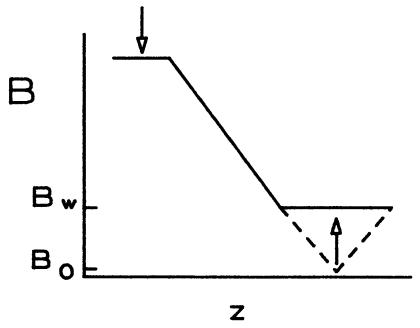

Figure 1.7.2: *Schematic diagram of the magnetic field profile of the trapping field in our experimental set-up. The solid line is the field at the wall, which has a minimal value B_w, the dashed line is the field along the axis of the cell. B_0 is the field in the trap minimum.*

between the minimum of the trap, where $B = B_0$, and the lowest field anywhere on the surrounding walls B_w, $\epsilon_{tr} = \mu_B(B_w - B_0)$. The relation eq. 1.3.1 which normally governs the ratio between bulk and surface density is then modified to

$$\sigma = n_0 \Lambda \exp[(\epsilon_a - \epsilon_{tr})/k_B T], \tag{1.7.1}$$

where n_0 is the density in the trap minimum. If $\epsilon_{tr} \gtrsim \epsilon_a$ the gas can come into thermal equilibrium with the walls without an increase in σ, so surface adsorption will no longer dominate at low temperatures.

A schematic drawing of the set-up of the experiment to evaluate this method of filling is shown in Fig. 1.7.2. The trap itself is the dip in the dashed line of the magnetic field, with the field at the wall indicated by the solid line. In the trapping region the field at the wall has the value B_w. To the left in Fig. 1.7.2 there is a region of high field with $B \gg B_w$. The reason for this is that we want to separate H$\uparrow$ and H$\downarrow$ rigorously, just as was done in experiments with H$\downarrow$, to avoid recombination through the singlet interaction. If a source of hydrogen atoms of both species is situated in the high-field region, H$\uparrow$ will move to the trap and thermalize there by interaction with the walls. Recombination will be determined by the overlap in the H$\uparrow$ and H$\downarrow$ densities, given by eq. 1.5.1.

After relaxation of trapped H$\uparrow$ to the high-field-seeking state the atoms will be pulled back into the high-field region, and most of these will reach a detector situated there. The probability that a relaxed atom goes to the detector is high because of the large opening cross-section of the detector compared to the opening of the dissociator. Thus the signal we detect will be proportional to the flux of atoms leaving the trap after relaxation, and not to the number of trapped atoms. A detailed description of the apparatus will be given

in Chapter 2.

The trapping fields are highly inhomogeneous in nature and therefore it will prove to be useful for the analysis to relate the total number of atoms N, pairs (N_2), triples (N_3) etc. to the density of atoms n_0, pairs $n_{2,0}$, triples $n_{3,0}$ etc. in the center of the trap. The effective volume V_{me} is defined by

$$V_{me} = \frac{N_m}{n_{m,0}} = \int_V \exp\left(\frac{-m\mu_B(B(\vec{r}) - B_0)}{k_B T}\right) \mathrm{d}\vec{r}, \tag{1.7.2}$$

where $B(\vec{r})$ is the field at any point. A small effective volume V_{me} results in higher central density n_0 for a given filling flux Φ, since for any m-th order loss process G_m, defined by

$$\dot{n} = -G_m n^m, \tag{1.7.3}$$

and averaged over the entire trapping region, the central density in steady state will be

$$n_0 = \left(\frac{\Phi}{G_m V_{me}}\right)^{1/m}. \tag{1.7.4}$$

If V_{me} varies strongly with temperature, this means the field B experienced by the atoms will also change with temperature.

1.8 Relaxation of H↑

The important decay mechanisms for trapped H↑ were calculated in detail by the Eindhoven theory group of B.J. Verhaar,[46] after a first publication made in collaboration with A. Lagendijk and I.F. Silvera.[47] Binary collisions lead to relaxation of atoms in the c and d states to the a or b state. Spin-exchange is the most efficient process in low field, but in the s-wave scattering regime it only occurs if two atoms in the c state collide. Other collisions between low-field seekers, i.e. cd and dd collisions, can lead to relaxation through magnetic dipolar interaction. The calculation of the rates is done by a coupled-channels method,[48] using the Kolos and Wolniewicz interatomic potentials,[2] and including the electron-electron and electron-proton magnetic dipole interaction (Sect.1.2)and the interatomic and intra-atomic (H_{hyp}) hyperfine interaction, already mentioned in eq.1.1.1.

The results of the calculations are plotted in Fig. 1.8.1 as event rates at $T = 0$K as a function of magnetic field. Clearly in low field the spin-exchange rate is considerably higher than the dipolar relaxation rate. The spontaneous polarization of the gas into the d state ensuing from this will be discussed in Chapter 3. The consequences of the strong field dependence of the rates for the comparison with experiment will also be discussed there. Note that the relaxation rates remain finite at zero temperature for all possible compositions (c and d) of a gas of low-field-seeking atomic hydrogen.

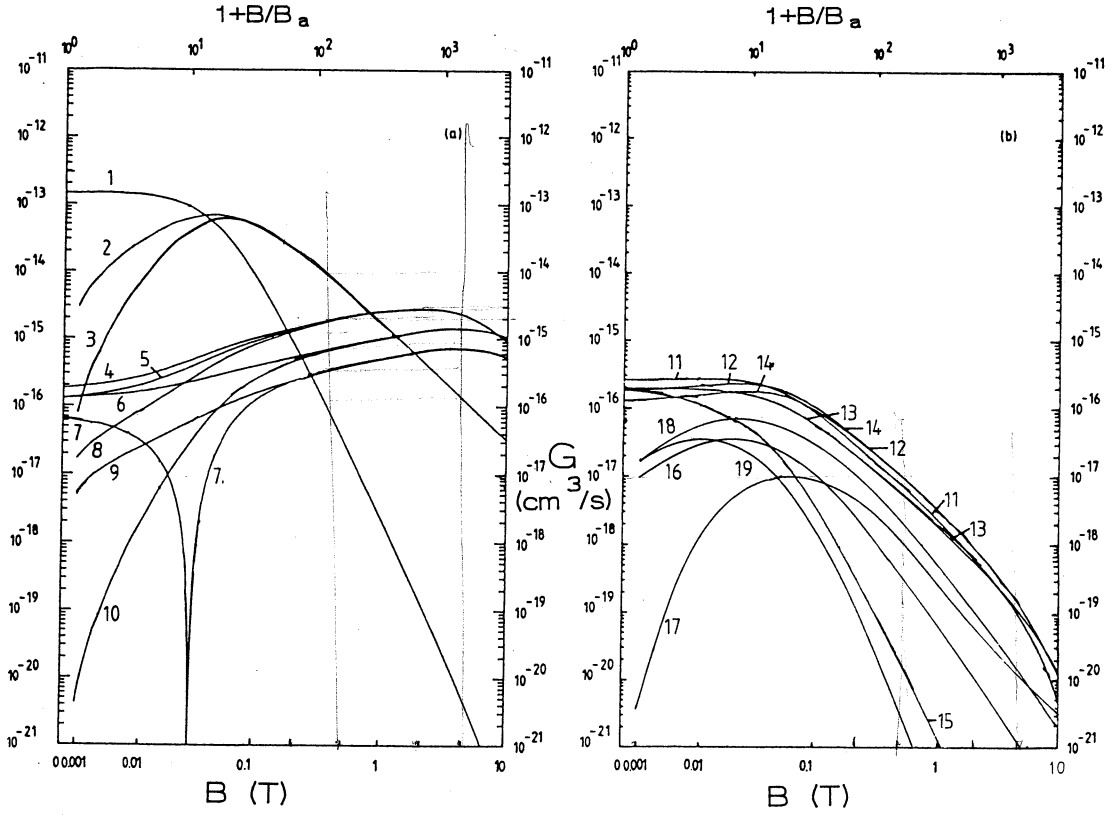

Figure 1.8.1: *The spin-exchange and dipolar relaxation event rates as a function of magnetic field calculated by the coupled-channels approach (after Stoof et al.[46]). The horizontal scale shows a gradual transition from a linear to a logarithmic scale as we plot* $1+B/B_a$ *logarithmically. Here* $B_a = a/16\mu_B = 3.17 \times 10^{-3}T$. *The curves correspond to the following rates:* $(1) : cc \rightarrow aa, (2) : cc \rightarrow bd, (3) : cc \rightarrow ac, (4) : dd \rightarrow aa, (5) : cd \rightarrow ab, (6) : dd \rightarrow ad, (7) : cd \rightarrow ac, (8) : cc \rightarrow bb, (9) : cd \rightarrow bd, (10) : cc \rightarrow bc, (11) : dd \rightarrow ac, (12) : cd \rightarrow aa, (13) : cd \rightarrow ad, (14) : cc \rightarrow ab, (15) : cc \rightarrow ad, (16) : dd \rightarrow cd, (17) : cd \rightarrow cc, (18) : cd \rightarrow bc, (19) : dd \rightarrow cc.$

A much simpler expression for the spin-exchange rate can found by expressing the rate constants in terms of the spin-exchange T-matrix elements.[46,49] The so-called degenerate-internal-state approximation was applied by Koelman *et al.*[49] for vanishing kinetic energy in the incoming channel ($T = 0$), but can be extended to $T \neq 0$.[46] This approach proves to be very accurate if the splitting of the internal energy levels is not to large, i.e. in low field, especially if a suitable choice is made for the energy in the in- and out-going channel. It turns out that taking half of the energy difference between initial and final state gives an optimum result.[46]

We will now calculate event rates on the basis of this approximation, following the notation of Ref. 1. The total number of scattering events per unit volume is

$$\frac{\Gamma}{V} = \frac{1}{2} n^2 \sum_{h_1,h_2} \hat{h}_1 \hat{h}_2 \Gamma_{h_1 h_2}, \tag{1.8.1}$$

where $\hat{h}_i$ is the fractional density of atoms in hyperfine state h_i. In terms of in-and outgoing states $\Gamma_{h_1 h_2}$ is

$$\Gamma_{h_1 h_2} = \frac{1}{2} \sum_{h_3,h_4} \Gamma_{h_1 h_2 \rightarrow h_3 h_4} \tag{1.8.2}$$

The rate of inelastic collisions ($h_1 h_2 \neq h_3 h_4$, with $h_3 h_4$ the outgoing states) is

$$\Gamma_{h_1 h_2 \rightarrow h_3 h_4} \equiv \bar{v} \bar{\sigma}_{h_1 h_2 \rightarrow h_3 h_4}, \tag{1.8.3}$$

where it is expressed in terms of the inelastic cross section σ and the relative velocity v. The cross section is

$$\sigma_{h_1 h_2 \rightarrow h_3 h_4}(k, k') = \left(\frac{1}{4\pi}\right)^3 \left(\frac{2\mu}{\hbar^2}\right)^2 \int \mathrm{d}\hat{k} \int \mathrm{d}\hat{k}' |\langle h_3 h_4 \vec{k}' | T | h_1 h_2 \vec{k} \rangle|^2. \tag{1.8.4}$$

Here μ is the reduced mass of the scattering pair, $\vec{k}$ and $\vec{k}'$ are the initial and final k-vectors and $\hat{k}$ denotes a unit vector. To calculate the dipolar relaxation rate in the Distorted Wave Born Approximation the T matrix is given by the electronic part of the dipolar interaction V_{dd} as given in section 1.2,

$$V_{dd} = \frac{\mu_0 \hbar}{4\pi} \frac{1}{r^3} \gamma_e^2 f(s_1, s_2), \tag{1.8.5}$$

where the function $f(s_1, s_2)$ is

$$\begin{aligned}
f(s_1, s_2) &= \sum_{m=-2}^{+2} \left(\frac{4\pi}{5}\right)^{1/2} T_2^m Y_2^{m*}(\hat{r}), \\
T_2^0 &\equiv \left(\frac{3}{2}\right)^{1/2} [s_{1,z} s_{2,z} - \frac{1}{4}(s_{1,+} s_{2,-} + s_{1,-} s_{2,+})] \\
T_2^{\pm 1} &\equiv \mp \left(\frac{3}{2}\right)^{1/2} (s_{1,\pm} s_{2,z} + s_{1,z} s_{2,\pm}) \\
T_2^{\pm 2} &\equiv \left(\frac{3}{2}\right)^{1/2} s_{1,\pm} s_{2,\pm}.
\end{aligned} \tag{1.8.6}$$

The spherical harmonics Y_2^{m*} describe the angular dependence. The cross section σ can be separated into a part depending on the momenta, i.e. on k, and a part depending on the projection of the states on the total spin basis $|SM_S IM_I\rangle$ of the two atom system. In the following we will treat the particles as distinguishable, which means we sum over nonsymmetrized states $|i)$. The relation between symmetrized and unsymmetrized states is[1]

$$|i\rangle = \frac{1}{2}\sqrt{2}[|i) + |-i)]. \tag{1.8.7}$$

One may show[50]

$$\sigma_{h_1h_2\to h_3h_4}(k,k') = \frac{24\pi}{5}a_{ee}^2|(h_3h_4|T_2^m|h_1h_2)|^2\left(\frac{k'}{k}\right)\left(\frac{2}{27}\right), \tag{1.8.8}$$

where a_{ee} is the electronic dipolar length scale,

$$a_{ee} \equiv \left(\frac{2\mu\mu_0}{4\pi}\right)\gamma_e^2. \tag{1.8.9}$$

Note that the velocity v in eq. 1.8.3 will be cancelled by k in the denominator in σ. It signifies the fact, already mentioned above, that the relaxation rate becomes independent of temperature for $T \to 0$. Furthermore we replace k' with the velocity in the final state

$$v_f = (2\Delta/\mu)^{1/2}, \tag{1.8.10}$$

where Δ is the energy difference between initial and final state

$$\Delta = E_{h_1} + E_{h_2} - E_{h_3} - E_{h_4}. \tag{1.8.11}$$

We can now write down expressions for the dipolar rates as a function of field for $T = 0$. The event rate becomes

$$\Gamma_{h_1h_2\to h_3h_4} = \left(\frac{16\pi}{45}\right)a_{ee}^2|(h_3h_4|T_2^m|h_1h_2)|^2 v_f. \tag{1.8.12}$$

The matrix elements are given in Ref. 1, and can be expressed as a function of magnetic field in terms of the angle θ of eq. 1.1.3

$$\begin{aligned} |(aa|T_2^{-2}|dd)|^2 &= \frac{3}{4}\cos^4\theta \\ |(ac|T_2^{-2}|dd)|^2 &= \frac{3}{2}\sin^2\theta\cos^2\theta \\ |(ad|T_2^{-1}|dd)|^2 &= \frac{3}{8}\cos^2\theta. \end{aligned} \tag{1.8.13}$$

Here we have only given the elements for those processes that do not vanish at $B = 0$. Transitions from the d state to the c or b state have $\Gamma = 0$ because $v_f \to 0$ as $B \to 0$, as can be inferred from eq. 1.1.2. For the transitions of eq. 1.8.13 we have $v_f \to \sqrt{2a/\mu}$ for $dd \to ac$ and $dd \to ad$ or $v_f \to \sqrt{4a/\mu}$ for $dd \to aa$ for $B \to 0$.

For low field ($B \leq 0.1$T) the results of the simplified calculation and the exact results from the coupled channels equation shown in Fig. 1.8.1 agree within a few percent. We return to this approximation in Chapter 3.

1.9 Thermalization in a trap

Thermalization of the particles in a trap is a non-trivial problem. A single particle entering a trapping field will simply move back and forth across the trap and never become trapped. Particles can only be trapped by applying another, non-conservative external force or by inter-particle collisions that redistribute energy. For the filling of our trap, we depend completely on the latter mechanism. Also, the collisions are essential for establishing thermal equilibrium in the gas, whatever the cooling mechanism.

As an example we calculate the energy redistributed per two-particle collision for the case of s-wave scattering, which is dominant at low energy. In the trap the initial situation is that all particles entering the trapping field have roughly the same energy and are coming in from all angles because of multiple wall collisions. Therefore we calculate the case of particles incoming with identical energy, averaged over all angles of incidence. This resembles quite closely the initial conditions for filling the trap.

The center-of-mass velocity of the particles is $\vec{V} = (\vec{v}_1 + \vec{v}_2)/2$, the relative velocity is $\vec{v} = \vec{v}_1 - \vec{v}_2$. The difference in kinetic energy of one particle before (E_i) and after (E_f) collision is

$$E_i - E_f = \frac{1}{2} m \vec{V}.(\vec{v}_i - \vec{v}_f), \tag{1.9.1}$$

where the $\vec{v}$'s are relative velocities and m is the mass of an atom. For particles with initially identical absolute velocity $|v_1| = |v_2|$ the product of center-of-mass velocity and relative velocity vanishes, so the energy difference in eq. 1.9.1 becomes $-(1/2)m\vec{V}.\vec{v}_f$. The probability of an angle β between $\vec{V}$ and $\vec{v}_f$ is equal for all β because of the s-wave scattering. Now we can calculate the average of the squared energy difference

$$\begin{aligned} \overline{(E_i - E_f)^2} &= \overline{(\frac{1}{2} m |\vec{V}||\vec{v}_f| \cos\beta)^2} \\ &= (\frac{1}{4} m^2 \overline{|\vec{V}|^2 |\vec{v}_f|^2}) \int_0^{\pi/2} \frac{2}{\pi} \cos^2\beta \mathrm{d}\beta \\ &= \frac{1}{2}(\frac{1}{4} m^2 \overline{|\vec{V}|^2 |\vec{v}_f|^2}). \end{aligned} \tag{1.9.2}$$

The product $\overline{|\vec{V}||\vec{v}_f|}$ is found by averaging over the angle α between the velocities of the incoming particles and can be expressed in terms of the initial velocity v_1

$$\begin{aligned} |\vec{V}| &= \frac{1}{2}|\vec{v}_1 + \vec{v}_2| = |\vec{v}_1| \cos(\alpha/2) \\ |\vec{v}_f| &= |\vec{v}_i| = 2|\vec{v}_1| \sin(\alpha/2). \end{aligned} \tag{1.9.3}$$

We assume that the incoming particles are distributed homogeneously over all angles α, so

$$\begin{aligned} \overline{|\vec{V}|^2 |\vec{v}_f|^2} &= v_1^4 \int_0^{\pi} \frac{1}{\pi} \sin^2\alpha \mathrm{d}\alpha \\ &= \frac{1}{2} v_1^4, \end{aligned} \tag{1.9.4}$$

and we find

$$\overline{(E_i - E_f)^2} = \frac{1}{4}(\frac{1}{2}mv_1^2)^2. \tag{1.9.5}$$

Expressed in terms of k_BT the root of this squared difference is $(3/4)(k_BT)$, to be compared with the root mean square of the energy difference between particles in a Maxwell-Boltzmann distribution $(3/2)^{1/2}(k_BT)$. From these numbers it seems reasonable to assume that the energy distribution in the gas will resemble that of a gas in internal thermal equilibrium after a few collisions.

1.10 Low Temperature Limit

Now we consider the number of elastic collisions in the gas in relation to the inelastic collisions that result in relaxation, e.g. loss of atoms. We will see that this imposes a fundamental limit on the temperature that can be established in a trapped gas.

The dominant elastic scattering process in low temperature H↑ is s-wave triplet potential scattering, which is proportional to the square root of the temperature. The event rate for elastic collisions per particle Γ_{th} is

$$\Gamma_{th} = (1/2)n\bar{v}\bar{\sigma} \approx 4n\pi a^2(8k_BT/\pi\mu)^{1/2}, \tag{1.10.1}$$

where a is the s-wave scattering length[21] and μ is the reduced mass. Since the inelastic scattering approaches a constant, finite value at zero temperature, as was noted above, there will be a temperature at which the life-time of the gas becomes comparable to the thermalization time-constant, and the gas, as an interacting system, can not be cooled below this temperature. We make an estimate of the temperature at which the inelastic and elastic collisions become comparable. The event rate for inelastic collisions per particle is $\Gamma_{inel} = n\Gamma_{h_1h_2\to h_3h_4}$, after eq. 1.8.12. The ratio of elastic and inelastic collisions in low field and at low temperature is, summing the relevant decay channels in eq. 1.8.13,

$$\frac{\Gamma_{th}}{\Gamma_{inel}} = \frac{45a^2(8k_BT/\pi\mu)^{1/2}}{a_{ee}^2\sum_{h_3,h_4}|(h_3h_4|T_2^m|dd)|^2v_f}. \tag{1.10.2}$$

In zero field this ratio is $4.6 \times 10^4\sqrt{T}$, with T in kelvin, and we see that at $T = 1\mu$K there will be approximately 46 elastic scattering events for every inelastic event. This temperature will therefore be a lower limit for cooling of atomic hydrogen in a magnetic trap, as was already noted by Koelman.[51] This limits the achievement of BEC to temperatures above this minimum, and consequently to samples of rather high density and short life-time.

In the following we first give detailed information on the apparatus used in the experiment (Chapter 2), then we will discuss the expected behavior of the gas on the basis of the theoretical predictions already mentioned[47,46] (Chapter 3), and finally the experimental results and some consequences for future experiments (Chapters 4 and 5) are discussed.

References

[1]I.F. Silvera, and J.T.M. Walraven, Prog. Low Temp. Phys. **X**, 139 (1986).

[2]W. Kolos, and L. Wolniewicz, Chem. Phys. Lett. **24**, 457 (1974).

[3]W. Kolos, and L. Wolniewicz, J. Mol. Spectrosc. **54**, 303 (1975).

[4]G. Herzberg, J. Mol. Spectrosc. **33**, 147 (1970).

[5]J.T. Jones Jr., M.H. Johnson, H.L. Meyer, S. Katz, and R.S. Wright, publication U-216 (Aeronutronic Systems Inc., a subsidiary of Ford Motor Company, 1958).

[6]I.B. Mantz, and D.O. Edwards, Phys. Rev. B **20**, 4518 (1979).

[7]W.N. Hardy, M.D. Hürlimann, and R.W. Cline, Jap. J. Appl. Phys. **26**, 2065 (1987).

[8]G.H. van Yperen, A.P.M. Matthey, J.T.M. Walraven, and I.F. Silvera, Phys. Rev. Lett. **47**, 800 (1981)

[9]R. Jochemsen, M. Morrow, A.J. Berlinsky, and W.N. Hardy, Phys. Rev. Lett. **47**, 852 (1981).

[10]I.F. Silvera, and V.V. Goldman, Phys. Rev. Lett. **45**, 915 (1980).

[11]V.V. Goldman, and I.F. Silvera, Physica B **107**, 515 (1981).

[12]D.O. Edwards, and I.B. Mantz, J. Phys. (France) **41**, C7-257 (1980).

[13]Y. Kagan, N.A. Glukhov, B.V. Svistunov, and G.V. Shlyapnikov (1988), to be published.

[14]A. Lagendijk, G.H. van Yperen, and J.T.M. Walraven, J. Phys. Lett. (France) **45**, 929 (1984).

[15]C. Lhuillier, and F. Laloë, J. Phys. (France) **43**, 197 (1982); C. Lhuillier, and F. Laloë, J. Phys. (France) **43**, 225 (1982).

[16]B.R. Johnson, J.S. Denker, N. Bigelow, L.P. Levy, J.H. Freed, and D.M. Lee, Phys. Rev. Lett. **52**, 1508 (1984).

[17]A. Einstein, Preuss. Akad. der Wiss. Sitzungsber. **3**, 18 (1925).

[18]S.R. de Groot, G.J. Hooyman, and C.A. ten Seldam, Proc. Roy. Soc. A **203**, 266 (1950).

[19]V.V. Goldman, I.F. Silvera, and A.J. Legget,Phys. Rev. B **24**, 2870 (1981).

[20]V. Bagnato, D.E. Pritchard, and D. Kleppner, Phys. Rev. A **35**, 4354 (1987).

[21]D.G. Friend, and R.D. Etters, J. Low Temp. Phys. **39**, 409 (1980).

[22]I.F. Silvera, and J.T.M. Walraven, Phys. Rev. Lett. **44**, 164 (1980).

[23]B.W. Statt, and A.J. Berlinsky, Phys. Rev. Lett. **45**, 2105 (1980).

[24]R.W. Cline, T.J. Greytak, and D. Kleppner, Phys. Rev. Lett. **47**, 1195 (1981).

[25]B.W. Statt, A.J. Berlinsky, and W.N. Hardy, Phys. Rev. B **31**, 3169 (1985)

[26]R. Sprik, J.T.M. Walraven, and I.F. Silvera, Phys. Rev. B **32**, 5668 (1985).

[27]D.A. Bell, H.F. Hess, G.P. Kochanski, S. Buchman, L. Pollack, Y.M. Xiao, D. Kleppner, and T.J. Greytak, Phys. Rev. B **34**, 7670 (1986).

[28]T. Tommila, E. Tjukanov, M. Krusius, and S. Jaakkola, Phys. Rev. B **36**, 6837 (1987).

[29]J.D. Gillaspy, I.F. Silvera and J.S. Brooks, Phys. Rev. B **38**, 9231 (1988).

[30]Y. Kagan, I.A. Vartanyants, and G.V. Shlyapnikov, Sov. Phys. JETP **54**, 590 (1981).

[31]L.P.H. de Goey, T.H.M. v.d. Berg, N. Mulders H.T.C. Stoof, B.J. Verhaar, and W. Glöckle, Phys. Rev. B **34**, 6183 (1986).

[32]L.P.H. de Goey, H.T.C. Stoof, J.V.M.A. Koelman, B.J. Verhaar, and J.T.M. Walraven, Phys. Rev. B **38**, 11500 (1988).

[33]L.P.H. de Goey, thesis, unpublished, Eindhoven (1988).

[34]H.T.C. Stoof, L.P.H. de Goey, B.J. Verhaar, and W. Glöckle, Jap. J. Appl. Phys. **26**, 251 (1986); H.T.C. Stoof, L.P.H. de Goey, B.J. Verhaar, and W. Glöckle, Phys. Rev. B **38**, 11221 (1988).

[35]J.D. Gillaspy, thesis, unpublished, Cambridge (MA) (1988).

[36]Y. Kagan, and G.V. Shlyapnikov, Phys. Lett. **130**, 483 (1988).

[37]J.P. Gordon, and A. Ashkin, Phys. Rev. A **21**, 1606 (1980)

[38]E.L. Raab, M. Prentiss, A. Cable, S. Chu, and D.E. Pritchard, Phys. Rev. Lett. **59**, 2631 (1987)

[39]R.V.E. Lovelace, C. Mehanian, T.J. Tommila, and D.M. Lee, Nature **318**, 30 (1985)

[40]I.F. Silvera, and C.C. Agosta, Proc. of the Third Int. Conf. on Spin-Polarized Quantum Systems, Torino, 1988.

[41]K.J. Kügler, W. Paul, and U. Trinks, Phys. Lett. **72B**, 422 (1978).

[42]A.L. Migdall, J.V. Prodan, W.D. Phillips, T.H. Bergeman, and H.J. Metcalf, Phys. Rev. Lett. **54**, 2596 (1985)

[43]W.H. Wing, Prog. Quantum Electron. **8**, 181 (1984).

[44]D.E. Pritchard, Phys. Rev. Lett. **51**, 1336 (1983).

[45]H.F. Hess, Phys. Rev. B **34**, 3476 (1986)

[46]H.T.C. Stoof, J.M.V.A. Koelman, and B.J. Verhaar, Phys. Rev. B **38**, 4688 (1988) and private communication.

[47]A. Lagendijk, I.F. Silvera, and B.J. Verhaar,Phys. Rev. B **33**, 626 (1986)

[48]R.M.C. Ahn, J.P.W.H. van den Eijnde, and B.J. Verhaar, Phys. Rev. B **27**, 5424 (1983)

[49]J.M.V.A. Koelman, H.T.C. Stoof, B.J. Verhaar, and J.T.M. Walraven, Phys. Rev. Lett. **59**, 676 (1987).

[50]J.P.H.W. van den Eijnde, C.J. Reuver, and B.J. Verhaar, Phys. Rev. B **28**, 6309 (1983).

[51]J.M.V.A. Koelman, thesis, Eindhoven (1988).

Chapter 2

Apparatus

2.1 The trapping magnet

The field that we use to trap hydrogen in our experiment is generated by combining a quadrupole field for radial confinement with a parabolic field for confinement along the z-axis. The application of a *non-zero* minimum B field geometry to trap neutral atoms was suggested in the literature by Pritchard.[1] A similar configuration is used by Hess.[2] Adjacent to the trap we include a region of high field ($B \approx 4.5$T), for production and detection of H$\uparrow$. The whole assembly is made to fit in a 138mm diameter, 278mm long stainless steel vacuum can, the same size of the magnet container used by Van Yperen *et al.*[3] in our cryostat. Hence no major changes had to be made to use the trap.

The quadrupole field is generated by four racetrack-shaped coils of the type shown in Fig. 2.1.1. The straight part of the racetracks is 150mm long, the wires are packed in a 10×10mm bundle. The inner distance between the inside and outside leg is 25mm. The coils are wound of copper-clad multifilament NbTi superconducting wire (Vacuumschmelze

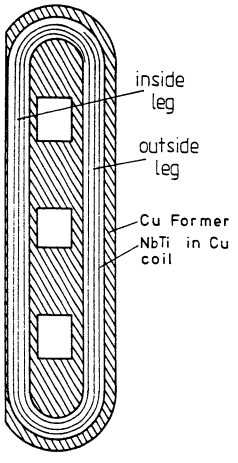

Figure 2.1.1: *A racetrack coil.*

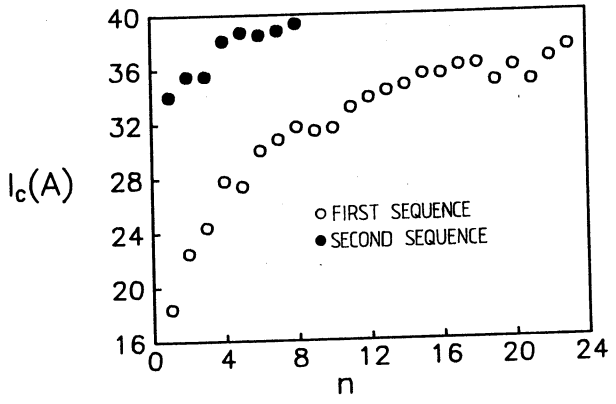

Figure 2.1.2: *Critical current of subsequent quenches in two cycles.*

F54, 0.2mm) on closed copper formers. During winding the wires are degreased with isopropyl alcohol (2-propanol) and the tension along the wires is kept at about 10N. Whenever possible we use copper in the construction of the magnets to avoid the creation of stresses by differences in thermal contraction. The formers act both as support for the wires and as a mold for impregnation with epoxy. The coils are vacuum-impregnated after winding with Stycast 1266 epoxy and cured at 60^{0}C under atmospheric pressure. Post-curing of the epoxy at 90^{0}C for two hours proved to be essential for high critical current. From a point of view of mechanical strength impregnating with Stycast 2850 GT is expected to be superior. This epoxy is unfortunately not suited for vacuum impregnation. We prefer impregnation *after* winding to assure optimum control over the winding process. Without entering into detail we note that the viscosity of the epoxy required a very careful impregnation procedure to render complete impregnation of the coils. In spite of a suggestion by Smith *et al.*[4] we decided to use epoxy for impregnation instead of a 'low strength' material such as wax, because on one side the former was left open to be fitted into a stainless steel yoke that accepts the four racetracks. We argued that epoxy would be less susceptible to degradation than wax when removing part of the mold to replace it with the yoke. Conceivable cavities between the impregnated wires and the yoke are filled with vacuum grease, to minimize the chances for motion of the wires.

To reach the design values for the fields the racetracks had to be trained by repetitive quenching (typically 25 times), in some cases doubling the initial critical current. There seems to be no unique cause of the 'training' problem of superconducting magnets, especially in non-solenoidal coils,[5] though it is thought training is connected with release of energy by wires under tension in the magnet. A typical training sequence is shown in

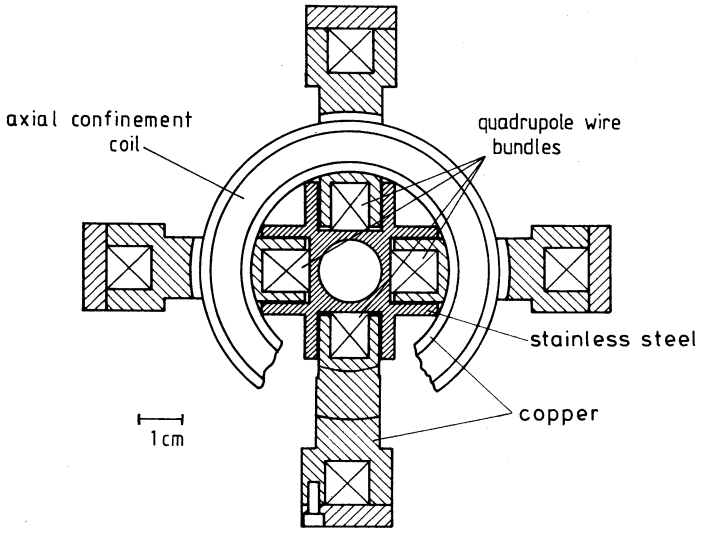

Figure 2.1.3: *Topview of the trapping magnets. The four inner wire bundles of the racetracks produce the quadrupole field. One of the axial confinement coils is shown.*

Fig. 2.1.2. We observe no degradation of the critical current on thermal cycling after the first two cycles. For all our racetracks the final critical current is over 85% of the short sample critical current as specified by the manufacturer.

The four racetracks are held on the inside by the central yoke, as shown in Fig. 2.1.3. This arrangement is chosen because of its radial symmetry and to avoid large spurious (i.e. non-quadrupolar) fields. The smallest distance between two diametrically situated racetracks is 18mm. The currents are parallel in diametrically situated racetracks, and anti-parallel in the pair at a right angle to them, thus creating a quadrupole field. Since there is a considerable outward force of 3200N at maximum current working on each of the racetracks, and because of the pressure exerted by the bundles within a racetrack due to mutual repulsion of the wires, the yoke holding the racetracks is made of stainless steel. The racetracks are electrically connected in series. The maximum current used is 36A, slightly less than their individual critical currents.

The axial confinement field is created by two dipole coils with 48mm inner diameter separated by 100mm. These coils are situated between the inside and the outside leg of the racetrack magnets, and are wound *in situ* with Niomax A60/25 wire. One of these coils is also shown in Fig.2.1.3. As for the other coils copper formers were used. Impregnation was done during winding with Stycast 1266. The dipole coils produce fields

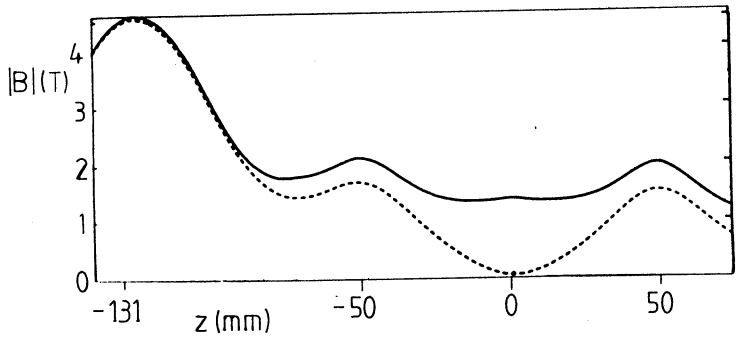

Figure 2.1.4: *Magnetic field profile of the magnet assembly along the z-axis. The solid line is the lowest field at the surface, the dashed line is the field along the axis of the cell. The high field region is located at the left, the center of the trap is at* $z = 0$.

of 1.5T ($z = +50$mm) and 1.7T ($z = -50$mm) respectively. For this 40A is required, well below the critical current. The field at $z = -50$mm is slightly higher than the one at $z = +50$mm to minimize a dip in the field profile (Fig. 2.1.4) between the high field region and the trapping field. At z=0 we include a small solenoid to enable trimming of the field minimum B_0. This coil also has an inner diameter of 48mm.

Below this assembly of magnets, which constitutes the trapping field, the high field region is situated. The high field is created by a single solenoid, length 50mm, with 44mm bore, mounted on an extension of the yoke holding the racetracks. This coil was wound with Vacuumschmelze F54, 0.3mm wire and also vacuum-impregnated with Stycast 1266. The center of this coil is at $z = -131$mm. During the experiments the coil was operated at 35A, producing a 4.5T central field, for safety reasons (possible damage to the cell through induced currents) well below the maximum current after training of 42A.

A cross section of the whole assembly, mounted on the stainless steel yoke that serves at the same time as the bore of the magnet can, is shown in Fig.2.1.5. The experimental cell is also shown. The free accessible bore is 16mm. The inner legs of the racetracks are in immediate proximity of the experimental cell, so field at the cell wall will be nearly equal to the maximum field created by a single racetrack. All coils are brought in persistent mode during the experiment to minimize evaporation of the main He bath. The home-made superconducting switches allow 16hr operation without loss of field exceeding 3% and withstood repeated deliberate quenching of the magnets.

The absolute value of the quadrupole field increases linearly as 0.2T/mm up to a distance of 5mm from the axis, beyond this distance non-linearities become significant.

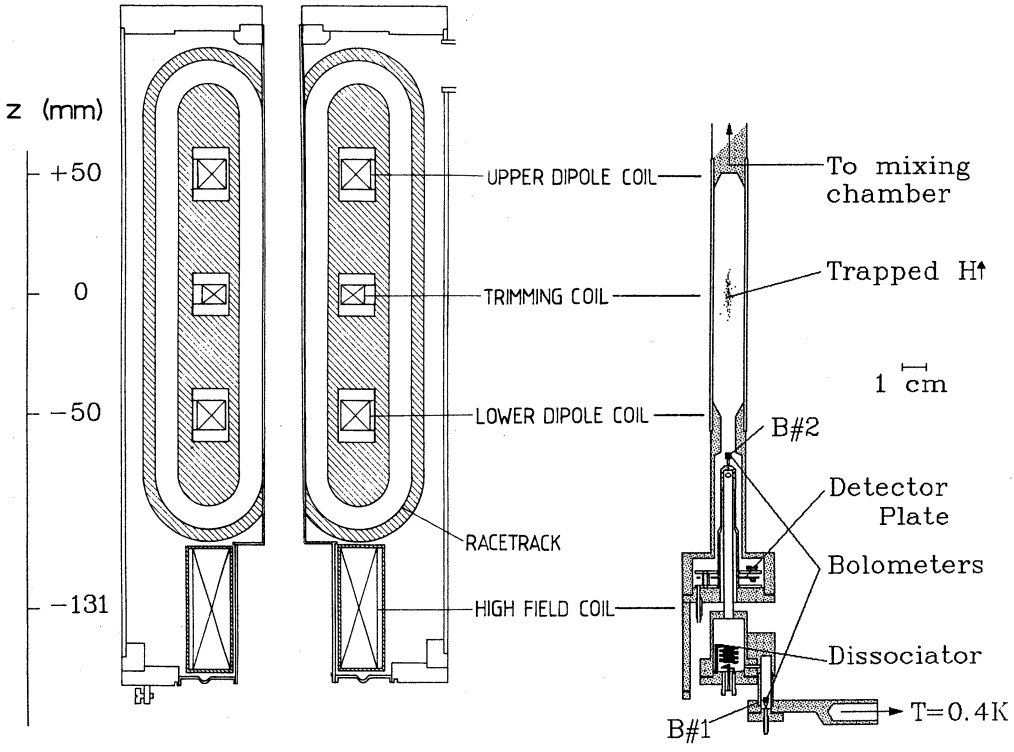

Figure 2.1.5: *The trapping magnet assembly in its tank and a cross section of the experimental cell. Two of the four racetracks are visible, and from top to bottom the upper confinement coil, the trimming coil, the lower confinement coil and the high field coil. We have indicated the height of the maxima and minima created by the solenoids in the experimental cell. The thermal link of the cell to the mixing chamber of the dilution refrigerator extends from the bore of the magnet on the top of the tank. In the cell the dissociator, some important bolometers, the detector plate and the location of the trapped gas are indicated.*

In the z-direction the quadrupole field decreases towards the ends of racetracks, this in combination with the increasing field of the axial confinement coils, is roughly described by $B = \beta z^2 + B_0$ with $\beta = 1.2 \times 10^{-3}\mathrm{T/mm^2}$. We find that the resulting total field near the wall is minimal at $z = 0$, so the depth of the trap, defined as the difference in potential energy between an H$\uparrow$ atom in the center of the trap and at the wall

$$\epsilon_{tr} = \mu_B(B_w - B_0), \tag{2.1.1}$$

is determined by the quadrupole field at this point. The absolute value of the magnetic fields with maximum current in all coils except the trim coil is shown in Fig. 2.1.4. The solid line is the field produced at the wall of the cell, the dashed line is the field along the axis. The field B_w is the minimum of the solid curve and B_0 the minimum of the dashed curve.

Approximating the magnetic field, using a linear term in the radial direction and the quadratic dependence in the z-direction, $B = B_0 + \alpha r + \beta z^2$, the effective volume V_{1e} may be calculated, and we find

$$V_{1e} = \frac{3\pi^{3/2}}{\alpha^2\sqrt{\beta}} \left(\frac{k_B T}{\mu_B}\right)^{5/2}. \tag{2.1.2}$$

Of course this relation is valid only in a limited temperature range. For high temperatures ($k_B T \gg \mu_B B$) the effective volume will be equal to the geometrical cell volume. For low temperature ($T < 5\mathrm{mK}$) the effective volume will be determined by the parabolic shape of the trap minimum. In a numerical integration over the volume using the exact fields used in the experiments, it is found that $V_{1e}T^{-5/2} = 35\mathrm{cm^3K^{-5/2}}$, within 5% for T between 100 and 200mK. In turn the analytic approximation deviates 5% from this result. For the data analysis we used the results of the numerical integration.

2.2 The Experimental Cell

A drawing of the cell (to scale) can be seen in Fig. 2.1.5. The body is made entirely of copper for maximum thermal conductivity. All copper parts are made of high purity copper, certified grade according to ASTM f68/77, manufactured by Outokumpu Oy (Finland). The copper of the trapping volume and all other parts to which the sample is exposed were electrolytically etched to remove magnetic impurities implanted by machining. Magnetic impurities should be removed since they cause transitions, i.e. spurious relaxation, between hyperfine states of atoms moving on or near the wall.[6–8]

The 'trapping' part of the experimental cell is a simple copper tube, placed inside the quadrupole magnet and the axial confinement coils. The wall thickness of this tube is chosen to be 1mm, in order to avoid large temperature gradients along the cell. The middle of the tube is located at the same height as the trimming coil of the magnetic

trap, its ends correspond to the local field maxima created by the axial confinement coils. The tube has an inner diameter as large as was allowable (13mm), given the bore of the quadrupole yoke and the required thickness of the copper wall. As discussed in the previous paragraph the quadrupole field increases approximately linearly with the radius, so according to eq. 2.1.1 the larger the diameter of the cell, the deeper the well depth of the trap. All in all the walls of cell coincide largely with a region outlined by the equipotential surface $\epsilon_{tr} = \mu_B B_w$ of the magnetic field.

The trapping section is connected to the upper and lower part of the cell by soft soldered joints. At the top the cell is connected to the mixing chamber of our dilution refrigerator. At the bottom the cell consists of two separate sections. The lowest section of the cell is the hydrogen dissociator, which is connected to the main body of the cell through a thin walled CuNi filling tube. The second section, containing the detector, annularly surrounds the CuNi tube. Both will be described in detail later. The dissociator and detector are responsible for most of the heat generated in the cell.

The dissociator is cooled independently by means of a copper rod and braid connected to the continuous heat exchanger at a point close to the still of the dilution refrigerator. A radiation shield, halfway in the CuNi-tube, is thermally anchored to the cold plate of the fridge.

Thermometers are situated above and below the trapping section of the cell. One is mounted on the copper rod connected to the mixing chamber, another on the bottom end of the cell, on the detection volume. They do not measure directly the temperature of the copper tube which is in thermal contact with the sample. At the lowest temperatures in this experiment the heat dissipated in the detector (20μW) causes fairly large temperature gradients over the length of the cell (as much as 10mK), and this gradient is the main source of uncertainty in the determination of the wall temperature T_w of the cell, although of course calculations can be made of the temperature of several parts of the cell, reducing the error well below the total gradient. Other thermometers are attached to the dissociator body and the thermal anchoring of the radiation shield.

The cell contains two bolometers. One (B#1) is situated in a volume directly connected to the dissociator also shown in Fig. 2.1.5. The second bolometer (B#2) is mounted on a cap on top of the filling tube, quite close to the trapping region, enabling us to destroy the H$\uparrow$-sample at will by evaporating the helium film.

The detector is situated in the high-field region, which is accessible only to high-field-seeking H$\downarrow$ because of the large Boltzmann factor (Sect. 1.7), whereas low-field-seeking H$\uparrow$ will collect in the trapping region, so detected atoms are always high-field seekers. The H$\uparrow$ gas in the trap can only be studied by monitoring the flux of atoms that leave the trap after relaxation.

The thermometers relevant to the experiment are all 200Ω Matsushita[9] carbon re-

sistors. The resistors are monitored with a four wire method described by Van Yperen.[3] They are connected in strings of four thermometers, through which a known current flows.

Calibration of the main carbon thermometer in the cell is done against a ^{3}He melting curve thermometer,[10] mounted on the copper rod that links the experimental cell to the mixing chamber of the dilution refrigerator. Calibration of the pressure transducer of the melting curve thermometer is done at the Van der Waals Laboratory of the University of Amsterdam.[11] We estimate the accuracy to be 1mK.

2.3 Detection

All hydrogen detection in this experiment is done with bolometric techniques already mentioned in section 1.5. The underlying mechanism is that the liquid helium film, which normally covers the entire surface of the cell, is removed from a part of the surface, and the heat deposited by the recombining hydrogen is detected.

Two types of bolometers are used. The simplest one is the carbon chip bolometer.[12] A small carbon chip (typically 2 × 1mm), cut out of a Speer resistor, is supported by two thin manganin wires, which also act as electrical leads. The chip is heated with a small electrical current, typically 70μA, sufficient to evaporate more helium from the chip than can be replenished by film flow along the supporting wires. This requires about 10μW for the bolometers in the cell. Once the film is 'burned off' the surface, hydrogen will recombine rapidly on the exposed substrate. The recombination heats up the chip, resulting in a drop of the resistance. At constant current the resulting voltage drop is a measure of the quantity of hydrogen that has recombined. Advantages of this method are the ease of construction and the sensitivity, disadvantages are the 'single shot' nature of the detection and the non-linearity of the bolometer response.

Our main detector is of the so-called 'pumping plate' type, first used by Berkhout *et al.*[13,14] The plate is a thin (0.1mm) foil, in our case made of brass with gold plating. The brass is used to reduce eddy current, induced by varying magnetic fields, which causes heating as well as exerting a force on the supporting wires. For the same reason there is a radial slit in the plate. The gold plating increases the heat conduction in the plate, so it reduces thermal gradients that could adversely influence the response time. The surface area of the foil is approximately 5cm^2. The relatively large area ensures that atoms in the proximity have a high probability of hitting the surface, i.e. it makes the device fast. Secondly a large part of the recombination energy is dumped in the plate, which ensures that we can rely on the calibration of Berkhout,[14] who used a device with similar dimensions. The plate is suspended by three thin (16μm diameter) tungsten wires, see Fig. 2.3.1. The wires are carefully stretched between copper poles attached to the upper and lower holding plates. The wires serve as mechanical support and also provide the

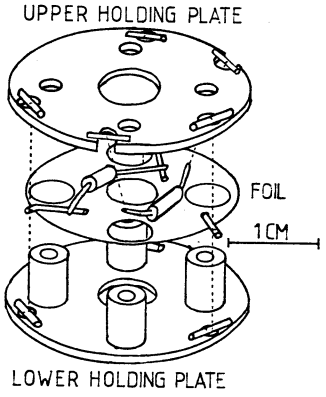

Figure 2.3.1: *The 'pumping plate' bolometer.*

electrical connection. The assembly has an annular shape to leave space for the filling tube extending from the dissociator into the cell. Two resistors are mounted on the plate with Stycast 2850 epoxy. One, a metal film resistor chosen for the weak temperature dependence of its resistance is used as a heater, the other, a Matsushita carbon resistor, as a thermometer.

The Matsushita is measured using the four wire method as mentioned in the previous section. The output of the lock-in amplifier measuring the resistance of the carbon resistor is supplied to an Oxford Instruments temperature controller, which in turn drives the heater. In this way the temperature of the plate can be stabilized at a preset value. The heater power is measured with a digital voltmeter, connected to a microcomputer for data storage, as shown in Fig. 2.3.2.

To detect hydrogen the plate is stabilized at a temperature of 1.3K, a temperature at which there will be no film on the plate (in steady state) and hydrogen will recombine on the surface. The stabilization temperature was selected for optimal signal to noise ratio. The power needed to keep the surface of the plate helium-free is about 20μW, determined by the number and size of the wires. Because the plate temperature is stabilized by the controller the recombination heat dumped in the plate will show up as a reduction of the heater power. We assume that, because of the similarity of the construction, the efficiency of this detector is equal to that reported by Berkhout *et al.*,[14] which means that $60 \pm 10\%$ of the recombination heat is dumped in the plate. For this reason we did not calibrate the device against another detector. Advantages of this detector are its linearity, up to a flux of 1.0×10^{14}at/s, being the equivalent of recombination energy to the externally supplied heater power, and the fact that it can be operated continuously to measure the

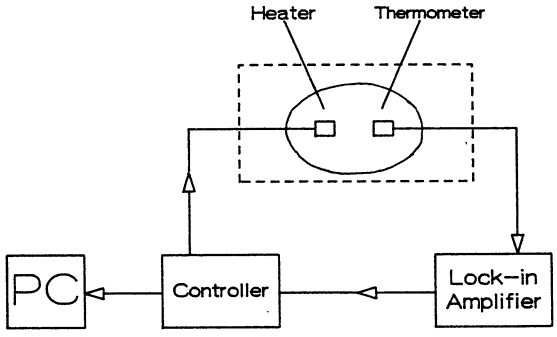

Figure 2.3.2: *Schematic diagram for the stabilization of the pumping plate temperature*

H↓ flux coming out of the trap. The noise of the detector is caused mainly by variations in the thermometer signal, predominantly at a frequency of about 0.5Hz, which led to a minimum detectable flux of about 2×10^{11}at/s. We ascribe this noise to motion of the plate or variation in the film flow over the tungsten wires.

Since our detection technique is destructive, and we do not want it to interfere with the natural decay of the trapped gas, the probability of a trapped atom to reach the detection site should be negligible. In equilibrium the atoms in the trap will have a Maxwell-Boltzmann distribution over the potential energy, so the chance to reach the detector, situated in the high-field region, will increase with temperature. The time constant for the decay of the gas as determined by the detector is found by calculating the flux of H↑ atoms Φ reaching it in proportion to the to number of particles in the trap $N = n_0 V_{1e}$. This flux is found by calculating the density at the entrance to the detector volume and using the approximation that the number of particles that will pass through there is $n\bar{v}A/4$, where $\bar{v}$ is the average atomic speed and A the area of the entrance. The density will be $n = n_0 \exp(-\mu_B(B_d - B_0)/k_B T)$, where B_d is the field at the detector. Now

$$\tau = \frac{4V_{1e}\exp(\mu_B(B_d - B_0)/k_B T)}{\bar{v}A}. \tag{2.3.1}$$

At 250mK we find $\tau \approx$800s, sufficient to introduce inaccuracies in our data. Therefore our experimental temperature range is limited to temperatures below 250mK.

2.4 The Dissociator

For our trapping experiment we replaced the room temperature dissociator used in earlier experiments in our group[15] with a cryogenic dissociator, developed on the basis of the design by Hardy *et al.*[16] The dissociator consists of a resonant electrical circuit, which

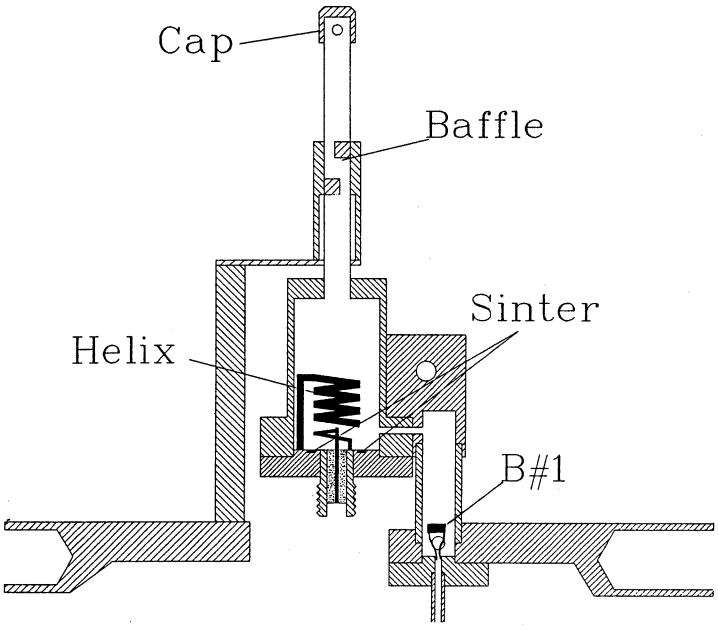

Figure 2.4.1: *The dissociator. Cap and baffle condense He-vapor and cool the hydrogen atoms moving to the trapping region. The sinter improves thermal contact between the He-film and the housing. Bolometer B#1 destroys H↓ which remains in the dissociator.*

creates a high electric field causing a discharge near a surface covered with a layer of solid H_2, in turn covered by a liquid helium film. The discharge gives rise to production of atomic hydrogen. The dissociator was designed as a compact source that would fit into the 40mm bore of the high field section (4.5T) of our trapping magnet. A maximum H↑ flux of 6×10^{12} at/s was observed, which is sufficient for our trapping experiment. The advantages of our design are the relatively simple and rugged construction, and the fact that it operates at comparatively low peak power levels.[17] Apart from a ceramic feedthrough the dissociator contains only metal (copper) components. This may be of interest because of the metals favorable outgassing properties, compared to epoxy, employed in several other low temperature dissociators.[17,18] For experiments with D, outgassing of H_2 from previous experiments can be a serious problem. Also, as we will see below, the operation of a low temperature dissociator may be positively influenced by good overall thermal conductivity.

The dissociator is shown in Fig. 2.4.1. It consists of a 3.5 turn, 7mm inner diameter helix,[19] situated in a 25mm long, 13mm inner diameter cylindrical cavity. The helix is

wound of 1mm copper wire with a pitch 0.5mm^{-1} and is supported by extending the upper end to the bottom of the cavity. Rf-coupling is done with a single turn loop at a distance of about 3mm from the helix. The loop and helix should be wound in opposite sense for optimal coupling.[20]

Because the helix is grounded at one end, it will sustain a $1/4\lambda$ mode. The cavity resonates at frequency $f = 718$ MHz, with a quality factor Q of about 300 at room temperature, increasing to 400 at low temperature. Some adjustment may be done by varying the distance between coupling loop and helix. In this way f, Q and reflected power at resonance can be changed. The maximal electric field E in the cavity is determined by the relation for the field energy stored in the cavity

$$\int_V \frac{1}{2}\epsilon_0 E^2 \mathrm{d}V = P_{in} Q/(2\pi f) \tag{2.4.1}$$

The electric field causes the acceleration of electrons and ions in the discharge thereby producing H. A discharge requires a certain minimal value of E. To achieve a high E field the reflected power has to be minimized, while maintaining as high a Q as possible. In practice we increase the coupling by bringing the loop closer to the helix until the Q starts to deteriorate. Apart from assuring a high field this procedure also implies optimal use of our amplifier by minimizing reflection losses. A schematic drawing of the electronic set-up is shown in Fig. 2.4.2.

The dissociator is loaded with about 3×10^{-4} mol of H_2, equivalent to a coverage of 750 monolayers if we assume the hydrogen to be distributed homogeneously over the cell and dissociator surface. This quantity proved to be sufficient for running the source for several months at a flux of order 10^{12}at/s. The characteristics of the superfluid helium film in the dissociator are not fully understood. From the fact that a small quantity of helium in the cell, not enough to saturate the film, results in reduction of the flux, we conclude that a very thin film affects the process adversely. Adding more helium leads to an increase in flux, but beyond a certain point the flux was found to be insensitive to addition of more liquid helium. We are not sure, however, that this point coincides with the film being saturated.

The mechanism for the production of H at low temperature is not accurately known,[17] but it is thought that electrons and ions are accelerated in a discharge in the He vapor, and, circling in μm-or mm-diameter cyclotron orbits respectively, strike the solid H_2 coating of the wall and release either H_2 or H. The atoms or molecules are subsequently ejected out of the film, after which molecules could be dissociated.

The discharge is operated between 0.50 and 0.65K. Whether the dissociator works at even lower temperatures is unknown, since it could not be cooled below 0.5K at the minimum power input. Dissipation of heat into the helical coil will cause evaporation of helium, so that the discharge is likely to start regardless the temperature of the housing for

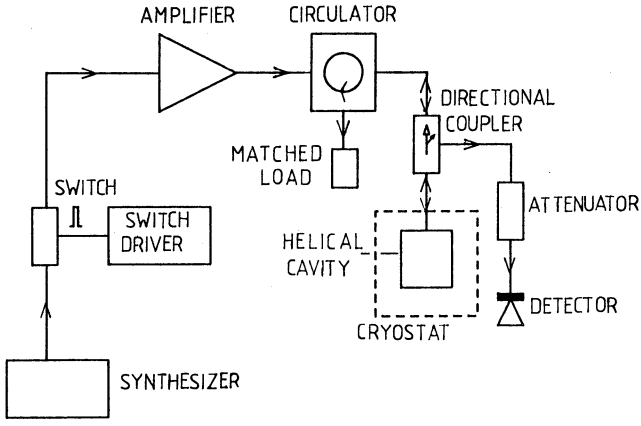

Figure 2.4.2: *Diagram of the set-up for supplying RF power and monitoring the dissociator. Circulator and load are included as protection for the amplifier output. By the use of a directional coupler the detector registers only reflected power.*

temperatures below 0.5K. A separate heater to provide some vapor at low temperature, as used by Helffrich *et al.*,[17] was not included for this reason. At temperatures above 0.65K the efficiency of the H production is strongly reduced. We note the similarity on this point between our results and those of Helffrich[17] for high-field-seekers, which leads us to suppose that the reduction is connected with the increasing vapor pressure of the helium. Above 0.65K the He density is of the order of 10^{16}cm^{-3}, which is at least an order of magnitude higher than the H density, and therefore most of the microwave power is absorbed by the He and does not result in production of H. This explanation could be tested by loading the cell with a large quantity of ^{3}He, which should result in a decrease of the temperature at which the dissociator starts to be less efficient.[21]

To strike a discharge a minimum power level of 20mW is needed in our geometry. Since a continuous heat input of 20mW would cause the dissociator to overheat, the power is supplied in pulses by inserting a fast RF switch between synthesizer and amplifier, as shown in Fig. 2.4.2. Typically we supplied 50μs pulses at a 50Hz repetition rate. After cooling down from room temperature, it was sometimes necessary to use full power (0.5W) for some time to initiate the discharge. During months of operation no special effort was needed to restart it. We did not include a radioactive source in or near the cavity, as was done elsewhere[18] to facilitate the initiation of the discharge. To monitor the presence of a

discharge one could look for the production of hydrogen, but a very simple indication is the reflected power level. The plasma will change the properties of the cavity drastically, leading to higher reflection.

We found the production of H by the dissociator to be roughly proportional to the average power input, with the following limitations: firstly the device should not be heated to temperatures above 0.65K, since then the atomic hydrogen flux deteriorates rapidly. Secondly the pulse duration should not be too short. We found the efficiency of H production to decrease for pulses shorter than 50μs. Long pulses, with pulse lengths up to 1ms, yield roughly equal amounts of H at the same average power input. Our most important conclusion is that for the production of large fluxes, cooling of the dissociator is a crucial factor. This is in accordance with earlier findings.[17,22,23]

Our present dissociator differs from a prototype version in two important respects, which result in a H-flux improvement by a factor of 3. At present we use a direct, metal-to-metal, connection of the helix to the rest of the cavity, instead of a support made of dielectric, Stycast 1266 epoxy. Further the designs differ by the inclusion of silver sinter in the bottom flange of the cavity in the new version. Both changes enhance the thermal contact between various components of the system.

With 100μW average input power we measured a flux of 2.2×10^{12} at/s (H$\uparrow$), which is an efficiency of about 0.8%. This is comparable to the results obtained with the MIT dissociator,[22] where a flux of 5×10^{12} is reported at 400μW average input power, or an efficiency of 0.5%. The efficiency for producing high-field seekers is different, a similar dissociator used in our group[24] for producing high-field seekers has an efficiency of 3%, equal to the result found by Helffrich *et al.*[17]

The dissociator is cooled by a thermal link connected close to the still to the continuous heat-exchanger of the dilution refrigerator. It is connected to the experimental cell through a 50mm long, 3.6mm inner diameter CuNi filling tube (see Fig. 2.4.1). The distance from dissociator to cell is only a few centimeters, which is small compared to distances used in other experiments.[17,18,22] Nevertheless by taking several precautions we manage to keep the heat load on the cell during operation well below 10μW, allowing a cell temperature below 45mK. Ignoring the contribution due to recombining hydrogen, heat will be transported mainly by helium vapor. Cooling of the helium inside the cavity was enhanced by the sinter in the bottom flange, increasing the total surface area by about a factor of ten. Halfway the filling tube we include an optically tight copper baffle to condense fluxing helium vapor. The baffle fits tightly inside the filling tube and blocks 60% of the cross sectional area of the tube over a length of 10mm. At the site of the baffle the outside of the filling tube is pinned to the cold plate of our refrigerator, typically having a temperature of about 0.2K. For similar reasons a copper cap, at cell temperature, was placed over the end of the filling tube, leaving only four holes sideways with a total area

approximately equal to the cross section of the tube.

A bolometer (B#1) situated in a separate volume, connected to the resonant cavity through a 1mm diameter hole, served to destroy atoms remaining in the dissociator (i.e. high-field seekers). The time-constant for the destruction was intended to be 0.15s, as estimated from the probability, in the case of Knudsen flow, of a high-field seeking atom to reach B#1. It was argued that high-field seekers would remain in the dissociator for a long time, while low-field seekers would be expelled well within 0.15s because of the high field. However, as will be shown in Section 4.3 a flux of high-field seekers spuriously entering the cell was detected up to more than a second after switching off the dissociator. This spurious flux is thought to be caused by compression of atomic hydrogen gas by a flux of evaporated helium. At a typical operating temperature of the discharge $T_d = 600$mK the density of the helium vapor in the cavity is $n_{He} = 4.5 \times 10^{15}\text{cm}^{-3}$. Using the H-He cross section as given by Jochemsen[25] we estimate that at this temperature the mean free path of the H atoms is smaller than the dimensions of the dissociator. We therefore expect the atoms to be carried along by the fluxing helium vapor, an effect similar to that observed in relation to our bottom-loading room temperature dissociators (HEVAC[26]). The compression of the H gas by H-He collisions will be equally strong for high and low-field seeking atoms. We assume that the helium vapor fluxes out of the cavity to the copper baffle in the filling tube to condense, and that the He atoms transfer their velocity in the z-direction $\frac{1}{2}\bar{v}_{He}$ to the H gas, where $\bar{v}_{He}$ is the average thermal velocity in helium vapor. We get the following expression for the hydrogen distribution in the tube:

$$J = (\frac{1}{2}\bar{v}_{He} \pm \mu)n - D\frac{\partial n}{\partial z}, \tag{2.4.2}$$

where D is the diffusion coefficient and μ is the Einstein mobility

$$\mu = \frac{D\mu_B}{k_B T}\frac{\mathrm{d}B}{\mathrm{d}z}. \tag{2.4.3}$$

The plus sign in eq. 2.4.2 applies to H$\uparrow$, the minus sign to H$\downarrow$. Since $\frac{1}{2}\bar{v}_{He}$ is a factor of ten larger than μ, it is clear that n_H in the low-field part of the filling tube will be bigger than one would expect for a Maxwell-Boltzmann distribution. If we set J to zero the compression ratio for H$\uparrow$ from cavity to baffle is 48, for H$\downarrow$ it is 24. The complete solution of eq. 2.4.2 is

$$n(z) = \left(n_0 - \frac{J}{1/2\bar{v}_{He} \pm \mu}\right)\exp[\frac{(1/2\bar{v}_{He} \pm \mu)z}{D}] + \frac{J}{1/2\bar{v}_{He} \pm \mu} \tag{2.4.4}$$

Inserting a typical experimental value for J of $4 \times 10^{13}\text{cm}^{-2}\text{s}^{-1}$ for H$\uparrow$ and $1 \times 10^{13}\text{cm}^{-2}\text{s}^{-1}$ for H$\downarrow$ we find compression ratios of 1 and 1.2 for H$\uparrow$ and H$\downarrow$ respectively. In the last part of the filling tube, between the first and the second baffle eq. 2.4.2 is reduced to

$$J = \pm\mu - D_k\frac{\partial n}{\partial z}, \tag{2.4.5}$$

where D_k is the Knudsen diffusion constant, since we are now in a regime of Knudsen flow, i.e. $\lambda_{mf} > a$, with a the tube radius, because we expect that most of the helium vapor condenses on the baffle. The diffusion constant is

$$D_k = \frac{2}{3} a \bar{v}, \tag{2.4.6}$$

where $\bar{v}$ is the average speed of the atoms. The solution of eq. 2.4.5 in our case is equal to eq. 2.4.4 if we leave out the He velocity term and replace D with D_k. In the experiment one expects the fraction of high-field seeking atoms in the flux to increase with dissociator temperature on the ground of this model. We will comment further on this in the section about experimental results.

Although the constrictions in the filling tube served very well to reduce the heat load on the cell, we ascribe to them a disadvantage too. When working with ^{4}He-covered surfaces, we found the filling of the cell with low-field seekers to be reduced when the temperature was lowered to 150mK. At 100mK only a small signal of high-field seekers could be detected. On a surface covered with a ^{3}He-^{4}He mixture, no such problem occurred down to our lowest experimental temperature of 80mK.

We believe the difficulty of loading the cell below 150mK with ^{4}He covered surfaces is due to surface recombination in the end of the filling tube. As was pointed out in Chapter 1 the separation of high and low-field-seekers, due to the magnetic field gradient, is such that no appreciable up-down recombination occurs in equilibrium. However, as was explained above, the helium evaporated in the discharge will compress both H$\uparrow$ and H$\downarrow$ in the filling tube. The recombination between H$\uparrow$ and H$\downarrow$ in high field ($B \gg 0.05T$) is orders of magnitude more efficient than recombination of H in either of the two electron spin states, and at low temperature this process takes place mainly on the surface. The higher binding energy of H on a pure ^{4}He surface ($\epsilon_a/k_B \approx$1K vs. 0.4K for the mixture) causes the reduced flux, when compared to the ^{3}He coverage. The recombination loss, calculated on the basis of H$\uparrow$ and H$\downarrow$ densities according to the compression effect as calculated above, would be

$$\frac{\mathrm{d}N}{\mathrm{d}t} = -A\lambda\bar{v}_s n_{H\downarrow} n_{H\uparrow} \Lambda^2 \exp(2\epsilon_a/k_B T). \tag{2.4.7}$$

Here $\lambda = 2.0 \times 10^{-9}$cm is a surface effective cross-length,[27,28] $\bar{v}_s$ is the average speed of atoms on the surface and A the surface area. At 100mK the number of atoms recombining in the filling tube will be $3 \times 10^{12}\mathrm{s}^{-1}$, to be compared with a flux of $5 \times 10^{11}\mathrm{s}^{-1}$. This is in accordance with the reduced flux found in the experiment.

Our conclusion is that if one wants to use this dissociator to fill a cell at a temperature, low relative to ϵ_a/k_B, a compromise has to be found between low heat load and optimum filling properties of the dissociator. We have attempted to fill our trap with deuterium, which has a considerably higher binding energy.[29] We encountered two major difficulties,

namely low flux and uncertainty whether the flux consisted of deuterium or a mixture of deuterium and hydrogen. This leads us to believe that removal of one or both of the constrictions would be advisable, because transport of D from dissociator to cell will be considerably more difficult than for hydrogen.[30]

References

[1]D.E. Pritchard, Phys. Rev. Lett. **51**, 1336 (1983).

[2]H.F. Hess, G.P. Kochanski, J.M. Doyle, N. Masuhara, D. Kleppner, and T.M. Greytak, Phys. Rev. Lett. **59**, 672 (1987).

[3]G.H. van Yperen, J.T.M. Walraven, and I.F. Silvera, Phys. Rev. B **30**, 2386 (1984); G.H. van Yperen, Thesis, University of Amsterdam (1984), unpublished.

[4]P.F. Smith, and B. Colyer, Cryogenics, 201 (april 1975).

[5]V.W. Edwards, C.A. Scott, and M.N. Wilson, Proc. 6th ICEC, 477 (1976).

[6]G.H. van Yperen, A.P.M. Matthey, J.T.M. Walraven, and I.F. Silvera, Phys. Rev. Lett. **47**, 800 (1981)

[7]R.W. Cline, T.J. Greytak, and D. Kleppner, Phys. Rev. Lett. **47**, 1195 (1981).

[8]B.W. Statt, A.J. Berlinsky, and W.N. Hardy, Phys. Rev. B **31**, 3169 (1985)

[9]Sinhachiro Saito, and Takashi Sato, Rev. Sci. Instrum. **46**, 1226 (1975).

[10]D.S. Greywall, and P.A. Busch, J. Low Temp. Phys. **46**, 451 (1982).

[11]For this we thank H. Luigjes and K.O. Prins of the Van der Waals Laboratory, University of Amsterdam.

[12]I.F. Silvera, and J.T.M. Walraven, Phys. Rev. Lett. **44**, 164 (1980).

[13]J.J. Berkhout, E.J. Wolters, R.v. Roijen, and J.T.M. Walraven, Phys. Rev. Lett. **57**, 2387 (1986).

[14]J.J. Berkhout, O.H. Höpfner, E.J. Wolters, and J.T.M. Walraven, Jap.J.Appl.Phys. **26**, 231 (1987) suppl. 26-3 (LT18).

[15]J.T.M. Walraven, and I.F. Silvera, Rev. Sci. Instrum. **53**, 1167 (1982).

[16]W.N.Hardy, M.Morrow, R.Jochemsen, and A.J.Berlinsky, Physica **109B** (1982), 1964.

[17]J.Helffrich, M.Maley, M.Krusius, and J.C.Wheatley, J. Low Temp. Phys. **66**, 277 (1987).

[18]B.W. Statt, W.N. Hardy, A.J. Berlinsky, and E. Klein, J. Low Temp. Phys. **61**, 471 (1985).

[19]W.W. Macalpine, and R.O. Schildknecht, Proc. IRE, 2099 (1959).

[20]A.F. Harvey, Microwave Engineering, p.480 (Academic Press, 1963).

[21]In another experiment with a similar dissociator we have loaded the cell with ^{4}He in such quantity that bulk liquid formed at the bottom of the cell. Addition of a comparable quantity of ^{3}He led to total disappearance of atomic hydrogen flux. However, in the setup used in that experiment the dissociator was situated above the experimental cell, i.e. the situation is comparable to an inverted heat pipe, and one expects the ^{3}He to remain in the lowest, coldest part so that no dense ^{3}He vapor can build up in the dissociator. Possibly the ^{3}He necessary to maintain a sufficient amount of vapor in the dissociator enters the dissociator by diffusion through the ^{4}He film. J.J. Berkhout, private communication.

[22]H.F.Hess, G.P.Kochanski, J.M. Doyle, T.J.Greytak, and D.Kleppner, Phys. Rev. A **34**, 1602 (1986).

[23]I.F. Silvera, private communication.

[24]J.J. Berkhout, private communication.

[25]R. Jochemsen, A.J. Berlinsky, and W.N. Hardy, Can. J. Phys. **62**, 751 (1984).

[26]I.F. Silvera, and J.T.M. Walraven, Phys. Rev. Lett. **44**, 164 (1980).

[27]A.P.M. Mattheij, J.T.M. Walraven, and I.F. Silvera, Phys. Rev. Lett. **46**, 668 (1981).

[28]R. Jochemsen, M. Morrow, A.J. Berlinsky, and W.N. Hardy, Physica **109&110B**, 2108 (1982).

[29]I.F. Silvera, and J.T.M. Walraven, Phys. Rev. Lett. 45, 1268 (1980).

[30]M.W. Reynolds, private communication.

Chapter 3

The Decay Process

3.1 The Onset of Polarization

Trapped H↑ will undergo relaxation to H↓ via spin exchange and magnetic dipolar interaction. The rates for these processes were calculated by Lagendijk *et al.*[1] and Stoof *et al.*[2] Spin exchange is a very efficient channel for relaxation for low fields as is the case in the trap. However, only collisions between atoms in the c state may lead to transitions through spin exchange in the s-wave scattering regime. Collisions between two d-state atoms or between a c-state and a d-state atom are less likely to lead to relaxation, since in this case relaxation may only be induced by the relatively weak dipolar interaction. This means that the c state should be rapidly depleted, leaving the gas in an almost pure d state.

When interpreting our results we use the relaxation rate constants as calculated by the degenerate-internal-state approximation mentioned in Chapter 1. The relaxation rate constants G give the change of the population of a hyperfine state h_i according to

$$\dot{n}_{h_1} = \sum_{h_2} \sum_{h_3 h_4} (1 + \delta_{h_1 h_2})(G_{h_3 h_4, h_1 h_2} n_{h_3} n_{h_4} - G_{h_1 h_2, h_3 h_4} n_{h_1} n_{h_2}). \tag{3.1.1}$$

We will only concern ourselves with relaxation of the c and d states, since high-field-seeking atoms in the a and b states are completely absent in the trap.

For the spin-exchange rates we get the following parametrization[2] of G in $\mathrm{cm^3 s^{-1}}$

$$G_{h_1 h_2, h_3 h_4} = (2 - \delta_{h_1 h_2})[(2\Delta + 3k_B T)/\mu)]^{1/2} \sigma_0 |(h_3 h_4 | P^{(0)} | h_1 h_2)|^2 \tag{3.1.2}$$

or

$$G_{h_1 h_2, h_3 h_4} = (2 - \delta_{h_1 h_2}) 3/2[(2\Delta + 5k_B T)/\mu)]^{1/2} \sigma_1 |(h_3 h_4 | P^{(0)} | h_1 h_2)|^2 \tag{3.1.3}$$

where μ is the reduced mass, $P^{(0)}$ is a projection operator on the total spin basis[3] $|0000\rangle$ for $l = 0$ and $|001 M_I\rangle$ for $l = 1$. The δ-function is included to enable us to use the tables

of the review article by Silvera and Walraven.[3] The spin exchange cross sections (cm^2) for $l = 0$ and $l = 1$ respectively are

$$\begin{aligned}\sigma_0 &= 14.4 \times 10^{-16}/[1 + 2.68 \times 10^{15}(\Delta + 3k_BT)] \\ \sigma_1 &= 77.0 \times 10^{12}\frac{(\Delta + 5k_BT)^2}{1 + 7.61 \times 10^{14}(\Delta + 5k_BT) + 4.5 \times 10^{30}(\Delta + 5k_BT)^2},\end{aligned} \tag{3.1.4}$$

and where eq. 3.1.2 refers to $l = 0$ ($cc \rightarrow bd$, $cc \rightarrow aa$ and $cc \rightarrow ac$) and eq. 3.1.3 to $l = 1$ ($cd \rightarrow ad$). The energy difference between initial and final states Δ,

$$\Delta = E_{h_1} + E_{h_2} - E_{h_3} - E_{h_4}, \tag{3.1.5}$$

should be expressed in erg. The projection yields

$$\begin{aligned}|(bd|P^{(0)}|cc)|^2 &= \frac{1}{4}\sin^2\theta\cos^2\theta \\ |(aa|P^{(0)}|cc)|^2 &= \frac{1}{2}\sin^4\theta\cos^4\theta \\ |(ac|P^{(0)}|cc)|^2 &= \frac{1}{4}\sin^2\theta\cos^2\theta(\sin^2\theta - \cos^2\theta)^2 \\ |(ad|P^{(0)}|cd)|^2 &= \frac{1}{4}\sin^2\theta\cos^2\theta.\end{aligned} \tag{3.1.6}$$

This parametrisation gives results very close, within 1%, to those of the coupled channels calculation for $B \ll 1$T and $T \ll 1$K. For $B \simeq 1.5$T and $T \simeq 0.3$K the deviation is 13%. In our experiment B and T are always below these values.

For the dipolar relaxation rates we refer to the expression for the event rate Γ given in section 1.8. The relation between event rates and relaxation rate constants is

$$G(h_1h_2 \rightarrow h_3h_4) = \frac{1}{2}\Gamma(h_1h_2 \rightarrow h_3h_4) \tag{3.1.7}$$

for $h_1 = h_2$ and

$$G(h_1h_2 \rightarrow h_3h_4) = \Gamma(h_1h_2 \rightarrow h_3h_4) \tag{3.1.8}$$

for $h_1 \neq h_2$. As in the case of the spin-exchange the orbital part has been factored out. The approximation of section 1.8 can be extended to finite temperature ($3k_BT \lesssim \Delta$) and non-zero magnetic field by multiplying the equation for the relaxation rate constant $G_{h_1h_2,h_3h_4}$ with an expression for the temperature dependence[2] to get

$$\begin{aligned}G_{h_1h_2,h_3h_4} &= (2 - \delta_{h_1h_2})\left(\frac{8\pi}{45}\right)a_{ee}^2|(h_3h_4|T_2^m|h_1h_2)|^2v_f \\ &\quad \left[1 - 1.440\frac{k_BT}{\Delta} + 1.797\left(\frac{k_BT}{\Delta}\right)^2\right].\end{aligned} \tag{3.1.9}$$

For somewhat higher temperature ($0.2 \lesssim \Delta/k_BT \lesssim 3$) we use the following expression for the event rate

$$G_{h_1h_2,h_3h_4} = (2-\delta_{h_1h_2})0.858\times 10^{-16}|(h_3h_4|T_2^m|h_1h_2)|^2 \left(\frac{k_BT}{a}\right)^{1/2}\left[1+1.401\frac{\Delta}{k_BT}-0.06181\left(\frac{\Delta}{k_BT}\right)^2\right]. \quad (3.1.10)$$

The T_2^m operator is defined in terms of second-rank tensor operators given in section 1.8, and contains the interatomic electron-electron dipolar interaction of eq. 1.2.2 in section 1.2. The matrix elements are

$$\begin{aligned}
|(aa|T_2^{-2}|dd)|^2 &= \frac{3}{4}\cos^4\theta \\
|(ac|T_2^{-2}|dd)|^2 &= \frac{3}{2}\sin^2\theta\cos^2\theta \\
|(ad|T_2^{-1}|dd)|^2 &= \frac{3}{8}\cos^2\theta \\
|(cc|T_2^{-2}|dd)|^2 &= \frac{3}{4}\sin^4\theta \\
|(cd|T_2^{-1}|dd)|^2 &= \frac{3}{8}\sin^2\theta \\
|(aa|T_2^{-1}|cd)|^2 &= \frac{3}{2}\sin^2\theta\cos^4\theta \\
|(ab|T_2^{-2}|cd)|^2 &= \frac{3}{8}\cos^4\theta \\
|(ac|T_2^{-1}|cd)|^2 &= \frac{3}{32}\cos^2\theta(\cos^2\theta-3\sin^2\theta)^2 \\
|(ad|T_2^{0}|cd)|^2 &= \frac{9}{16}\sin^2\theta\cos^2\theta \\
|(bc|T_2^{-2}|cd)|^2 &= \frac{3}{8}\sin^2\theta\cos^2\theta \\
|(bd|T_2^{-1}|cd)|^2 &= \frac{3}{32}\cos^2\theta \\
|(cc|T_2^{-1}|cd)|^2 &= \frac{3}{16}\sin^2\theta(\cos^2\theta-\sin^2\theta)^2 \\
|(ab|T_2^{-1}|cc)|^2 &= \frac{3}{2}\sin^2\theta\cos^4\theta \\
|(ad|T_2^{-1}|cc)|^2 &= \frac{3}{2}\sin^4\theta\cos^2\theta \\
|(bb|T_2^{-2}|cc)|^2 &= \frac{1}{32}\cos^4\theta \\
|(bc|T_2^{-1}|cc)|^2 &= \frac{3}{8}\cos^2\theta(\cos^2\theta-\sin^2\theta). \quad (3.1.11)
\end{aligned}$$

The value of the dipolar relaxation rate constants calculated in this way reproduces within 2% the result of the coupled channels calculation of Stoof *et al.*[2] for low field ($B < 0.1$T) and temperature ($T < 0.6$K). Note that for instance the minimum in the rate constant

of the transition $cd \rightarrow ac$ (curve 7 in Fig. 1.8.1) is reproduced by the matrix element $|(ac|T_2^{-1}|cd)|^2$. In higher fields the results can be inaccurate. To extend the calculations to higher values of the magnetic field at finite temperature one should multiply the result for $T = 0$ from the coupled channels calculation, shown in Fig. 1.8.1, with the temperature dependence given in eqs. 3.1.9 and 3.1.10. The rates listed here are all for transitions from higher to lower energy of the spin states. The probability of the inverse processes is found by multiplying with a Boltzmann factor $\exp(-\Delta/k_BT)$.

To compare our experimental results with the calculated values we have to average over the density distribution and take into account the field and temperature dependence of the rate constants. For the thermal averaging we assume the trapped gas to be distributed according to thermal equilibrium, so

$$n_{h_i}(\vec{r}) = n_{0,h_i} \exp[-\mu_B(B(\vec{r}) - B_0)/k_BT_g] \tag{3.1.12}$$

where n_{0,h_i} is the density of hyperfine state h_i in the center of the trap and the exponent represents the Boltzmann-distribution over the field. The time scale in which equilibrium is reached will be considered later. We can describe the evolution of the populations of the c and the d state by using eq. 3.1.1. We make a summation over initial and final states of processes that have their initial states in common, by defining

$$\begin{aligned}
G^c_{cc} &\equiv -2G_{cc,aa} - G_{cc,ac} - 2G_{cc,bd} \\
G^d_{cc} &\equiv G_{cc,bd} \\
G^c_{cd} &\equiv -G_{cd,aa} - G_{cd,ab} - G_{cd,ad} - G_{cd,bd} + G_{cd,cc} - G_{cd,dd} \\
G^d_{cd} &\equiv -G_{cd,aa} - G_{cd,ab} - G_{cd,ac} - G_{cd,bc} - G_{cd,cc} + G_{cd,dd} \\
G^c_{dd} &\equiv 2G_{dd,cc} + G_{dd,ac} + G_{dd,cd} \\
G^d_{dd} &\equiv -2(G_{dd,aa} + G_{dd,ac} + G_{dd,cc}) - G_{dd,ad} - G_{dd,cd}.
\end{aligned} \tag{3.1.13}$$

In the calculation we use the total number of trapped atoms N and the effective volumes V_{me} as defined in section 1.7,

$$V_{me} = \frac{N_m}{n_{m,0}} = \int_V \exp\left(\frac{-m\mu_B(B(\vec{r}) - B_0)}{k_BT}\right) \mathrm{d}\vec{r}, \tag{3.1.14}$$

because we have to incorporate the effects of the distribution over the trap, as described in eq. 3.1.12. Now the change of the numbers of atoms can be written as

$$\begin{aligned}
\dot{N}_c &= \int_V (G^c_{dd} n_d^2 + G^c_{cd} n_c n_d + G^c_{cc} n_c^2) \mathrm{d}\vec{r} \\
\dot{N}_d &= \int_V (G^d_{dd} n_d^2 + G^d_{cd} n_c n_d + G^d_{cc} n_c^2) \mathrm{d}\vec{r}.
\end{aligned} \tag{3.1.15}$$

The equations for $\dot{N}_{h_1}$ can be rewritten, using the absolute number of particles of a species N_{h1} ($N_{h1} \equiv n_{0,h1} V_{1e}$). We account for the two-particle nature of the relaxation

process in connection with the density distribution by introducing a new effective volume V_γ:

$$V_\gamma \equiv V_{1e}^2/V_{2e}. \tag{3.1.16}$$

We relate the relaxation rate constants G to their value in field B_0, written as G_0.The parameter γ accounts for the field dependence of the rates:

$$\gamma_{h_1h_2}^{h_3} = \frac{\int_V G_{h_1h_2}^{h_3}(B,T)\exp[-2\mu_B(B(\vec{r})-B_0)/k_BT]\mathrm{d}\vec{r}}{\int_V G_{0h_1h_2}^{h_3}(T)\exp[-2\mu_B(B(\vec{r})-B_0)/k_BT]\mathrm{d}\vec{r}}. \tag{3.1.17}$$

Finally we abbreviate the rate constants by writing

$$R_{h_1h_2}^{h_3} \equiv \gamma_{h_1h_2}^{h_3} G_{0h_1h_2}^{h_3}. \tag{3.1.18}$$

The evolution of the populations of eqs. 3.1.15 is now given by

$$\begin{aligned} V_\gamma \dot{N}_c &= R_{dd}^c N_d^2 + R_{cd}^c N_c N_d + R_{cc}^c N_c^2 \\ V_\gamma \dot{N}_d &= R_{dd}^d N_d^2 + R_{cd}^d N_c N_d + R_{cc}^d N_c^2. \end{aligned} \tag{3.1.19}$$

The relaxation rate of the trapped gas as a whole depends on the composition of the gas. As Lagendijk *et al.*[1] pointed out the gas is expected to polarize in the d state quickly due to the fast spin exchange rate. We make an estimate for the time scale in which polarization arises. The ratio $\hat{c} \equiv N_c/N_d$ is a measure for the polarization of the gas. Its time derivative is

$$\frac{\mathrm{d}\hat{c}}{\mathrm{d}t} = \frac{\dot{N}_c}{N_d} - \hat{c}\frac{\dot{N}_d}{N_d}. \tag{3.1.20}$$

Combining equations 3.1.19 and 3.1.20 results in a third-order equation for $(\mathrm{d}\hat{c}/\mathrm{d}t)$:

$$\frac{1}{N_d} V_\gamma \frac{\mathrm{d}\hat{c}}{\mathrm{d}t} = R_{dd}^c + \{R_{cd}^c - R_{dd}^d\}\hat{c} + \{R_{cc}^c - R_{cd}^d\}\hat{c}^2 - R_{cc}^d\hat{c}^3. \tag{3.1.21}$$

In steady state $(\mathrm{d}\hat{c}/\mathrm{d}t) = 0$. The steady state value of $\hat{c}$ is denoted by $\hat{c}_0$. We expect $\hat{c}_0$ to be small, but not zero because of the term R_{dd}^c. For sufficiently small $\hat{c}_0$ one may neglect the third order term, and eq.3.1.21 may be solved to yield

$$\begin{aligned} \hat{c}_0 &= \frac{R_{dd}^d - R_{cd}^c}{2(R_{cc}^c - R_{cd}^d)} + \left(\frac{-R_{dd}^c}{R_{cc}^c - R_{cd}^d}\right)^{1/2}\left(1 - \frac{(R_{cd}^c - R_{dd}^d)^2}{4R_{dd}^c(R_{cc}^c - R_{cd}^d)}\right)^{1/2} \\ &\approx \frac{R_{dd}^d - R_{cd}^c}{2(R_{cc}^c - R_{cd}^d)} + \left(\frac{-R_{dd}^c}{R_{cc}^c - R_{cd}^d}\right)^{1/2}. \end{aligned} \tag{3.1.22}$$

In our geometry at temperatures below 200mK the approximation is never more than 6% off. For our trap $\hat{c}_0$ varies from 2.5% at 100mK to 4% at 200mK. The contribution of c state atoms to the flux $\dot{N}$ can be found by adding eqs. 3.1.15. For steady state $(\hat{c} = \hat{c}_0)$ it is found that this contribution is at most 1% at $T = 100$mK or 2.5% at $T = 200$mK.

We next estimate the time constant τ_{pol} for the gas to reach the steady state. Again using eq.3.1.21 to second order, we find a solution of the form

$$\hat{c}(t) = \frac{(\hat{c}_i - \hat{c}_0)\exp(\alpha t)}{1 + (\hat{c}_i - \hat{c}_0)\beta/\alpha(1 - \exp(\alpha t))} + \hat{c}_0, \tag{3.1.23}$$

where $\hat{c}_i$ is the value of $\hat{c}$ at $t = 0$, and the coefficients are

$$\begin{aligned} \alpha &= (N_d/V_\gamma)\{2(R^c_{cd} - R^d_{cd})\hat{c}_0 + (R^c_{cd} - R^d_{dd})\}, \\ \beta &= (N_d/V_\gamma)(R^c_{cd} - R^d_{cd}). \end{aligned} \tag{3.1.24}$$

The coefficients α and β both contain the density of d-state atoms, which itself is time-dependent. However, the decay of the d state is expected to be much slower than the build-up of polarization, so as a first approximation of the c-state decay we treat the d state density as constant. For a typical density in our experiment ($n_0 = 10^{14}\text{cm}^{-3}$) and typical initial polarization c_i ($\hat{c}_i = 0.15$) $\tau_{pol} = 3$s. As long as $\hat{c} > \hat{c}_0$, $\dot{N}$ will be higher than we would expect for a fully polarized gas. We will call this Enhanced Initial Decay (EID), because it disappears quickly after the dissociator has been switched off. The time-constant of this enhancement is roughly half of τ_{pol}, since relaxation is quadratic in the density. This means that after a fairly short time of about 10s, depending on the initial polarization, the trapped gas is polarized to a high degree in the d state. This point will be addressed further below.

In the experiment we measure the number of atoms leaving the trap, so we should calculate

$$\dot{N} = \sum_{h_1,h_2,h_3,h_4} \int_V (1 + \delta_{h_3 h_4}) G_{h_1 h_2, h_3 h_4}(B(\vec{r}), T) n_{h_1}(\vec{r}) n_{h_2}(\vec{r}) \mathrm{d}\vec{r} \tag{3.1.25}$$

where the summation should be made over *high-field-seeking* final states h_3, h_4 only. This can be accomplished by adding eqs. 3.1.15. We introduce the relaxation rate constant $G_{h_1 h_2}$ by summing $G^{h_3}_{h_1 h_2}$ over h_3 so that one gets the rate constants for high-field-seeking final states only:

$$\begin{aligned} G_{cc} &= G^d_{cc} + G^c_{cc} \\ G_{cd} &= G^d_{cd} + G^c_{cd} \\ G_{dd} &= G^d_{dd} + G^c_{dd}. \end{aligned} \tag{3.1.26}$$

and we define $\gamma_{h_1 h_2}$ analogous to eq. 3.1.17

$$\gamma_{h_1 h_2} = \frac{\int_V G_{h_1 h_2}(B,T)\exp[-2\mu_B(B(\vec{r}) - B_0)/k_B T]\mathrm{d}\vec{r}}{\int_V G_{0 h_1 h_2}(T)\exp[-2\mu_B(B(\vec{r}) - B_0)/k_B T]\mathrm{d}\vec{r}}. \tag{3.1.27}$$

Now we rewrite eq. 3.1.25 as

$$V_\gamma \dot{N} = E_{dd} N_d^2 + E_{cd} N_c N_d + E_{cc} N_c^2, \tag{3.1.28}$$

where

$$\begin{aligned} E_{dd} &= \gamma_{dd} G_{dd} \\ E_{cd} &= \gamma_{cd} G_{cd} \\ E_{cc} &= \gamma_{cc} G_{cc}. \end{aligned} \tag{3.1.29}$$

The effective rates E that determine $\dot{N}$ are not identical to the rates R that govern the population dynamics of the hyperfine levels, because the transitions between the low-field seeking c and d states that do not produce high-field seekers (such as $dd \rightarrow cd$), do not affect $\dot{N}$.

The dipolar relaxation determines the decay of the doubly polarized gas, and this is the rate we can extract from our data if we ignore the initial period corresponding to the time-constant for c-state decay. If we take out the dipolar relaxation rate constant E_{dd} eq. 3.1.28 can be rewritten as

$$V_\gamma \dot{N} = \frac{E_{dd} N_d^2}{(1+\hat{c})^2} \left(1 + \frac{E_{cd}}{E_{dd}} \hat{c} + \frac{E_{cc}}{E_{dd}} \hat{c}^2\right). \tag{3.1.30}$$

For $\hat{c} = \hat{c}_0$ this means

$$V_\gamma \dot{N} \approx E_{dd} N_d^2 \tag{3.1.31}$$

where the error is less than 2.5% for our experimental conditions. Now $\gamma_{dd} G_{dd}$ can be extracted if the other quantities in eq.3.1.31 are known.

A tempting possibility is the extraction of the spin-exchange rate from the data by looking at the EID due to the population of the c state $\hat{c}_i > \hat{c}_0$. To this end we expand eq.3.1.30 in terms of $\hat{c}$ to second order and get

$$V_\gamma \frac{\dot{N}}{N^2} = E_{dd}\{1 + (\theta - 2)\hat{c} + (\eta + 3 - 2\theta)\hat{c}^2\} \approx E_{dd}(1 + \eta \hat{c}^2), \tag{3.1.32}$$

where $\theta = E_{cd}/E_{dd}$ and $\eta = E_{cc}/E_{dd}$. The approximation is correct for $\hat{c} > 0.1$ for $T \approx 100$mK or $\hat{c} > 0.15$ for $T \approx 200$mK. Using eq. 3.1.23 for $\hat{c}$ we can make an estimate of the time constant of the EID, i.e. of $1+\eta\hat{c}^2$. In a crude approximation $\tau \approx \{2(\hat{c}_i - \hat{c}_0)\beta\}^{-1}$. At the highest temperature this period may be as long as 2s, for typical experimental conditions.

On the basis of the theoretically predicted rate constants and the calculations discussed in this section we expect that a trapped sample of hydrogen gas (H$\uparrow$) rapidly polarizes into the doubly polarized state and after that slowly decays because of dipolar relaxation. Observation of the number of atoms that has undergone relaxation ($\dot{N}$) should enable us to verify the predicted rates and their field dependence.

3.2 Thermalization

Since the data analysis of our measurements is based on the assumption of thermal equilibrium in the gas it is important to know the temperature of the gas, and also the time in which thermal equilibrium is reached. A simple model, based on collision rates of the particles, gives some insight into this problem. We distinguish between the temperature of the trapped gas T_g and the temperature of the surrounding walls T_w. We first consider the internal equilibrium, and thereafter the route to equilibrium of the gas with its surroundings.

If we want to speak of the gas temperature T_g it is obvious that there should be internal thermal equilibrium in the trapped gas. This is determined by the interatomic collision time τ_c, which we assume to be equal to thermalization time, since collisions are very efficient in redistributing energy, as was pointed out in section 1.9. The collision time can be found by calculating the total rate of two-body collisions per unit volume $\Gamma^{(2)}/V$ (higher order collisions will be absent). In general $\Gamma^{(2)}$ will be related to the number of pairs of atoms, their relative velocity v and the cross section σ by

$$\frac{\Gamma^{(2)}}{V} = \frac{1}{2} n^2 v \sigma. \tag{3.2.1}$$

In our case we find

$$\Gamma^{(2)} = \frac{1}{2}\int_V n^2(\vec{r})\bar{v}2^{7/2}\pi a^2 \mathrm{d}\vec{r} = n_0^2 \bar{v} 2^{5/2}\pi a^2 V_{2e}, \tag{3.2.2}$$

where $a = 0.72$Å is the s-wave scattering length,[4] and we have assumed the collisional cross section $8\pi a^2$ for particles in the same hyperfine state. We have used the average *relative* velocity $\sqrt{2}\bar{v}$, where $\bar{v}$ is the average velocity in the laboratory frame. The collision time is $\tau_c^{-1} = \Gamma^{(2)}/n_0 V_{1e} \approx 2^{5/2}\pi a^2 \bar{v}(N/V_\gamma)$. For $n_0 = 10^{12}\mathrm{cm}^{-3}$ (the densities in this experiment are always higher than this) and $T_g = 80$mK this means $\tau_c \approx 3$s.

As was mentioned in section 1.9 collisions are essential for trapping, a single particle can not be trapped. When we start to fill the trap by sending in atoms, the atoms will be distributed all over the trapping volume, and each has an energy $\epsilon > \epsilon_{tr}$. To get atoms into the trap energy has to be extracted by exerting some force on them (for instance laser cooling), or energy has to be redistributed by collisions. We rely entirely on the latter mechanism. Note that this means the average energy per particle ϵ_{tr} is unchanged. We will return to the problem of removing this energy later. Once a small number of atoms become trapped, the density of the atoms in the trap center starts to increase rapidly, since the collision probability for the atoms moving across the cell becomes much higher. We estimate the threshold for the start of trapping under our experimental conditions. The expression for the two-body collision rate differs from eq. 3.2.2 in several respects. The effective volume V_{2e} has to be replaced by the cell volume V, and we use $4\pi a^2$ instead

of $8\pi a^2$ for the cross section, since the gas will not yet be polarized into the d state. The spatial and velocity distribution also change because of the magnetic field, but we assume that the product $n\bar{v}$ is constant. The collision rate becomes

$$\Gamma^{(2)} = n^2 \bar{v} 2^{3/2} \pi a^2 V. \tag{3.2.3}$$

The average interatomic collision time is given by $\tau_c^{-1} = \Gamma^{(2)}/nV$. The threshold time depends on the filling flux, since some density has to build up before collisions will start to trap atoms efficiently. This time is of the order of one second for a typical experimental filling flux, when a density $n \approx 3 \times 10^{11}\text{cm}^{-3}$ is reached. This time constant is comparable to the time constant of our detector, so that we do not expect to see any delay between the first atoms entering the trapping region and the start of the trapping in the measurements. With a more sensitive detector, allowing smaller flux, τ could be made longer.

Next we examine thermalization of the gas to the wall temperature T_w. This requires collisions of atoms with the wall. An atom having a total energy exceeding ϵ_{tr} will either collide with a wall or move into a region where the field is higher than ϵ_{tr}/μ_B. In both cases the atom will return to the trapping region. However, note that the energy of the atom may be changed when it returns. In case of specular reflection from a wall[5] or of an atom driven back by a field gradient the energy is conserved. But if the atom enters a surface-bound state it will return after some time with an average energy corresponding to the wall temperature T_w. The latter process leads of course to thermalization of the gas to the wall temperature ($T_g = T_w$). The rate at which energy is exchanged can be found using a simple model in which we assume that each sticking event will contribute an amount $2k_B(T_g - T_w)$.

The heat flow is

$$\dot{Q} = \alpha_a \int_A \frac{1}{2} n(\vec{r}) \bar{v} k_B (T_g - T_w) \mathrm{d}\vec{r} \tag{3.2.4}$$

where α_a is the accommodation coefficient,[6] $\bar{v}$ is the average speed of the atoms and the integral is taken over the surface of the cell. Implicitly we have assumed detailed balance between the flux of particles going to and coming from the wall. The density near the wall (n_w) is in fact the density at the edge of the trap, so it is the product of the density in the center of the trap and the Boltzmann-factor of the full trap depth:

$$n_w = n_0 \exp[-\epsilon_{tr}/k_B T_g]. \tag{3.2.5}$$

If we replace the surface by an effective surface A_{1e}, defined as

$$A_{1e} \equiv \int_A \exp[\mu_B (B_w - B(s))/k_B T_g] \mathrm{d}s, \tag{3.2.6}$$

with B_w as defined in section 1.7 eq. 3.2.4 becomes

$$\dot{Q} = \frac{\alpha_a}{2} n_w \bar{v} k_B (T_g - T_w) A_{1e}. \tag{3.2.7}$$

In our geometry $A_{1e}T^{-1/3} \approx 40\text{cm}^2\text{K}^{-1/3}$ for maximum trap depth ($\epsilon_{tr} = 0.92\text{K}$). The exponential temperature dependence of n_w in eq. 3.2.5 implies that heat exchange between gas and wall is strongly suppressed at low temperature, due to the small number of particles that reach the wall. To calculate the rate of change of the temperature we need to know the heat capacity of the gas. The internal energy of the gas consist of a kinetic term,

$$U_{kin} = \frac{3}{2} N k_B T_g \tag{3.2.8}$$

and a term representing the potential energy,[7]

$$U_{pot} = N \int_V \mu_B (B(\vec{r}) - B_0) \exp\left\{ \frac{-\mu_B (B(\vec{r}) - B_0)}{k_B T_g} \right\} \mathrm{d}\vec{r}. \tag{3.2.9}$$

If we use the approximation for the field $B(r,z) = B_0 + \alpha r + \beta z^2$ we get a contribution of $2k_BT_g$ from the integration over r and $k_BT_g/2$ from the z direction, so after summation

$$U_{pot} = \frac{5}{2} N k_B T_g \tag{3.2.10}$$

Numerically U_{pot} is found to be $2.3k_BT_g$ between 100 and 200mK. The total energy is simply $U = U_{pot} + U_{kin} \approx 4Nk_BT_g$. Now the temperature will change at a rate $\dot{T} = (\mathrm{d}T/\mathrm{d}U)\dot{Q}$, and the time constant of thermalization to wall temperature τ_w, $\tau_w^{-1} = \dot{T}/(T_g - T_w)$, becomes

$$\tau_w^{-1} = \frac{1}{8} \alpha_a \bar{v} \frac{A_{1e}}{V_{1e}} \exp\left\{ \frac{-\epsilon_{tr}}{k_B T_g} \right\}. \tag{3.2.11}$$

Clearly τ_w may become long if $k_BT_g \ll \epsilon_{tr}$. For maximum trap depth and T_g =80mK we calculate $\tau_w \approx 17\text{s}$.

Thermal coupling between gas and wall requires not only collisions of atoms with the wall. Subsequent to the wall collisions interatomic collisions of the atoms are needed to transport heat between the wall and the trapped gas. This will be the dominant barrier if the interatomic collision time τ_c is longer than the product of sticking probability[5] s and the time it takes a particle to cross the cell. Consider a particle with energy ϵ_{tr}, sufficient to reach the wall. If such a particle moves across the cell diametrically, we can calculate the collision probability with another particle

$$P_c = \int_0^{\epsilon/\mu_B\alpha} 16 n_0 \pi a^2 \exp\left\{ \frac{-\mu_B \alpha r}{k_B T_g} \right\} \mathrm{d}r = \frac{16 n_0 \pi a^2 k_B T_g}{\mu_B \alpha} \{1 - \exp\left(\frac{-\epsilon_{tr}}{k_B T_g} \right)\}, \tag{3.2.12}$$

where we have assumed the linear field dependence $B = \alpha r$ of the trap. In our experiment P_c will be smaller than one, i.e. a particle coming from the wall has a considerable chance to hit the wall again, before colliding with trapped atoms. As we have seen the exponential factor is small, so eq 3.2.12 can be written as

$$P_c = \frac{16 n_0 \pi a^2 k_B T_g}{\mu_B \alpha}. \tag{3.2.13}$$

For T_g = 100mK and $n_0 = 10^{14}\text{cm}^{-3}$, $P_c \approx 0.01$. Since collisions are essential for thermalization of the gas to wall temperature, we have to modify equation 3.2.7 for the heat transport by multiplying with P_c. However, this also effects the accommodation factor in the same equation, because a particle with energy ϵ_{tr} will have multiple wall collisions, each having a sticking probability s and thus having a probability to contribute to thermalization. Only an atom that enters a surface bound state can return to the trapping region with an energy corresponding to the wall temperature T_w. If $k = 1/P_c$ is the average number of wall collisions of an atom before a collision with another atom, the probability that there is no sticking event is $(1-s)^k$, and consequently the probability that it does contribute to thermalization is $s_e = 1-(1-s)^k$. In the limit for the mean free path much larger than the dimensions of the cell, as in our experiment, P_c is small, s_e will be nearly 1, so nearly all atoms that reach the wall will contribute to thermalization and α_a is effectively also equal to 1. Now eq. 3.2.7 becomes

$$\dot{Q} \approx \frac{1}{2} P_c n_0 \bar{v} k_B (T_g - T_w) A_{1e} \exp\left(\frac{-\epsilon_{tr}}{k_B T_g}\right). \tag{3.2.14}$$

The thermalization rate has become density dependent and eq. 3.2.11 will be altered to

$$\tau_w^{-1} \approx \frac{1}{8} P_c \bar{v} \frac{A_{1e}}{V_{1e}} \exp\left(\frac{-\epsilon_{tr}}{k_B T_g}\right). \tag{3.2.15}$$

A relation between the gas to wall thermalization time constant τ_w and the internal thermalization rate of the gas can be found by replacing the collision probability for an atom crossing the cell P_c with the ratio between the time τ_d it takes a particle to cross the cell and the time constant of interatomic collision τ_c, so $P_c \approx \tau_d/\tau_c$. Furthermore we can replace the product $\tau_d \bar{v}$ by the cell diameter d, so that

$$\tau_w \approx \tau_c 8 \frac{V_{1e}}{V_d} \exp\left(\frac{\epsilon_{tr}}{k_B T_g}\right), \tag{3.2.16}$$

where $V_d = A_{1e} d$ is a volume of the same order as the physical cell volume, and therefore an order larger than V_{1e} for our experimental conditions. It is clear that τ_w can become very long for low temperatures. For T_g =80mK we find a τ_w of more than three minutes and even at T_g =100mK we get $\tau_w \approx$ 18s. At T_g = 125mK the time constant is about one second.

Comparing with τ_w we see that at low temperatures ($T_g \leq$120mK) the gas-to-surface accommodation rate will dominate the overall thermalization rate ($\tau_c \ll \tau_w$). At higher temperatures τ_{th} is always shorter than the response time of the detector, 0.5s.

To see how the slow thermalization affects our results at low temperature, we should consider the heat input in the gas. First of all, the gas enters the trap carrying an energy equal to the well depth plus the thermal energy of the atoms. The thermal energy depends

on the thermalization of the gas coming out of the dissociator, at about 600mK, into the cell. The filling tube (see Fig. 2.4.1) contains a radiation shield at a temperature not exceeding 200mK. From the last part of the filling tube, which is at cell temperature, to the trap an atom will on the average collide about 30 times with the walls. Taking into account the sticking probability[5] one expects the atoms to be thermalized to cell temperature when they reach the trap. On entering the trap the internal energy will therefore be $U_i = (3/2)Nk_BT_w + NU_p$, where the potential energy $U_p \geq \epsilon_{tr}$ is determined by the magnetic field at the site of the last sticking event. The kinetic contribution can be ignored, since $(3/2)k_BT_w \ll U_p$. As discussed the energy of the gas in the trap $U \approx 4Nk_BT_g$. If we assume the internal thermalization of the gas to be faster than the gas-to-surface thermalization, the temperature immediately after filling would be $T_g \approx \epsilon_{tr}/4k_B$, 250mK for maximum trap depth. This means that during the filling stage the gas will tend to be above cell temperature and will cool down to T_w after filling at a rate determined by T_g through eq. 3.2.15.

The way in which equilibrium is reached is probably the most important difference between this experiment and those carried out at MIT.[8,9] In the MIT set-up the gas cools by a kind of evaporation until its temperature (T_g) is well below the temperature corresponding to the depth of the trap, i.e. $T_g \ll \epsilon_{tr}/k_B$. This evaporation occurs because H↑ atoms with energy higher than ϵ_{tr} can escape from the trap. Atoms reaching the boundary of the lower axial confinement coil (lower pinch coil) will move into another low-field-region, taking with them energy at least equal to ϵ_{tr}, and do not return. Since only atoms with lower energy remain, and since collisions in the gas will produce more atoms with $\epsilon \geq \epsilon_{tr}$ the gas will continue to cool, although the cooling rate will slow down as temperature and density drop. By setting ϵ_{tr} lower, the final temperature can be lowered in principle into the μK regime.[8] Masuhara *et al.*[9] have reached a temperature of 3.0mK with this technique.

3.3 Heating

Three mechanisms actively affect the temperature of the trapped gas, two of which heat the gas up, one cools it down. The first heating mechanism arises from recoil in the relaxation process. It applies to relaxation events in which one high-field seeking and one low-field seeking atom is formed, for instance $dd \rightarrow ad$. If the low-field seeking atom remains trapped, due to recoil half of the relaxation energy will be transferred to the trapped gas. The second heating process is caused by the spatial variation of the two-body collision rate over the trap. The collisions will take place mainly in or near the center of the trap, since the two-body collision rate scales with the square of the density. Because collisions cause relaxation this means the average potential energy carried by

atoms leaving the trap after relaxation will be smaller the average potential energy of all trapped atoms. The third mechanism leads to cooling if the gas is doubly polarized. The dominant relaxation process of the d-state polarized gas, dipolar relaxation, is slower in low field, i.e. in the center, than in high field. Because a disproportionately large number of atoms comes from high field after relaxation, the potential energy carried out of the trap tends to be more than what would be expected if one uses some averaged rate over the whole volume. Since the effects work in opposite directions it is not possible to tell beforehand whether the temperature of the gas will rise or fall.

The heating caused by the two-body nature of the relaxation process can be calculated fairly well analytically. As in eq. 3.2.9 we can calculate the average potential energy in the two-particle distribution by

$$U_{2,pot} = N \int_V \mu_B(B(\vec{r}) - B_0) \exp[2\mu_B(B(\vec{r}) - B_0)/k_B T_g] \mathrm{d}\vec{r}. \tag{3.3.1}$$

Using the approximation $B(r,z) = B_0 + \alpha r + \beta z^2$ of the field we get $U_{2,pot} = (5/4)N k_B T_g$ instead of $U_{pot} = (5/2)N k_B T_g$ of eq. 3.2.10. The total amount of heat carried off by the atoms will be

$$\dot{Q} = \frac{11}{4} \dot{N} k_B T_g. \tag{3.3.2}$$

We now define the excess heat input $\dot{Q}_e$ as the difference between the energy actually carried by particles that leave the trap and the average energy per particle in the trap times $\dot{N}$

$$\dot{Q}_e = \dot{Q} - (U/N)\dot{N} = -\frac{5}{4} \dot{N} k_B T_g. \tag{3.3.3}$$

Under adiabatic conditions (this means the gas is isolated from the wall and evaporative cooling is not applied) the heating can be expressed as

$$\dot{T} = (\mathrm{d}T/\mathrm{d}U)\dot{Q}_e = -\frac{5}{16}(\dot{N}/N) T_g. \tag{3.3.4}$$

For a fully parabolic trap these figures would be $\dot{Q} = (9/4)\dot{N} k_B T_g$ and $\dot{T} = -(1/4)(\dot{N}/N) T_g$.

The recoil contribution to the heat production may only be estimated or calculated numerically. The energy released by the relaxation is $2\mu_B B$, half of which will remain in the trap because it is carried by the low-field-seeking atom. This means the average energy added to the trapped gas will be $\mu_B B$ per relaxation event and since this is equal to the potential energy of colliding atoms, which will be distributed according to the two-particle distribution, the average energy added will be equal to $U_{2,pot}$, or $(5/4)k_B T_g$ per event. Taking the case of a d-state polarized gas, the most important channels are $dd \rightarrow aa$ and $dd \rightarrow ad$. For the temperatures we are considering the atoms will be in relatively high field ($B \geq 0.05$T) and contributions from other channels will be at least an order of magnitude smaller.[2] The $dd \rightarrow ad$ rate is about 0.3 times the total rate,

$\gamma_{dd,ad}G_{dd,ad} \approx 0.3\gamma_{dd}G_{dd}$, and this ratio does not depend strongly on temperature, so an estimate of the relaxation energy heat input would be

$$\dot{Q} \approx -0.4\dot{N}k_BT_g. \tag{3.3.5}$$

The effect of the field dependence of the rates can hardly be treated in any other way than numerically, because the field experienced by the atoms will change strongly with temperature. A rough estimate can be made by making a linear fit to the rate for the fields we are concerned with, i.e. $G = G_0 + G_1B$, for the most important dipolar relaxation rates. Now the integration to find the average energy of the relaxed particles

$$U_{rel} = \int_V G(B(\vec{r}))[\mu_B(B(\vec{r}) - B_0) + U_{kin}] \exp[-2\mu_B(B(\vec{r}) - B_0)/k_BT_g]\mathrm{d}\vec{r} \tag{3.3.6}$$

can be carried out. With this approximation and the simplified fields we find a quadratic term in the average energy, resulting in $\dot{Q} = 2.78\dot{N}k_BT_g$ at 100mK instead of the 2.75 of eq. 3.3.2, so this is a negligible correction at low temperature, while at high temperature the gas to wall thermalization ensures that heating effects play no role.

Finally the temperature dependence of the relaxation rates could also be considered, however since it is much weaker than the field dependence, one expects its effect to be entirely negligible.

The conclusion is that two mechanisms will tend to heat the trapped gas under conditions where thermal contact with the wall is poor. Effectively the energy carried off by particles after relaxation will be $\dot{Q} = 2.4\dot{N}k_BT_g$, to be compared with the average energy of about $4Nk_BT_g$ of particles in the trap, or in terms of the excess heat input defined in eq. 3.3.3

$$\dot{Q}_e = -1.6\dot{N}k_BT_g. \tag{3.3.7}$$

The heating effect is proportional to the relaxation rate and therefore to the square of the total number of particles N^2, whereas the heat content and the transport of heat to the wall are proportional partly to N and partly to N^2, so the heating effects are expected to be strongest at high density. It follows from eq. 3.3.7 that adiabatically the gas should heat up at a rate of about $\dot{T} = 0.4(\dot{N}/N)T_g$.

The conditions in our trap are not adiabatic since we still have thermal contact with the walls. A steady state temperature can be calculated by equating the heating discussed in the present section, $\dot{Q}_e \approx 1.6\dot{N}k_BT_g$, to the heat transport to the walls given by eq. 3.2.14. If we assume that internally the gas is always in thermal equilibrium ($\tau_c \ll \tau_w$) the temperature difference between gas and wall is given by

$$T_g - T_w \approx \frac{0.2\gamma_{dd}G_{dd}\mu_B\alpha V_{2e}}{\pi a^2\bar{v}k_BA_{1e}} \exp\left(\frac{\epsilon_{tr}}{k_BT_g}\right). \tag{3.3.8}$$

One can easily evaluate this expression by iteration for various temperatures T_w, since only the terms with the strongest temperature dependence have to be taken into account.

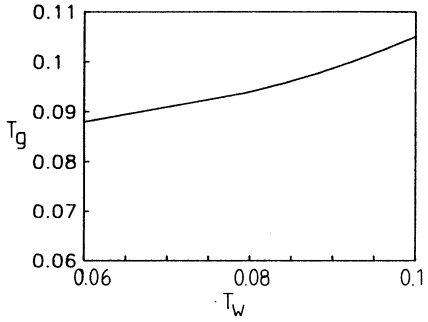

Figure 3.3.1: *Temperature of the trapped gas T_g as a function of the wall temperature T_w for maximum well depth $\epsilon_{tr}/k_B = 0.92K$.*

As is expected considering the thermalization time constant the trapped gas does not cool far below 100mK for maximum trap depth. In Fig. 3.3.1 T_g is plotted as a function of T_w. Note that in the temperature range depicted here T_g does not become independent of T_w. This means that the gas is not completely isolated in the sense that there is no influence of the surrounding walls, even for a trap depth more than ten times higher than the gas temperature.

References

[1]A. Lagendijk, I.F. Silvera, and B.J. Verhaar,Phys. Rev. B **33**, 626 (1986)

[2]H.T.C. Stoof, J.M.V.A. Koelman, and B.J. Verhaar, Phys. Rev. B **38**, 4688 (1988) and private communication.

[3]I.F. Silvera, and J.T.M. Walraven, Prog. Low Temp. Phys. **X**, 139 (1986).

[4]D.G. Friend, and R.D. Etters, J. Low Temp. Phys. **39**, 409 (1980).

[5]J.J. Berkhout, E.J. Wolters, R.v. Roijen, and J.T.M. Walraven, Phys. Rev. Lett. **57**, 2387 (1986).

[6]J. Helffrich, M.P. Maley, M. Krusius, and J.C. Wheatley, Phys. Rev. B **34**, 6550 (1986).

[7]V. Bagnato, D.E. Pritchard, and D. Kleppner, Phys. Rev. A **35**, 4354 (1987).

[8]H.F. Hess, Phys. Rev. B **34**, 3476 (1986).

[9]N. Masuhara, J.M. Doyle, J.C. Sandberg, D. Kleppner, and T.J. Greytak Phys. Rev. Lett. **61**, 935 (1988).

Chapter 4

Experiments with Atomic Hydrogen in a Magnetic Trapping Field

R. van Roijen, J.J. Berkhout, S. Jaakkola, and J.T.M. Walraven

Abstract

We describe the loading of a minimum-B-filed trap with neutral atomic hydrogen cooled through thermal exchange with liquid-helium surfaces. We monitor the gas during filling and decay by observing the atoms which are ejected from the trap as a result of spin-exchange and magnetic dipolar relaxation. The stability of the gas is unaffected if we change the wall coverage from pure ^{4}He to dilute ^{3}He and ^{4}He mixtures. The maximum trapped density is $3 \times 10^{14}\text{cm}^{-3}$ at about 100mK. The limiting decay rate is attributed to dipolar relaxation and found to agree with theory for both magnitude and field dependence.

(Phys. Rev. Lett. **61**, 931 (1988))

Experiments with Atomic Hydrogen in a Magnetic Trapping Field

R. van Roijen, J. J. Berkhout, S. Jaakkola,[a] and J. T. M. Walraven
Natuurkundig Laboratorium, Universiteit van Amsterdam, Valckenierstraat 65, 1018 XE Amsterdam, The Netherlands
(Received 16 May 1988)

We describe the loading of a minimum-B-field trap with neutral atomic hydrogen cooled through thermal exchange with liquid-helium surfaces. We monitor the gas during filling and decay by observing the atoms which are ejected from the trap as a result of spin exchange and magnetic dipolar relaxation. The stability of the gas is unaffected if we change the wall coverage from pure ^{4}He to dilute ^{3}He and ^{4}He mixtures. The maximum trapped density is 3×10^{14} cm^{-3} at about 100 mK. The limiting decay rate is attributed to dipolar relaxation and found to agree with theory for both magnitude and field dependence.

PACS numbers: 32.80.Pj, 67.65.+z

Surface-free confinement of neutral gases is opening up exciting new dimensions to condensed-matter and atomic physics. For atomic hydrogen, trapping concepts are particularly challenging because of the potential of H gas to undergo a transition to a Bose-Einstein condensed (BEC) state. Although liquid-helium surfaces provide the weakest conceivable attraction to the H atom and have thus enabled a wealth of interesting experiments,[1,2] it has been observed[3-6] that the achievement of BEC would require the rigorous suppression of surface recombination. Once this was recognized, proposals were made to eliminate the influence of surfaces altogether by use of static[7] or dynamic[8] trapping technique. The behavior and manipulation of trapped atomic hydrogen (and deuterium) have been discussed by various authors,[9-13] for the reason that trapping techniques may open the route to submillikelvin temperatures and to density-to-temperature ratios $n^{2/3}/T\approx6.3\times10^{13}$ cm^{-2} K^{-1} as required for BEC. Unfortunately, the Maxwell equations do not allow the construction of static traps for atoms in high-field-seeking spin states (a and b, referred to as H$\downarrow$) but only for the less stable low-field seekers (states c and d, denoted by H$\uparrow$).[14] Here a, b, c, and d are the hyperfine states of H in its electronic ground state in order of growing energy.

The first observation of trapped neutral atoms was made by Migdall *et al.*[15] using a laser-cooled beam of Na atoms in combination with an anti-Helmholtz magnetic quadrupole trap. Recently, Hess *et al.*[16] succeeded in trapping up to 5×10^{12} H$\uparrow$ atoms in a magnetic field minimum. The operating densities were near 10^{13} cm^3 at temperatures of about 40 mK, corresponding to $n^{2/3}/T\approx10^{10}$ cm^{-2} K^{-1}. A mixture of all four hyperfine states of H was blown into the trapping region with a single pulse from the dissociator. The field gradients led to rapid spatial separation of H$\uparrow$ and H$\downarrow$. In the rarified regime where the escape time of energetic H$\uparrow$ atoms was shorter than the interatomic collision time, Hess *et al.* could demonstrate "evaporative" cooling of the gas to below the wall temperature. The gas was studied destructively by our dumping into a magnetic resonance detector the atoms remaining in the trap after a certain holding time.

In this Letter we report on a novel approach to study H$\uparrow$ in a magnetic confinement geometry. A bolometric detection method is employed which does not destroy the sample in the trap and enables us to arrange experiments much like conventional experiments with H$\downarrow$.[1,2] The trap is filled with H$\uparrow$ until a steady state is reached between filling flux and the flux of H$\downarrow$ atoms escaping the trap due to spin-exchange and magnetic dipolar relaxation to the high-field-seeking states. As in the experiments of Greytak and co-workers, no direct thermometry is available for the gas. Our approach is to minimize temperature-related uncertainties by positioning walls and a high-field (4 T) barrier, avoiding the added complexity of evaporative cooling. The H-atom coverage on the surfaces is suppressed by the depth of the trap so much that all second-order surface processes, surface recombination in particular, become insignificant. At the same time the collision rate of the atoms with surfaces remains sufficiently large to enable thermalization with the environment. This method enables us to reach higher densities and to determine accurately the dipolar relaxation rate. We study filling of the trap and relaxational decay for temperatures ranging from 80 to 225 mK. We obtain a maximum density $n_0=3\times10^{14}$ cm^{-3} at the trap center at $T\approx100$ mK, corresponding to a total of $N=4\times10^{13}$ atoms or $n^{2/3}/T\approx4.5\times10^{10}$ cm^{-2} K^{-1}. The stability of the sample is found to be the same for surfaces covered with either pure ^{4}He or with ^{3}He/^{4}He mixtures, convincingly demonstrating the suppression of surface adsorption. By observing the H$\downarrow$ emerging from the trap, we determine the rate G_{dd} at which d-state atoms are converted into high-field seekers. This conversion-rate constant may be expressed in terms of the event rates for dipole-diple relaxation as defined in Ref. 9: $G_{dd}\equiv2G^d_{ddaa}+G^d_{ddac}+G^d_{ddad}$. For $T=100$ mK and $B=0.05$ T, we find $G_{dd}=1.1(2)\times10^{-15}$ cm^3/s, improving on the result of Hess *et al.*[16] to be compared

with the theoretical value[9] $G_{dd}=1.2\times10^{-15}$ cm^3/s. In extracting our results, we are sensitive to the field dependence of the relaxation channels.

Our trapping configuration is similar to that advocated by Pritchard[17] and Hess.[7] The field is generated by a system of eight superconducting coils operated in persistent mode. Four radially oriented racetrack-shaped coils provide a quadrupole field for radial confinement of the gas. At maximum current the quadrupole field is $\simeq$1.4 T at the surface of the sample cell ($r=6.5$ mm, see Fig. 1). Axial confinement is achieved with a couple of dipole coils positioned at $z=+50$ mm and $z=-50$ mm near the ends of the racetracks. These coils produce fields of 1.7 and 1.5 T, respectively. The field strength at the B-field minimum was adjusted to $B=0.05$ T by use of a trim coil at $z=0$. At the lower end of the racetracks, $z=-131$ mm, there is a 4.4-T cylindrical coil which serves to separate H$\uparrow$ and H$\downarrow$. The well depth of the trap is defined by $\epsilon_{tr}=\mu_B\Delta B$, where μ_B is the Bohr magneton and ΔB is the difference between the lowest value of the field on any surface of the sample cell and the values at the field minimum. For our configuration $\epsilon_{tr}/k_B=0.92$ K.

All surfaces of the experimental cell shown in Fig. 1 are covered with liqiuid helium. A mixture of H$\uparrow$ and H$\downarrow$ is produced in the high-field zone ($B=4$ T) by rf discharge at low temperatures ($T\leq650$ mK) with the techniques pioneered by Hardy *et al.*[18] Our dissociator is an all-metal $\frac{1}{4}\lambda$ helical cavity with $Q\approx300$. It resonates at 718 MHz and is driven with 0.1-W$\times$50-μs pulse at a repetition rate of 50 Hz. The H$\downarrow$ fraction, favoring the high field, is trapped in the dissociator region, where it is continuously removed by forced recombination on a helium-free bolometer surface (B#1). The low-field-seeking H$\uparrow$ flux ($\Phi\uparrow\leq5\times10^{12}$/s) is guided up through a thin-walled german silver (GS) tube (3.6-mm inner diameter) to a low-field region ($B\leq1.5$ T) bounded by the walls of a cylindrical copper cell, symmetrically surrounding the B-field minimum. Thermometry is done against a ^{3}He melting-curve thermometer. We find an optimum H$\uparrow$ filling flux at a dissociator temperature of 600 mK. No evaporative cooling takes place as the H$\uparrow$ atoms cannot escape the low-field region and surface adsorption times are much shorter than the lifetime of the sample. We monitor the trapped gas continuously by observing the H$\downarrow$ flux escaping from the trap because of magnetic relaxation. For this purpose a "pumping plate" detector[19] is mounted in high field ($B=4$ T) at the annularly shaped lower end of the copper cell. We assume that the recombination heat is detected with an efficiency of 60% $\pm$ 10%.[19] The minimum detectable flux is 2×10^{11} atom/s. A second bolometer (B#2) enables us to trigger recombination of the trapped H$\uparrow$ and is included for calibration purposes.

We plot our data as $V_\gamma\dot{N}/N^2$ versus time t as shown in Fig. 2. $N(t)$ is obtained by integration of the observed flux $\dot{N}$ over the time interval (t,∞). V_γ is the effective volume of the trap with the gas temperature T_g assumed to be equal to the wall temperature T_w, as defined below. To compare with theory, we calculate $\dot{N}(t)$ by averaging the field and temperature-dependent relaxation rates of Stoof, Koelman, and Verhaar[9] over a thermal density distribution. The contribution due to any individual rate is written as

$$\dot{N}=(\gamma_0 G_0/V_\gamma)N_{h1}N_{h2}, \tag{1}$$

where G_0 is the rate constant for the process under consideration, evaluated for the conditions at the center of the trap, and

$$\gamma_0\equiv\int\{G(\mathbf{r})/G_0\}[n(\mathbf{r})/n_0]^2d\tau/V_{2e}$$

includes all effects due the field dependence of the rate. The effects associated with the density profiles are incor-

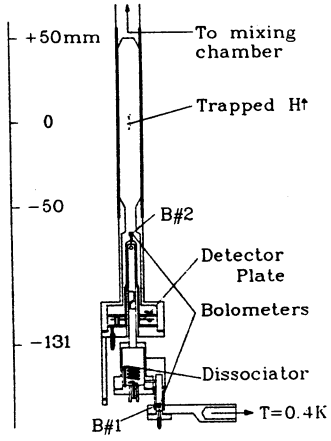

FIG. 1. Schematic drawing of the experimental cell.

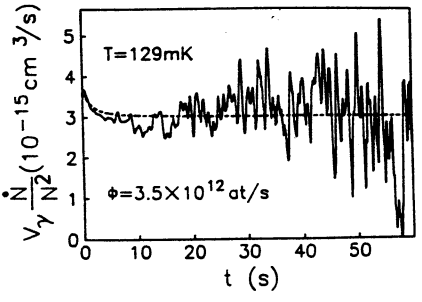

FIG. 2. Typical decay curve plotted as $V_\gamma\dot{N}/N^2$. ϕ is the H$\uparrow$ filling flux; the dashed line is a simulation.

porated in the effective volume $V_\gamma \equiv V_{1e}^2/V_{2e}$, where $V_{me} \equiv \int [n(\mathbf{r})/n_0]^m d\mathbf{r}$. N_{hi} refers to the total number of atoms in the trap in hyperfine state hi. For our trap, $V_\gamma T_g^{-5/2} \approx 180$ cm^3 K$^{-5/2}$ and $V_{1e} T_g^{-5/2} \approx 34$ cm^3 K$^{-5/2}$. The field dependence gives rise to important corrections. When T_g is varied from 80 to 225 mK, theory predicts γ_0 to increase from 2.1 to 3.5 for the dipolar relaxation processes ($\gamma_0 \equiv \gamma_{dd}$), while γ_0 decreases for spin exchange ($\gamma_0 \equiv \gamma_{cc}$) from 0.28 to 0.08 over the same range. Notice that the temperature dependence of the γ factors reflects the field dependence of the rates as with increasing temperature the atoms sample higher fields in the trap. As spin exchange is very fast and only affects the c-state atoms ($cc \rightarrow aa, ac, bd$), preferential escape of c-state atoms leads to a sample which consists almost exclusively of d-state atoms.[9] This is observed as an enhanced initial decay (EID) during up to 8 s after the discharge is switched off (see dashed curve in Fig. 2 for a simulation of this effect). Below 100 mK, the EID is dominated by another effect which leads to a reduced initial decay (RID) for up to 15 s, which we attribute to incomplete thermalization to T_w. According to theory the asymptotic decay is described to within 3% by $V_\gamma \dot{N}/N^2 \equiv \gamma_{dd} G_{dd}$.

In Fig. 3 we plot the results for the overall second-order decay rate $\gamma_0 G_0 \equiv V_\gamma \dot{N}/N^2$ vs T obtained by discarding the EID-RID period of 15 s. For ^{4}He-covered surfaces, data were taken for $135 < T < 225$ mK (open circles). Above 225 mK, systematic errors arise from recombination of H↑ on the plate due to the far tail of the He↑-density distribution extending to high field. Below about 135 mK we had insufficient flux to fill the trap because of surface recombination in the filling tube. To reach lower temperatures, 1% ^{3}He was added to the cell (filled circles in Fig. 3) which is known to reduce the adsorption energy from $\epsilon_a \approx 1$ K to $\epsilon_a \approx 0.4$ K and hence also the surface recombination.[1,2] However, under these conditions heat conduction by ^{3}He vapor makes the plate unreliable for $T > 160$ mK. Near 80 mK, we were limited by refrigerator power. The theoretical result for $\gamma_{dd} G_{dd}$ is given by the solid curve in Fig. 3. The dashed curve corresponds to G_{dd} for $B = 0.05$ T and shows the small intrinsic temperature dependence of the dipolar rate. The good agreement with the solid curve demonstrates the importance of the γ_{dd} average and reflects the increase of the dipolar rate with growing field. After dividing our data by γ_{dd}, we find $G_{dd} = 1.1(2) \times 10^{-15}$ cm^3/s for $T = 100$ mK and $B = 0.05$ T. In view of the strong temperature dependence of V_γ, we infer that the gas in the trap is thermalized to T_w. In principle, the deviation of the data with respect to the solid curve below 100 mK may be explained by our assuming T_g to be 8 mK higher than T_w as illustrated by the dotted curve in Fig. 3. We believe this effect not to be significant because of a 17% systematic error not included in the error bars of Fig. 3 and related to the uncertainty in absolute calibration of the detector. Comparing the open and filled circles, we note that our results are insensitive to the type of helium coverage. Hence the H↑-surface density {scaling as $\exp[(\epsilon_a - \epsilon_{tr})/k_B T]$} must be small, as is to be expected for $\epsilon_{tr} \gtrsim \epsilon_a$.

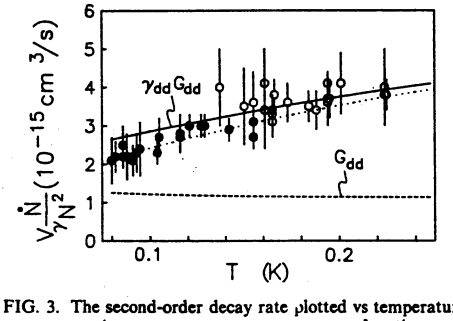

FIG. 3. The second-order decay rate plotted vs temperature (open circles: ^{4}He wall coverage; filled circles: ^{3}He/^{4}He coverage). Dashed line: Theoretical result for the bottom of the trap. Solid line: Including the field average. Dotted line: See text.

To describe the filling of the trap we assume that initially, i.e., before entering the trap, the internal energy of the gas is driven by $U_i = \frac{3}{2} N k_B T_w + N U_p$, where the average potential energy $U_p \approx \epsilon_{tr}$ is determined by the magnetic field at the site of the last sticking event. Once in the trapping region, most of the potential energy is converted irreversibly into kinetic energy within a few interatomic collision times, after which the gas may be characterized by a well-defined temperature T_g (not necessarily equal to T_w) and has an internal energy given by $U_f \approx 4 N k_B T_g$.[20] To fill the trap no volume work is done by the gas against the environment. In the adiabatic limit ($U_i = U_f$) and starting with $T_w \ll \epsilon_{tr}/k_B$ the gas temperature should therefore increase to $T_g \approx \frac{1}{4} \epsilon_{tr}/k_B$, 250 mK for our trap. In practice, some heat will be carried off to the walls during the filling and by atoms that escape after relaxation. In addition, the inelastic nature of the relaxation process gives rise to some internal heating. The rate at which energy is carried off to the walls is given by

$$\dot{Q} = 4(N/\tau_w) k_B (T_g - T_w), \tag{2}$$

where

$$\tau_w^{-1} = \tfrac{1}{8} a \bar{v} (A_{1e}/V_{1e}) \exp[-\epsilon_{tr}/k_B T_g]$$

is the gas-to-surface thermal accommodation rate, $a/T_g \approx 0.5$ K^{-1} is the accommodation coefficient[21] and $\bar{v} = (8 k_B T_g/\pi m)^{1/2}$ the average atomic speed. The effective surface area $A_{1e} T_g^{-1/3} \approx 40$ cm^2 K$^{-1/3}$ is obtained by integration of the relative surface coverage over the walls of the sample cell. The exponential temperature dependence of τ_w arises from the ratio of density in the center of the trap to that near the wall and

varies from 1×10^5 at 80 mK to 60 at 225 mK. At 80 mK, τ_w is about 17 s. The interatomic collision rate τ_c^{-1} may be estimated from $\tau_c^{-1}\approx 2^{3/2}\pi a^2\bar{v}(N/V_\gamma)$, where $a=0.72$ Å is the s-wave scattering length. For $n_0=10^{12}$ cm^{-3} and $T_g=80$ mK, one calculates $\tau_c\approx 3$ s. For our experimental conditions, with central densities up to 3×10^{14} cm^{-3}, the overall thermalization rate, $\tau_{\rm th}^{-1}=1/(\tau_c+\tau_w)$, is either faster than the response time of our detector or limited by the surface accommodation rate. The observed RID's can be explained if we assume that just after switching off the discharge, the gas is at a slightly higher temperature ($\Delta T<10$ mK) than the walls and cools down to T_w in 10–15 s. Even a small ΔT should show up as a substantial RID because of the strong temperature dependence of V_γ. The observed $\tau_{\rm th}$ is roughly in agreement with the above model, but the exponential character of its temperature dependence seems to be absent and if we compare with a computer simulation, the observed RID's are too large. This point deserves further study.

Our results show that even for our relatively high densities the temperature has to be reduced by 3 orders of magnitude to reach BEC. Extrapolating we estimate that our current technique is applicable down to approximately 55 mK. For cooling to the optical quantum limit (2 mK), we propose to use a Lyman-α optical cooling method. Since this leaves the number of particles unaffected, densities over 10^{14} cm^{-3} should be attainable at temperatures below 10 mK. As G_{dd} remains constant while τ_c diverges as $T^{-1/2}$, such initial conditions are vital to aim successfully for BEC with an evaporative cooling method.

During revision of the manuscript we received a copy of unpublished work by Masuhara *et al.*, reporting $T_g=3$ mK and $n_0=7.6\times10^{12}$ cm^{-3}.[22]

The authors wish to thank the Eindhoven theory group for providing us with detailed information on the relaxation processes. We thank B. Hébral for his aid in developing the low-temperature dissociator, O. H. Höpfner for his overall technical support, and R. J. D. Manuputy, J. Mosk, I. Setija, and K. van der Werf for their contributions in constructing the trap coils. One of us (S.J.) thanks the University of Amsterdam for hospitality and the Wihuri Foundation and the academy of Finland for travel grants. This work is part of the research program of the Stichting voor Fundamenteel Onderzoek der Materie (FOM), which is finanically supported by the Nederlandse Organisatie voor Wetenschappelijk Onderzoek (NWO).

[a]Permanent address: Wihuri Physical Laboratory, University of Turku, Finland.

[1]I. F. Silvera and J. T. M. Walraven, in *Progress in Low Temperature Physcis*, edited by D. F. Brewer (North-Holland, Amsterdam, 1986), Vol. 10, p. 139.

[2]T. J. Greytak and D. Kleppner, in *New Trends in Atomic Physics*, edited by G. Grynberg and R. Stora (Elsevier, Amsterdam, 1984), Vol. 2, p. 1125.

[3]R. Sprik, J. T. M. Walraven, and I. F. Silvera, Phys. Rev. B **32**, 5668 (1985).

[4]D. A. Bell, H. F. Hess, G. P. Kochanski, S. Buchman, L. Pollack, Y. M. Xiao, D. Kleppner, and T. J. Greytak, Phys. Rev. B **34**, 7670 (1986).

[5]T. Tommila, E. Tjukanov, M. Krusius, and S. Jaakkola, Phys. Rev. B **36**, 6837 (1987).

[6]J. D. Gillapsy, I. F. Silvera, and J. S. Brooks, to be published.

[7]H. F. Hess, Phys. Rev. B **34**, 3476 (1986).

[8]R. V. E. Lovelace, C. Mehanian, T. J. Tommila, and D. M. Lee, Nature (London) **318**, 30 (1985).

[9]A. Lagendijk, I. F. Silvera, and B. J. Verhaar, Phys. Rev. B **33**, 626 (1986); H. T. C. Stoof, J. M. V. A. Koelman, and B. J. Verhaar, to be published, and private communication.

[10]T. Tommila, Europhys. Lett. **2**, 789 (1986).

[11]V. Bagnato, D. E. Pritchard, and D. Kleppner, Phys. Rev. A **35**, 4354 (1987).

[12]J. M. V. A. Koelman, H. T. C. Stoof, B. J. Verhaar, and J. T. M. Walraven, Phys. Rev. Lett. **59**, 676 (1987).

[13]R. V. E. Lovelace and T. J. Tommila, Phys. Rev. A **35**, 3597 (1987).

[14]W. H. Wing, Prog. Quantum Electron. **8**, 181 (1984).

[15]A. L. Migdall, J. V. Prodan, W. D. Phillips, T. H. Bergeman, and H. Metcalf, Phys. Rev. Lett. **54**, 2596 (1985).

[16]H. F. Hess, G. P. Kochanski, J. M. Doyle, N. Masuhara, D. Kleppner, and T. J. Greytak, Phys. Rev. Lett. **59**, 672 (1987).

[17]D. E. Pritchard, Phys. Rev. Lett. **51**, 1336 (1983); V. S. Bagnato, G. P. Lafyatis, A. G. Martin, E. L. Raab, R. N. Ahmad-Bitar, and D. E. Pritchard, Phys. Rev. Lett. **58**, 2194 (1987).

[18]W. N. Hardy, M. Morrow, R. Jochemsen, B. W. Statt, P. R. Kubik, R. M. Marsolais, and A. J. Berlinsky, Phys. Rev. Lett. **45**, 453 (1980).

[19]J. J. Berkhout, O. H. Höpfner, E. J. Wolters, and J. T. M. Walraven, Jpn. J. Appl. Phys. **26**, Suppl. No. 3, 231 (1987).

[20]Because of anharmonicity and bounding walls, U decreases from $U=3.83Nk_BT$ at 80 mK to $U=3.62Nk_BT$ at 225 mK (see also Ref. 11).

[21]J. Helffrich, M. P. Maley, M. Krusius, and J. C. Wheatley, Phys. Rev. B **34**, 6550 (1986).

[22]N. Masuhara, J. M. Doyle, J. C. Sandberg, D. Kleppner, T. J. Greytak, H. F. Hess, and G. P. Kochanski, following Letter [Phys. Rev. Lett. **61**, 935 (1988)].

Chapter 5

Experimental Results

5.1 Introduction

In this chapter we discuss details of the experimental procedure and results. Commonly the trap is filled by sending in a flux of low-field-seeking atoms until a density of a few times 10^{14}cm^{-3} is reached in the center of the trap. Then the flux is stopped and the decay is monitored and analyzed to extract the dipolar relaxation rate.

5.2 Data Acquisition

Our primary detection method is observing the decay of the trapped gas by measuring the flux of atoms leaving the trapping region after relaxation. The pumping plate detector[1] (see section 2.3), situated in the high-field region, enables us to monitor this flux continuously. To be able to discriminate between systematic effects and noise even in the tail of the decay signal, where signals are of the order of the noise of our detector, corresponding to $2 \times 10^{11}\text{at/s}$, we applied signal averaging to increase the signal-to-noise ratio. The necessary reproducibility of the flux produced by the dissociator is good (within 5%) from one cycle in the averaging procedure to another, if two conditions are met. There has to be sufficient surface coverage of the dissociator with molecular hydrogen, and the temperature of the dissociator should be kept constant. If there is not sufficient molecular hydrogen in the dissociator the flux will be very irregular, with variations by a factor of three within the time-scale of the filling part of a single cycle, typically one minute. The dissociator operated reliably at an estimated surface coverage of a thousand monolayers. Variation of the dissociator temperature causes variations in the flux at equal input power, with a maximum at a temperature of approximately 650mK. Equally important, also the ratio between the number of high-field and low-field-seeking atoms in the flux varies with temperature (this aspect is discussed in the next section). To guarantee reproducibility

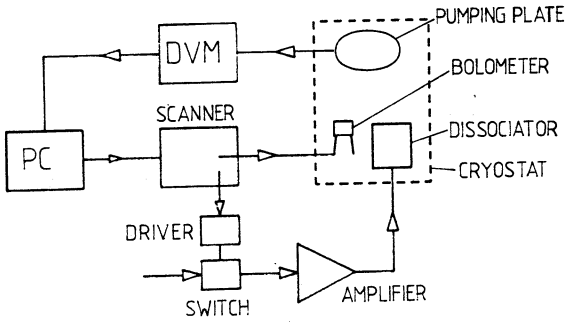

Figure 5.2.1: *Schematic drawing of the control and data acquisition of the experiment. PC= microcomputer, DVM= digital voltmeter.*

the dissociator temperature had to be stabilized, or alternatively, the first few cycles have to be discarded because the dissociator temperature has not reached a steady state yet.

The experiment is controlled by a microcomputer through an IEEE interface. The set-up is shown schematically in Fig. 5.2.1. The microcomputer triggers a scanner at the start of each measurement cycle. With the scanner the bolometers and the dissociator may be activated in any desired sequence. The dissociator is switched on and off by sending a trigger signal to a pulse generator, which in turn controls the RF-switch of the dissociator (see Sect. 2.4).

The computer continuously registers and stores the signal from the digital volt meter connected to the pumping plate detector. After a maximum of 20 cycles the measurements or a selection of them are averaged. The number of cycles is limited by available computer memory.

5.3 Trapping of H↑

To assure that the atoms observed with the pumping plate detector originate from the trap and not from some unintended reservoir of the much more stable H↓ in high field, we have an independent method to establish the presence of H↑ gas in the trap. This is done by activating B#2. This bolometer is located at the edge of the trapping field, where $B = 1.5$T (see Fig. 2.1.5). We can only detect the trapped atoms in this way if activating B#2 triggers recombination of all the trapped gas within a short period (a few seconds at most). If we calculate the H↑-density near the bolometer n_b, we can find the number of atoms that will hit the detector, using the equation of the flux on a surface $\phi = n\bar{v}A/4$,

where $\bar{v}$ is the average velocity, n_b the density and A the bolometer surface. Assuming a Maxwell-Boltzmann distribution over the trap the density will be

$$n_b = n_0 \exp\left(\frac{-\mu_B(B_b - B_0)}{k_B T_g}\right). \tag{5.3.1}$$

Here $B_0 = 0.05$T is the field in the trap center and $B_b = 1.5$T the field at the bolometer site. It follows that the time-constant for the detection of the sample by B#2 will be

$$\tau_b^{-1} = -\dot{N}/N = \left(\frac{\bar{v}A}{4V_{1e}}\right) \exp\left(\frac{-\mu_B(B_b - B_0)}{k_B T_g}\right). \tag{5.3.2}$$

At T =170mK we find $\tau_b \approx 2$s, whereas at 135mK this has become 10s.

As we expect on the grounds of these estimates we can detect a signal on B#2 at 170mK, steadily growing if the dissociator had been operated longer before triggering the bolometer. After 10s of filling we have $1.5 - 6 \times 10^{13}$ atoms in the trap, where the large uncertainty is due to the calibration of the bolometer. Because other bolometers were continuously used to deplete all other parts of the cell of H and because the signal persists for some time, up to one minute, after switching off the dissociator, we know that the atoms must be H$\uparrow$ from the trapping region.

At 135mK we detect no atoms on B#2. This is to be expected because the time constant for detection has become quite long. Nevertheless B#2 still destroys the trapped sample even at low temperatures by collisions of evaporated helium atoms with H$\uparrow$. The flux of helium evaporated by the bolometer power (12μW) is, in view of the H-He cross section,[3] sufficient to blow the atoms out of the trap, after which they have an equally high probability to hit the bolometer surface or to become trapped again. Therefore activating the bolometer for 10 seconds will empty the trap at any temperature. An alternative application of the bolometer could be to do evaporative cooling if there is a radiation shield situated between the bolometer and the trapped gas. In that case only the atoms having sufficient energy to reach the bolometer surface in field B_b, i.e. $\epsilon \geq \mu_B(B_b - B_0)$, are destroyed, and the remaining trapped gas will have lower temperature.

We have tried to observe the effect of the Majorana transitions, mentioned in section 1.7, by increasing the current in the trimming coil so that the resulting magnetic field in the center is opposed to that of the dipole coils and there is a zero-field region somewhere between the trimming coil and the dipole coils. The zero-field has no discernible effect on the decay rate as long as the change in the current was such that the effective volume V_γ was not drastically altered. This is not surprising if we estimate the number of transitions from H$\uparrow$ to H$\downarrow$ by assuming that an atom will undergo a transition if the rate of change of the direction of the field it experiences is higher than or equal to the Larmor frequency[2] $\omega_0 = \gamma B$, where γ is the gyromagnetic ratio. In our case the quadrupole field at the center of the trap changes direction fastest. To estimate the transition rate we let atoms pass

through the trap center, where there is only the quadrupole field, with gradient $\partial B/\partial r$. If v is the velocity of the atoms the rate of change of the direction of the field is about v/r. The radius of the area in which the condition for Majorana transitions is met is given by

$$r^2 \leq \frac{v}{\gamma(\partial B/\partial r)}. \tag{5.3.3}$$

If we take $v = \bar{v}$ and a gradient of about 2T/cm, the radius r of the transition region is about 10^{-4}cm, and the loss of H$\uparrow$, calculated by taking the flux trough this area, is negligible compared to the decay caused by other mechanisms.

5.4 Composition of the Flux

The composition of the flux is a point of concern in the analysis of our data. In the signal of the pumping plate we can not distinguish between high-field seekers (H$\downarrow$) coming directly out of the dissociator and atoms that are the product of relaxation of low-field seekers (H$\uparrow$) in the trap. Due to the helium vapor compression described in the section on the dissociator (chapter 2), H$\downarrow$ will enter the cell in spite of the field gradients in the filling tube and recombine on the pumping plate immediately, adding a spurious signal to the decay in the trap.

The existence of a direct high-field seekers signal was indicated by two phenomena: one is the persistence of a pumping plate signal even if the cell bolometer (B#2) is continuously activated, the other a reduction of the flux by 15 to 25% by switching on B#1, which is situated near the dissociator, as can be seen in Fig. 2.4.1.

A typical experiment is shown in Fig. 5.4.1. We observe the pumping plate power, where the reduction in heating power reflects the heat load on the pumping plate due to recombining hydrogen. The offset of the signal, being the heating power at zero flux, is subtracted, and the signal is converted to hydrogen atom flux, assuming a 60% efficiency in detecting the recombination energy.[1] In Fig. 5.4.1 the flux is plotted as a function of time. We record the zero flux signal for some time before and after the experiment, to make sure we have a proper base line. This is important in connection with the analysis. Fig. 5.4.1 is made by averaging over 10 cycles.

At $t = -62$s the dissociator is switched on, but because bolometer B#2 is activated no H$\uparrow$ can collect in the trap. This is done to give an impression of the H$\downarrow$ spuriously reaching the detector. As can be seen the H$\downarrow$ signal slowly increases with time. This is a temperature effect, because the dissociator warms up during the measurement. We have established this by looking at the flux with B#2 activated throughout a measurement cycle. At a dissociator temperature of about 550mK the share of spurious high-field seekers in the signal is estimated to be 30%, but at high temperature ($T_d \approx 650$mK) it is more than 50%. This is in accordance with the vapor compression model described in

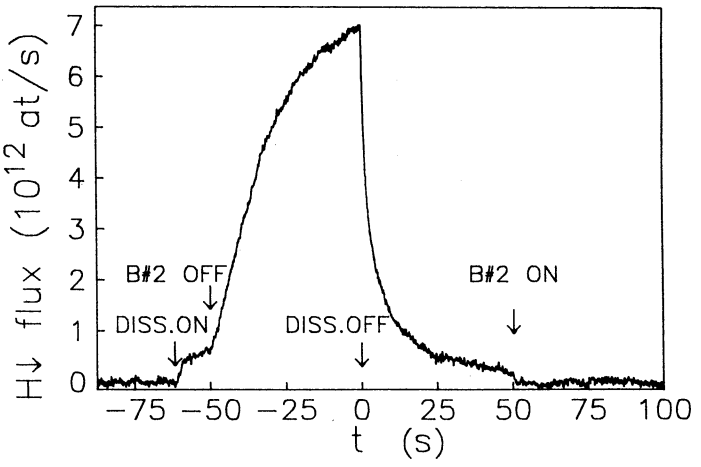

Figure 5.4.1: *A typical measurement cycle: the flux of atoms coming out of the trap vs. time. At $t = 0$ the dissociator is switched off.*

section 2.4. We have also explored the dependence on the field in the high field zone on the composition of the flux. Changing this field from 3T to 4.5T under otherwise identical conditions led to a reduction of the direct H↓ flux by one-third. If the force of the magnetic field would be the only force acting on the atoms one would expect an effect of the order of $\exp(\mu_B \Delta B / k_B T)$, with ΔB the change in field and T the dissociator temperature, in this case giving a reduction by a factor of 5. The fact that the change is much smaller supports the vapor compression model.

The other indication of the direct H↓ flux is the effect of bolometer B#1 on the flux. Triggering of B#1 leads to a reduction of the flux by approximately 20%. It is highly improbable that B#1 destroys an appreciable number of low-field seekers, so this reduction has to be a reduction of direct H↓ flux. Apparently B#1, when activated, is not so efficient that the spurious high-field seekers flux may be completely suppressed. During the experiments B#1 was triggered continuously, to reduce the spurious high-field seekers signal as well as possible.

The direct flux was observed to disappear within two seconds after the dissociator is switched off. Therefore the analysis is carried out ignoring the first two seconds of the decay signal, unless stated otherwise.

5.5 Analysis of the Data

We now continue the discussion of the cycle shown in Fig. 5.4.1. At $t = -50$s B#2 is switched off, and the growing density of trapped H↑ gives rise to an increasing flux

of relaxed atoms to the detector in the high field region. The flux saturates when the density in the trap has reached a steady state value $n_0 = (\Phi/G_2V_{2e})^{1/2}$, as was mentioned in Sect. 1.7. Then the dissociator is turned off ($t_0 = 0$) and the sample starts to decay. Finally at $t_1 = 50$s B#2 is switched on again, destroying what is left of the H$\uparrow$ sample. The reason for the destruction of the sample by triggering B#2 is that it assures a proper baseline ($\dot{N} = 0$) at the beginning and the end of a cycle, which we need to determine $\dot{N}$ accurately.

Next the decay signal can be analyzed to extract the rate G. Note that the rate constant depends both on the magnetic field, which varies considerably over the trap, and the density distribution. We therefore express the effective rate as a product of the rate in the field minimum G_{dd}, and a factor γ_{dd} which accounts for the field dependence as described in section 3.1. The atoms in the trap will on the average experience a higher field at higher temperature, since a higher total energy of an atom will allow it to reach a higher potential energy ($\mu_B B(\vec{r})$). The intrinsic temperature dependence of the rate G_{dd} is weak in our experimental range, so the change in the effective rate $\gamma_{dd}G_{dd}$ with temperature is due to the field dependence. The rate constant G_{dd} varies from 1.1×10^{-15} to 1.2×10^{-15} for T going from 200 to 100mK, the parameter γ_{dd} from 3.5 to 2.3 over the same temperature range.

For the analysis we rewrite eq. 3.1.31 as

$$-V_\gamma \frac{\dot{N}}{N^2} \approx \gamma_{dd} G_{dd}. \tag{5.5.1}$$

The effective volume can well be approximated by $V_\gamma T^{-5/2} = 180\text{cm}^3\text{K}^{-5/2}$ over the temperature range of this experiment. For the approximation in eq. 5.5.1 to be valid the period of EID must be over. N is found by integrating the signal $\dot{N}$ over t, and adding the number of atoms destroyed at the end of a cycle $N(t_1)$. The procedure for finding $N(t_1)$ is described below.

Plotted as $-V_\gamma \dot{N}/N^2$ the data look like Fig. 5.5.1. Note the EID during the first 5 seconds, and also note how the noise increases towards the end, signifying the decreasing signal. The 'flat' part of the decay (after the EID) is taken to be equal to $\gamma_{dd}G_{dd}$, with the correction factor for residual spin-exchange given in eq. 3.1.32. To calculate $N(t_1)$ we evaluate the function for a second order decay process, starting at some time t

$$N(t_1) = \frac{1}{(1/N(t)) + (\gamma_{dd}G_{dd}/V_\gamma)(t_1 - t)}. \tag{5.5.2}$$

The number $N(t)$ is calculated from $\dot{N}(t)$ by using the relation

$$N(t) = \left(\frac{V_\gamma \dot{N}(t)}{\gamma_{dd}G_{dd}}\right). \tag{5.5.3}$$

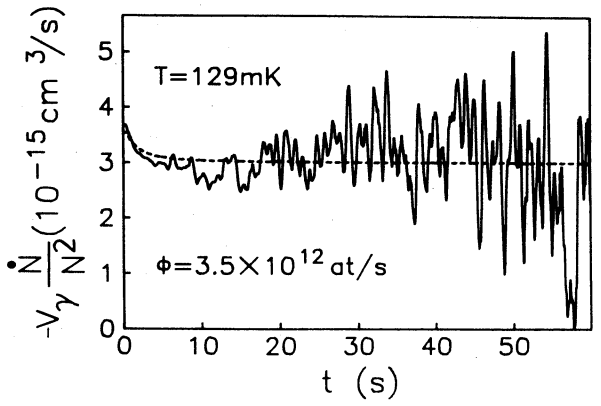

Figure 5.5.1: *The data plotted as $-V_\gamma \dot{N}/N^2$ vs. time. The dashed line is a simulation using the theoretically predicted decay rates. Note the EID during the first few seconds.*

This expression contains the value of $\gamma_{dd}G_{dd}$, which we want to find. However, we can insert here as a first approximation the theoretical value and correct this value by iteration of eq. 5.5.1 and 5.5.3. The result of this procedure should be that the curve of $-V_\gamma(\dot{N}/N^2)$ as a function of t is flat, i.e. it does not have a positive or negative slope. A positive slope indicates a too low number of atoms assumed to be destroyed by B#2, a negative slope indicates that $N(t_1)$ was estimated too high, and therefore the flatness of the curve is the indication that $N(t_1)$ is estimated correctly.

The data in Fig. 5.5.1 show EID because the gas is not yet doubly polarized immediately after switching of the dissociator. As we expected on the basis of the calculations in section 3.1 the EID, caused by rapid loss of c-state atoms through spin-exchange, disappears after a few seconds. Relation 5.5.1 holds for the rest of the curve, because the correction, of the order of 1% (sect. 3.1), due to the remaining spin-exchange, is negligible compared to other errors. There are three important contributions to the uncertainty in $\gamma_{dd}G_{dd}$. The first is, obviously, the noise in the pumping plate signal, as can be seen in Fig. 5.5.1. The second is the calibration of the pumping plate, of which the detection efficiency has an uncertainty of 17%, as given by Berkhout *et al.*[1] The ratio $\dot{N}/N^2$ depends inversely on this efficiency so the contribution to the error in $\gamma_{dd}G_{dd}$ is of the same size. The third contribution to the uncertainty is the uncertainty in the gas temperature T_g. We have plotted the data as a function of the wall temperature T_w, which is known quite accurately. However, we expect T_g to differ from T_w at temperatures of about 100mK and below for maximum trap depth ϵ_{tr}, as was stated in section 3.2 and 3.3. The latter is a

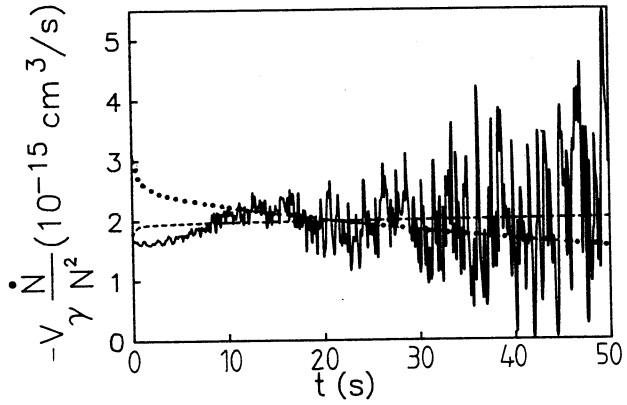

Figure 5.5.2: *The data plotted as $-V_\gamma \dot{N}/N^2$ vs. time, at $T_w = 85mK$, showing RID. The dashed line is a simulation using the theoretically predicted decay rates and including heating effects, the dotted line is a simulation were the gas is assumed to be at wall temperature T_w all the time.*

systematic error, and will be addressed separately.

Data recorded at low temperature, $T_w \leq 120$mK, show another feature shortly after t_0. As was remarked in Chapter 3 thermalization with respect to the cell temperature T_w will be slow, and possibly incomplete, with a time constant τ_w of the order of 10s, at these temperatures. If we plot the data in the way described above, using the value of V_γ belonging to T_w, we will underestimate V_γ, since $T_w < T_g$, and $V_\gamma \propto T_g^{5/2}$. This means the product $-V_\gamma \dot{N}/N^2$ will appear lower at the start of the decay, but approaches a steady state value, not necessarily equal to that expected for $T_w = T_g$, after some time, so the initial higher gas temperature will show up as Reduced Initial Decay (RID) in the analysis. An example of this is shown in Fig. 5.5.2.

The results of the analysis of all the measurements performed with maximum trap depth are plotted in Fig. 5.5.3. Data were taken with surface coverages of ^{4}He and a mixture of ^{4}He and 0.25% ^{3}He, with a binding energy of $\epsilon_a/k_B = 1.00$K[4] and 0.4K respectively. With pure ^{4}He coverage, we were unable to extend the measurements below 140mK. This may be understood in terms of recombination in the filling line as was discussed in Sect. 2.4. With ^{3}He added, the surface recombination problem is eliminated, and the cell temperature can be lowered until the heat load on the dilution refrigerator, coming mainly from the pumping plate, prohibits further cooling. On the high temperature end of the measurement range ($T \approx 225$mK) we are limited by direct recombination of trapped H↑ on the pumping plate, as explained in section 2.4. In the presence of ^{3}He the experiment

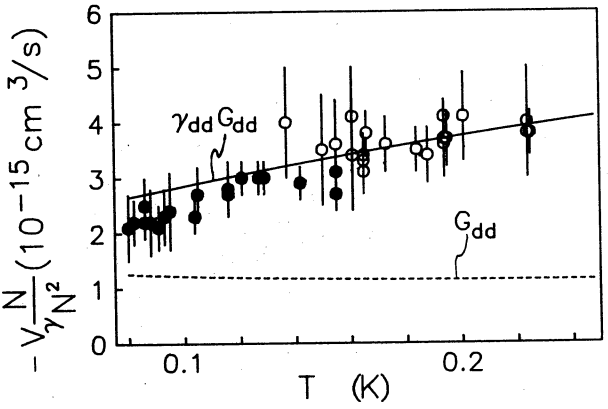

Figure 5.5.3: *The results $-V_\gamma \dot{N}/N^2$ plotted as a function of temperature (T_w), for maximum trap depth. Open circles stand for measurements done with ^{4}He covered surface, closed circles for ^{3}He-^{4}He. The solid line is the theoretical value, the dashed line is the rate constant G_{dd} for $B = B_0$.*

are limited to temperatures below 160mK. Vapor pressure causes heat transport through the gas phase, which strongly affects the power required to operate the pumping plate. Small variations in cell temperature then lead to large changes in the ^{3}He pressure, and accordingly to noise in the pumping plate signal. In spite of the small overlap between the points taken with the both types of surface coverage, it is clear from Fig. 5.5.3 that the measured relaxation rate does not depend on the value of ϵ_a. This is another indication that the atoms are trapped indeed, and that the decay process takes place in the trapped gas.

The agreement between the experimental data and theory[5,6] is quite good, as can be seen from the solid line in Fig. 5.5.3. Note that the field dependence of G_{dd}, incorporated in γ_{dd}, is reflected by the difference between the dashed line (the rate for $B = B_0$) and the solid line. This means the theoretical prediction is verified over a range of fields from 0.05 to approximately 1T. However, the error bars of the points in Fig. 5.5.3 do not include the uncertainty in the calibration of the pumping plate, so all points could be shifted up and down by this error. The experimental value for the relaxation rate through magnetic dipolar relaxation, incorporating only the error due to pumping plate noise and calibration, is $G_{dd} = 1.1(2) \times 10^{-15}$cm^3/s at $T_g = 100$mK and $B = 0.05$T. If we correct for the systematic error due to the heating of the gas at 100mK, as given in section 3.3, we find $G_{dd} = 1.2(2) \times 10^{-15}$cm^3/s, in good agreement with the theoretical value[5] $G_{dd} = 1.2 \times 10^{-15}$cm^3/s.

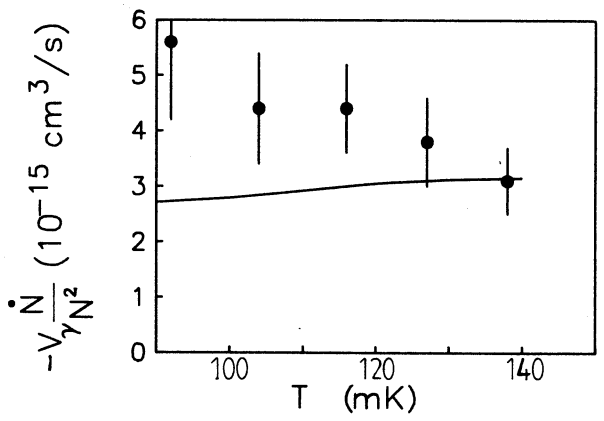

Figure 5.5.4: *The results $-V_\gamma \dot{N}/N^2$ plotted as a function of temperature (T_w), for reduced trap depth. The solid line is the theoretical prediction for $\gamma_{dd} G_{dd}$.*

A number of decays were taken with a reduced ϵ_{tr}, driving the quadrupole coil with 18A, half of the normal value. Because this leads to a different distribution of the gas and hence to a different value of γ_{dd} the results, shown in Fig. 5.5.4, can not be directly compared with those in Fig. 5.5.3. Furthermore the condition $\epsilon_a \lesssim \epsilon_{tr}$ implies that this experiment can only be done with a ^{3}He covered surface. We will comment on the large deviation at low temperature in Fig. 5.5.4 later.

5.6 Simulation of the experiment

When the sample is almost fully polarized in the d-state, the analysis can be done by calculating $-V_\gamma \dot{N}/N^2$. To be able to say something about transient effects, such as the c-state decay and the thermalization of the sample, we cannot rely on such a simple procedure. Therefore we have simulated the experiment. In the simulation H$\uparrow$ gas flows into the trapping region. We assume a Maxwell-Boltzmann distribution of the gas, which means we consider the gas to be always in internal thermal equilibrium. In our opinion this assumption is justified because the time-scale for internal equilibrium is always shorter than other relevant time-scales, as was pointed out in section 3.2. In the simulation the atoms enter the trap with high potential energy (equal to the trap depth), and all other heating processes, described in sections 3.2 and 3.3, are included. The flux is taken to consist of equal numbers of c and d-state atoms. We use magnetic fields generated by an expansion for dipole coils and a linear term for the quadrupole coils, and integrating the theoretical relaxation rates over the volume.

Results of the simulation have been included in Figs. 5.5.1 and 5.5.2 (the dashed lines). It can be seen that in both cases the simulation agrees with the final, steady state value of $-V_\gamma \dot{N}/N^2$ of the experimental result, steady state meaning here that the fraction of c state atoms does not change anymore. More interesting is the transient, initial behavior. The experimental data show a peak during the first second which is not there in the simulation. We attribute this to a spurious flux of H$\downarrow$, as was explained in sect. 5.4. After this we can see EID in Fig. 5.5.1, both in the simulation and the experiment. This is a general feature of all measurements done at temperatures above 120mK. However, the agreement between both results does not mean the predicted value for spin-exchange can be verified, since it turns out that the EID seen in the simulation is quite insensitive for the exact value of the spin-exchange. From the fact that EID is visible in the measurements we can conclude that G_{cc} exists and is considerably larger than G_{dd}.

The rate constants plotted in Fig. 5.5.4 deviate from the theoretical prediction at low temperature. In principle this could be due to a higher dipolar relaxation rate constant, but the analysis and simulation indicated that this is not the case. The procedure described in section 5.5 for estimating the number of atoms destroyed at the end of a measurement cycle, $N(t_1)$, does not give consistent results here, i.e. the final result for $\gamma_{dd}G_{dd}$, giving a flat curve of $-V_\gamma \dot{N}/N^2$ vs. t, does not agree with the value of $\gamma_{dd}G_{dd}$ needed to calculate the corresponding $N(t_1)$. Furthermore there is a systematic curvature in these plots, strongly suggesting that the decay is not a pure second order process. As is to be expected there is also little agreement between simulation and experiment in this case. However, full agreement could be restored by including a first order relaxation process, taking place at the wall. A very likely candidate for this is relaxation from the d-state to the c-state induced by magnetic impurities on the surface.[7] The measurements in Fig. 5.5.4 are more sensitive to this than others because the surface coverage will be higher since ϵ_{tr} is lower, according to eq. 1.7.1. The impurity fraction needed to induce a relaxation as strong as the one observed in these measurements is estimated to be 5×10^{-4}. This is much higher than the fraction 2×10^{-6} that was found in our analysis of the high purity copper. The impurities may be the result of machining, since it is known[8] that machining can implant concentrations of iron this high. However, to avoid this we have electrolitically etched the copper after machining. Possibly the soldering that was done after the etching, to put the cell together, has somehow introduced magnetic material. For completeness we have included the impurity relaxation in all simulations, although this has no visible effect on the agreement with the other measurements. The theoretical prediction for $\gamma_{dd}G_{dd}$ shown in Fig. 5.5.4 is based only on dipolar relaxation, and therefore there is a discrepancy with the measurements that grows as the temperature is lowered.

5.7 Experimental results on thermalization

In the case of RID there is also a general agreement between experiment and simulation on the basis of the model given in sect. 3.2 and 3.3. Moreover the simulation is sensitive for the inclusion of the heating effects and the bottleneck in the thermalization between gas and wall described in section 3.2. If we take the gas to be in thermal equilibrium throughout the cycle, a simulation shows a much higher decay rate than the experimental data. This can be seen in Fig. 5.5.2, where we show the experimental data and a simulation (the dotted line) where we take the gas to be constantly at the same temperature as the wall, $T_g = T_w$. In an earlier publication[9] we attributed the RID to the a combination of the exponentially decreasing H↑ density near the wall and the accommodation rate. This did not bring full agreement with the experimental data, as we remarked in the Letter.[9] Now we have used an improved thermalization model, taking into account the rate of collisions between the particles that have been bound to the wall and the rest of the gas. The agreement between simulation and experiment is better, especially at the lowest temperatures. The result of the simulation is also shown in Fig. 5.5.2 by the dashed line. However still, if we look at all our low temperature results it seems that there is a systematic effect of the RID being larger in the experiment than in the simulation during the first ten seconds or so. This could be due to a higher energy of incoming particles than the ϵ_{tr} used in the model, since particles will enter the trapping region having their last *sticking* wall-collision at a site of higher potential energy than ϵ_{tr}. If the value of the sticking probability is smaller than what we have taken it to be[1] this would lead to higher gas temperature too. It could also be that our view of the thermalization problem is still not complete.

According to the simulation the temperature of the gas does not become equal to the wall temperature ($T_g > T_w$), even after the RID. This is not surprising if we consider the time constant for thermalization τ_w calculated in section 3.2, and the steady state temperatures calculated in section 3.3. For a temperature $T_g = 80$mK we found a τ_w of more than three minutes, i.e. much longer than the duration of the experiment. It means we expect the gas to be warmer than T_w, even after the RID. According to this, the value of $-V_\gamma \dot{N}/N^2$ should also reflect the higher gas temperature, because of the strong temperature dependence of V_γ. This can be seen more clearly if we plot the data as $-\dot{N}/N^2$ vs. T_w, as is done in Fig. 5.7.1. We expect the ratio $\dot{N}/N^2$ to become independent of temperature below the value of T_w where τ_w becomes much longer than the duration of the experiment. Unfortunately this temperature is nearly equal to the lowest temperature that could be reached. In combination with the uncertainty in $\dot{N}/N^2$ the result is that these data alone give no conclusive evidence for incomplete thermalization, although it can be seen in Fig. 5.7.1 that the points below $T_w \approx 100$mK have values of $\dot{N}/N^2$ corresponding

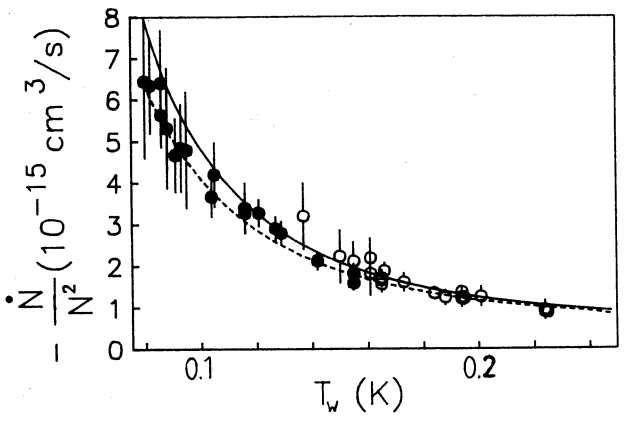

Figure 5.7.1: *$-\dot{N}/N^2$ plotted as a function of temperature (T_w), for maximum trap depth. Open circles stand for measurements done with ^4He covered surface, closed circles for ^3He-^4He. The solid line is the theoretical prediction for $\gamma_{dd}G_{dd}/V_\gamma$, the dashed line is calculated for $T_g = T_w + 8mK$. The plot reflects the strong reduction of V_γ with decreasing T_g.*

to temperatures higher than T_w.

However, summing the rather convincing appearance of RID and the tendency towards a constant $\dot{N}/N^2$, the reduction in the thermalization rate is a phenomenon clearly observed in this experiment, while the proposed thermalization mechanism offers, in our view, the best explanation for it.

5.8 Conclusion

This experiment has shown the feasibility of filling a magnetic trap with low-field-seeking atomic hydrogen at moderately high densities. The maximum density is three orders of magnitude higher than that achieved in trapping experiments with Na-atoms.[10] We have confirmed the theoretically predicted magnetic dipolar decay rate constant[5] over the range of magnetic fields relevant for traps. A reliable value for the spin-exchange rate could not be extracted, but it is justified to say that the gas polarizes rapidly (within 10s) to a steady, doubly polarized state. A lower bound on the temperatures reached in an experiment like this is set by the slowing of the gas-to-wall thermalization rate with temperature. Setting aside limits introduced by peculiarities of our experimental setup, and taking into account the heating mechanisms mentioned in Chapter 3, trapping atoms in a magnetic trap and cooling the gas by wall collisions can be used to achieve a temperature of approximately

45mK at a density of about $10^{14}cm^{-3}$. It is clear that additional techniques, such as evaporative cooling[11,12] or laser cooling,[13] should be applied to move the frontier further towards the quantum degeneracy regime.

References

[1]J.J. Berkhout, O.H. Höpfner, E.J. Wolters, and J.T.M. Walraven, Jap.J.Appl.Phys. **26**, 231 (1987) suppl. 26-3 (LT18).

[2]N.F. Ramsey, Molecular Beams, p.115 (Oxford University Press, 1985).

[3]R. Jochemsen, A.J. Berlinsky, and W.N. Hardy, Can. J. Phys. **62**, 751 (1984).

[4]W.N. Hardy, M.D. Hürlimann, and R.W. Cline, Jap. J. Appl. Phys. **26**, 2065 (1987).

[5]H.T.C. Stoof, J.M.V.A. Koelman, and B.J. Verhaar, Phys. Rev. B **38**, 4688 (1988) and private communication.

[6]A. Lagendijk, I.F. Silvera, and B.J. Verhaar,Phys. Rev. B **33**, 626 (1986)

[7]B.W. Statt, A.J. Berlinsky, and W.N. Hardy, Phys. Rev. B **31**, 3169 (1985)

[8]R. Sprik, J.T.M. Walraven, G.H. Van Yperen, and I.F. Silvera, Phys. Rev. B **34**, 6172 (1986).

[9]R. Van Roijen, J.J. Berkhout, S. Jaakkola, and J.T.M. Walraven, Phys. Rev. Lett. **61**, 931 (1988).

[10]E.L. Raab, M. Prentiss, A. Cable, S. Chu, and D.E. Pritchard, Phys. Rev. Lett. **59**, 2631 (1987).

[11]H.F.Hess, G.P. Kochanski, J.M. Doyle, N.Masuhara, D.Kleppner and T.J.Greytak, Phys. Rev. Lett. **59**, 672 (1987).

[12]N. Masuhara, J.M. Doyle, J.C. Sandberg, D. Kleppner, and T.J. Greytak Phys. Rev. Lett. **61**, 935 (1988).

[13]T.W. Hijmans, O.J. Luiten, I. Setija, and J.T.M. Walraven, submitted to J. Opt. Soc. Am. **B**.

Summary

In this thesis we investigate a new way of stabilizing a gas of atomic hydrogen (H) at very low temperature. The temperature can be reduced, compared to the 'classical' type of experiments with H, if we suppress the interaction between the gas and the walls of the container in which it is kept. With the aid of new cooling techniques it should be possible to observe quantum degeneracy in an almost ideal Bose gas.

In Chapter 1 we review some general characteristics of atomic hydrogen. The H atom consists of only one proton and one electron. It is possible to give a good quantummechanical description of this atom in its electronic ground state in terms of the spins of the composing particles, which will prove to be of use to us. By applying Bose-Einstein Statistics we find the values of density and temperature which have to be achieved to reach Bose-Einstein Condensation (BEC). BEC occurs when a macroscopic number of particles enters the ground state of the gas.

An H atom will be attracted (high-field seeker) or repelled (low-field seeker) by a magnetic field depending on the eigenstate it is in. Until recently H was stabilized by confining it at low temperature (around 500mK) in a cell in high magnetic field. The high field excluded the low-field seeking atoms to suppress recombination. All surfaces had to be covered with liquid helium, which has the lowest binding energy for H. The small but finite binding energy of the surface leads to a surface recombination rate which increases with lower temperature. To get rid of the surface one can use a magnetic trap. A combination of a quadrupole and a dipole field creates a high field at the surface and a low field in the middle of a cell. Low-field seeking atoms will collect in the center of such a cell, whereas high-field seekers are expelled. The density of atoms in the trap is limited by a relaxation process that changes low-field seekers into high-field seekers. Relaxation is induced by collisions between atoms through spin-exchange and magnetic dipolar interaction.

In Chapter 2 we describe the construction of the cell and the magnet system. There are four race-track magnets for the quadrupole field and three solenoids to create the dipole field. Apart from these magnets there is a single large solenoid which creates a high field to separate high- and low-field seeking atoms. In the high field part of the cell the dissociator, which creates H by a discharge at low temperature, is situated. When constructing the cell we have to make sure that there is sufficient thermal conductivity between various components and that detectors are properly located. A bolometric detector which registers the flux of H atoms coming out of the trap after relaxation is situated in the high field region. We also describe the cryogenic dissociator and mention some of its characteristics.

In Chapter 3 we consider the expected behavior of the gas in the trap on the basis

of theoretical predictions for relaxation rates. We show that only atoms in one of the eigenstates remain, because atoms in the other state relax quickly due to spin-exchange. The decay rate of the remaining, polarized gas depends strongly on the size and shape of the trap. We derive expressions to enable comparison between theory and experiment. We also look at thermal equilibrium. It turns out that internal equilibrium in the gas is always reached quickly, due to frequent interatomic collisions. However, if the temperature of the gas is lowered the trapped sample will be concentrated more and more in the trap center, and the number of collisions of atoms with the wall is reduced. Therefore for very low wall temperatures, compared to the energy corresponding to the trap depth, the gas can not be cooled to wall temperature. Furthermore there are processes, related to relaxation, which tend to heat the trapped sample.

A concise report of the experimental results is given in Chapter 4, which was published in Physical Review Letters. In this Chapter a short description of all important aspects of the experiment can be found.

Chapter 5 contains the results of the experiment. We check whether the gas is in the trap, and monitor the decay of the trapped sample. From the analysis of the flux of relaxed atoms we learn that the gas polarizes quickly into one state. The decay rate agrees very well with the theoretical prediction for dipolar relaxation. The filling method used in this experiment leads to high central density ($n = 3 \times 10^{14}\text{cm}^{-3}$). This seems to be a practical limit for experiments with trapped hydrogen, since the life time of the gas is only a few seconds at this density. We also see that it becomes difficult to cool the gas below a certain temperature, as is expected on the basis of the model described in Chapter 3. Therefore an additional cooling mechanism will have to be applied to reach the quantum degenerate regime.

Samenvatting

In dit proefschrift wordt een nieuwe techniek beschreven om onderzoek aan een gas van atomair waterstof (H) te doen bij zeer lage temperatuur. De temperatuur kan aanzienlijk verlaagd worden in vergelijking met 'klassieke' experimenten met H als we erin slagen de interaktie tussen het waterstof en het materiaal van de wanden van de experimenteercel te onderdrukken. Mede met behulp van nieuwe koeltechnieken zou het mogelijk moeten zijn om gedegenereerde quantumverschijnselen waar te nemen in een vrijwel ideaal Bose systeem.

In Hoofdstuk 1 worden enkele algemene kenmerken van atomair waterstof besproken. Het H-atoom bestaat uit slechts één elektron en één proton. Het is mogelijk voor dit atoom in de electronische grondtoestand een goede quantummechanische beschrijving te geven, waarbij voor ons doel met name de magnetische eigenschappen, die bepaald worden door de spin van electron en proton, van belang zijn. Toepassing van Bose-Einstein statistiek laat zien aan welk criterium van dichtheid en temperatuur voldaan moet worden om de zogenoemde Bose-Einstein Condensatie waar te nemen. Bose-Einstein Condensatie treedt op wanneer een macroscopisch aantal deeltjes in de grondtoestand van het gas komt.

Afhankelijk van de eigentoestand waarin een atoom zich bevindt zal het worden aangetrokken of afgestoten door een magneetveld. We noemen zo'n atoom een hoog- resp. laagveld-zoeker. Stabilisatie van atomair waterstof werd tot dusver altijd gedaan door opsluiting in een koude cel (rond 500mK) waarbij een hoog magneetveld zorgde voor grote stabiliteit doordat slechts één van de twee electron-spin toestanden voorkwam, namelijk de hoogveldzoeker. De wand van de cel werd bedekt met een film van vloeibaar helium, die slechts een geringe bindingsenergie heeft voor een H-atoom. Toch maakt de bindingsenergie van het oppervlak het onmogelijk om het waterstof zeer koud te maken omdat een oppervlakte-recombinatie proces de levensduur van het gas juist bij lage temperatuur sterk bekort. Om toch verder af te kunnen koelen is de magnetische valkuil bedacht. Door middel van combinatie van een quadrupool-en een dipoolveld kan men in een experimenteercel het veld ter plaatse van de wand hoger maken dan in het midden van de cel. Laagveldzoekende atomen zullen zich dan in het midden verzamelen en de dichtheid op de wand, bepalend voor de recombinatie-snelheid, wordt onderdrukt door een factor die exponentieel van de temperatuur en potentiaal-diepte van de valkuil afhangt. De dichtheid van atomen in de valkuil wordt dan beperkt door een relaxatie proces, waarbij laagveldzoekers in hoogveldzoekers worden omgezet. De relaxatie wordt teweeg gebracht door onderlinge botsingen van atomen, via spin exchange en magnetische dipool wisselwerking.

De constructie van de cel en het stelsel magneten dat de valkuil vormt is beschreven in Hoofdstuk 2. Naast racetrack-magneten voor het quadrupoolveld en solenoiden voor

het dipoolveld van de valkuil bevat het stelsel een grote solenoide om de scheiding tussen hoog-en laagveldzoekende atomen volledig te maken. In het hoge veld bevindt zich een dissociator, die door middel van een ontlading H produceert bij lage temperatuur. Bij het bouwen van de cel moet rekening gehouden worden met onder meer warmtegeleiding en de juiste plaatsing van detectoren in het magneetveld. In het hoge veld gebied zit een bolometrische detector die de flux van H atomen uit de valkuil meet.

In Hoofdstuk 3 wordt bekeken wat we aan de hand van de theoretische voorspellingen verwachten van het gedrag van de atomen in de valkuil. We laten zien dat door snel verval van de atomen in één bepaalde laagveldzoekende hyperfijntoestand er polarisatie optreedt in de andere toestand. De snelheid waarmee het gepolariseerde gas vervalt hangt sterk af van vorm en diepte van de valkuil. Hiervoor worden uitdrukkingen afgeleid zodat het mogelijk is de metingen met de theorie te vergelijken. We bekijken ook het thermisch evenwicht in het gas, dat zich in ons experiment altijd snel blijkt in te stellen, en de afkoeling van het gas naar de celtemperatuur, die bereikt moet worden door de schaarse botsingen van atomen met de celwand. Naarmate het gas afkoelt concentreert het zich in het minimum van de valkuil en neemt het aantal botsingen met de wand af, waardoor de afkoeling steeds langzamer gaat. Bovendien zijn er processen die het gevangen gas opwarmen.

Hoofdstuk 4 bevat een beknopt verslag van de experimentele resultaten, eerder gepubliceerd in Physical Review Letters. In dit hoofdstuk wordt in het kort een beschrijving van het gehele experiment gegeven.

Hoofdstuk 5 gaat over de uitvoering van het experiment. We gaan na of het gas zich in de valkuil bevindt, en hoe snel het vervalt naar de hoogveldzoekende toestand. Hiertoe wordt de flux van hoogveldzoekers die uit de valkuil komt geanalyseerd. Het blijkt dat het gas, zoals verwacht, snel polariseert en dat de resultaten zeer goed overeenkomen met de theoretische verwachting voor dipolaire relaxatie. Met de gebruikte vulmethode worden hoge dichtheden gehaald ($n = 3 \times 10^{14}\text{cm}^{-3}$). Wegens de levensduur van slechts enkele seconden die het gas bij deze dichtheid heeft, lijkt het niet erg zinvol om naar nog hogere dichtheid te streven. De afkoeling van het gas naar de temperatuur van de wand is inderdaad vertraagd, waardoor we op grond van het eerder beschreven model kunnen stellen wat de laagste temperatuur is die met deze methode gehaald kan worden. Naast de in dit proefschrift beschreven technieken zal er nog een additioneel koelmechanisme moeten zijn om het gedegenereerde quantum regime te bereiken.

Nawoord

Ik zou een verkeerde voorstelling van zaken geven als ik deed alsof dit proefschrift louter door eenzame arbeid van de promovendus tot stand is gekomen. Experimentele natuurkunde bedrijven zonder samen te werken is schier onmogelijk, en als men zich bovendien verheugt in het stimulerende gezelschap dat ik de afgelopen jaren gehad heb, ook onwenselijk.

Allereerst moet ik mijn promotor Jook Walraven noemen, die nauw betrokken was bij alle stadia van het experiment en mij langs vele theoretische en experimentele kliffen geleid heeft, en tevens het nodige heeft bijgedragen aan de leesbaarheid en begrijpelijkheid van dit boekje. Onvervangbaar in menig opzicht was Jaap Berkhout, met wie ik vele, soms hilarische discussies aangaande de mengkoeler gevoerd heb. Ook bij het meten was hij dikwijls behulpzaam. Simo Jaakkola came to us in the hour of need and made a large contribution to the construction of the trap and the cell. Bij het uitvoeren van het experiment heb ik verder hulp gehad van de studenten Jos Mosk, Ib Lunding en Irwan Setija en van Tom Hijmans. Otto Höpfner was betrokken bij alle constructie-technische aspecten van het experiment, en Karel v.d. Werf en Ron Manuputy namen het mechanische gedeelte van de valkuil voor hun rekening. Aan Nico Jonker en Herman Pothoven is het te danken dat de voor cryogene experimenten onontbeerlijke vloeistoffen telkens in voldoende mate voorhanden waren. Heel wat elektronische en computer problemen werden snel verholpen door deskundige tussenkomst van Paul Langemeijer. Glaswerk en vacuumapparatuur werden verzorgd door Bert Zwart. Ton Riemersma en Hugo Schlatter waren altijd bereid om mij van allerlei technische materialen en hulpmiddelen te voorzien, terwijl andere grote en kleine benodigdheden door respectievelijk Ton Jensen en Klaas van Paasschen aangevoerd werden. Zonder ettelijke door Mariet Bos verzorgde brieven zou mijn carriere als promovendus waarschijnlijk voortijdig geeindigd zijn.

Ook van buiten het laboratorium heb ik dikwijls adviezen en hulp gehad. In de eerste plaats dient het werk van de groep van Boudewijn Verhaar van de Universiteit Einhoven genoemd te worden. Henk Stoof en Vianney Koelman bezorgden ons betrouwbare berekeningen van relaxatie-snelheden. Tevens heb ik geprofiteerd van de ervaring met de constructie van magneten op het FOM-instituut voor Plasmafysica. Ing. Manintveld was zo vriendelijk de door ons berekende veldsterkte te controleren. I have conducted fruitful discussions with Takao Mizusaki of Kyoto University about many aspects of the experiment. Meritt Reynolds of the University of British Columbia has kindly shared his experience with deuterium with me.

Naast de mensen die ik al genoemd heb wil ik iedereen die deel uitmaakt(e) van de groep Spectroscopie van de Verdichte Materie bedanken voor de uitstekende sfeer en de talloze al dan niet constructieve opmerkingen, vooral tijdens de hectische bijeenkomsten

op vrijdagmiddag. Rudolf Sprik en Ad Lagendijk lieten mij delen in hun kennis. Pedro de Vries was altijd bereid om mijn worstelingen met de theorie aan te horen. En voorzover er, ondanks deze voortreffelijke lieden, toch eenzaamheid is bij de voorbereiding op de promotie, werd die aanzienlijk verlicht doordat het leuker is samen met Mick Baggen eenzaam te zijn dan alleen.